GEM TN-92-116
Rev. A

GEM Magnet Engineering Design Report

R. Stroynowski - Southern Methodist University

P.G. Marston, J. Minervini, R.D. Pillsbury Jr., Z. Piek, R.L. Myatt, B.A. Smith, J.D. Sullivan, P.H. Titus, R. Vieira - Massachusetts Institute of Technology, Plasma Fusion Center

T. Altenbach, J. Bowers, A. Chargin, G. Deis, A. House, W. Hsu, C. Johnson, D. Ng, G. Oberst, L. Pedrotti, R. Warren, S. Wineman, R. Yamamoto - Lawrence Livermore National Laboratory

M. Harris, N. Martovetsky, P. Reardon, W.J. Wisniewski - Superconducting Supercollider Laboratory

B. Smith - Los Alamos National Laboratory

December 18, 1992

GEM Magnet Engineering Design Report

R. Stroynowski

Southern Methodist University, Dallas,
TX 75275.

M. Harris, N. Martovetsky,
P. Reardon, W. J. Wisniewski

Superconducting
Supercollider Laboratory,
Dallas, TX 75237.

P. G. Marston, J. Minervini,
R. D. Pillsbury, Jr., Z. Piek,
R. L. Myatt, B. A. Smith,
J. D. Sullivan, P. H. Titus,
R. Vieira

Massachussetts Institute
of Technology
- Plasma Fusion Center,
Cambridge, MA 02139

T. Altenbach, J. Bowers,
A. Chargin, G. Deis, A, House,
W. Hsu, C. Johnson, D. Ng,
G. Oberst, L. Pedrotti,
R. Warren, S. Wineman,
R. Yamamoto

Lawrence Livermore National
Laboratory , Livermore, CA
94550.

B. Smith

Los Alamos National Laboratory
Los Alamos, NM 87545

TABLE OF CONTENTS

1.0 Executive Summary 1

2.0 Overview 2

3.0 Magnet Design and Global Performance Requirements 9
- 3.1 Magnet Design and Performance Requirements 9
- 3.2 Interface Requirements 11
- 3.3 Requirements Summary 12

4.0 Magnetic Field Design 13
- 4.1 Basis for Design Evaluation 13
- 4.2 Magnetic Field and Force Analysis 15

5.0 Cold Mass Design Description 24
- 5.1 Coil Design 25
- 5.2 Module Structural Support 27
- 5.3 Coil Joints 30
- 5.4 Conductor Design & Manufacture 33
- 5.5 Coil Module Assembly 42
- 5.6 Structural Analysis Introduction and Summary 44

6.0 Coil Assembly Design 58
- 6.1 Vacuum Vessel 58
- 6.2 Thermal Radiation Shields 67
- 6.3 Cold Mass Supports 69
- 6.4 Magnet System Assembly 74

7.0 Forward Field Shapers 84
- 7.1 Vacuum Vessel Interface 85
- 7.2 Temperature changes during cold mass activation 85
- 7.3 Forward Field Shaper Support Structure 86
- 7.4 Operational Requirements 86
- 7.5 Design Criteria 86
- 7.6 Description of Possible Failures 87
- 7.7 Documentation 87
- 7.8 Summary of Design Calculations 87

8.0 Central Support 91

9.0 Cryogenic System 93
- 9.1 System Description 93
- 9.2 Analysis 96

10.0 Magnet Power Supply and Protection Systems 104
- 10.1 Magnet Power Supply System 104
- 10.2 Magnet Protection System 109

11.0 Magnet Control System 112

12.0 Installation Scheme for Magnet Components in the Experimental Hall 113

13.0 Magnet Facilities at the SSCL 118

14.0 ES&H CONSIDERATIONS 121

15.0 Magnet Research and development 124

16.0 Schedule 126

1.0 EXECUTIVE SUMMARY

This report summarizes the present conceptual design of the GEM magnet. The current design is the result of a collaborative effort of a team of physicists and engineers from the MIT Plasma Fusion Center, the Lawrence Livermore National Laboratory and the SSC Laboratory. The design has benefited significantly from advice from numerous panels of international magnet experts who have reviewed it during the last year, particularly from the continuing involvement of the Rutherford Appleton Laboratory group which played a major role in selection of the concept and design of the conductor and of the winding scheme.

All major parameters of the magnet, including its field strength, length, radius and the choice of the type of conductor, are now frozen to allow this very large magnet to be constructed within the project schedule. The magnet design described in this report fulfills all of the performance requirements and meets cost and schedule objectives of the GEM experiment. All design choices made to date are conservative. Consideration of options for improving the design, reducing the cost, and streamlining the schedule are continuing. Thus, minor changes to this conceptual design may be expected, but these will be improvements on an already viable design.

A vigorous R&D program is being pursued to resolve the few remaining issues relating to conductor manufacturing and winding. This effort must run in parallel with completion of the design, which will be continued and finished by the contractor selection for final design, fabrication, assembly and installation so that the magnet will be ready by March 1997.

The overview section of this report contains a general description of the magnet and the considerations leading to particular choices of its parameters. Each of the subsequent chapters addresses aspects of the magnet design, construction and operation in greater detail.

2.0 OVERVIEW

The construction of the SSC will open new physics territory for exploration: unprecedented high energy proton-proton collisions studied at high luminosity. A major goal of the SSC is the search for massive new particles. Among these are the Higgs scalar boson which is expected in the Standard Model of electroweak interactions and additional families of particles which include supersymmetric particles, technicolor particles, leptoquarks, etc.[1] The greatest physics discovery potential lies among the particles emitted at large transverse momentum, as has been demonstrated at the CERN and FNAL colliders.

Most of the processes of interest are difficult to separate from the background due to well known strong interaction processes. The expected signatures of the decays of new particles, which are more readily distinguishable from these backgrounds, are high energy photons, charged leptons emitted at large transverse momentum, and multiple jets of charged and neutral particles. The goal of the GEM experiment is to discover these new particles with a detector optimized to measure high energy photons, electrons and muons, and which also maintains the possibility of measuring the energy and direction of hadronic jets. In addition, production of new particles is expected to have very small cross sections and the experiment must be able to operate at the high luminosity planned for the SSC accelerator.

In order to identify rare processes within the large background, GEM needs very good muon momentum resolution and very good energy and position resolution for electrons and photons. This requirement leads us to minimize the amount of intervening material in front of the electromagnetic calorimeter and to measure the muon tracks inside a magnetic field. This leads to the present detector concept in which a solenoidal magnet with very large radius encompasses muon tracking stations and electromagnetic calorimeter inside the coil. The baseline design of the GEM experiment is shown[2] in Fig. 2-1. The muon momentum measurement goals for the central region and a desire to minimize the constraints on the muon chamber precision, lead naturally to a very large radius, long solenoid to provide sufficient lever arm for muon tracking. This is limited by constraints on the cost of the magnet, experimental hall and surface facilities necessary for magnet construction as well as the number of chamber channels and segmentation[3,4] of the muon system. The size of the magnet, both in radius and in length, results from cost optimization for the combination of the magnet, the muon system and the size of the experimental hall. This optimization also took into account a range of the field strength basics in which the application of technologies considered for other detector components appeared reliable.

---

[1]The physics opportunities available at the SSC are described in the GEM Letter Of Intent , GEM TN-92-49.
[2]GEM Experiment Baseline design, GEM TN-92-76.
[3]J. Sullivan, GEM Magnet Options, GEM.TN-91-37.
[4]G.Deis, GEM Magnet and Muon System Cost Model.

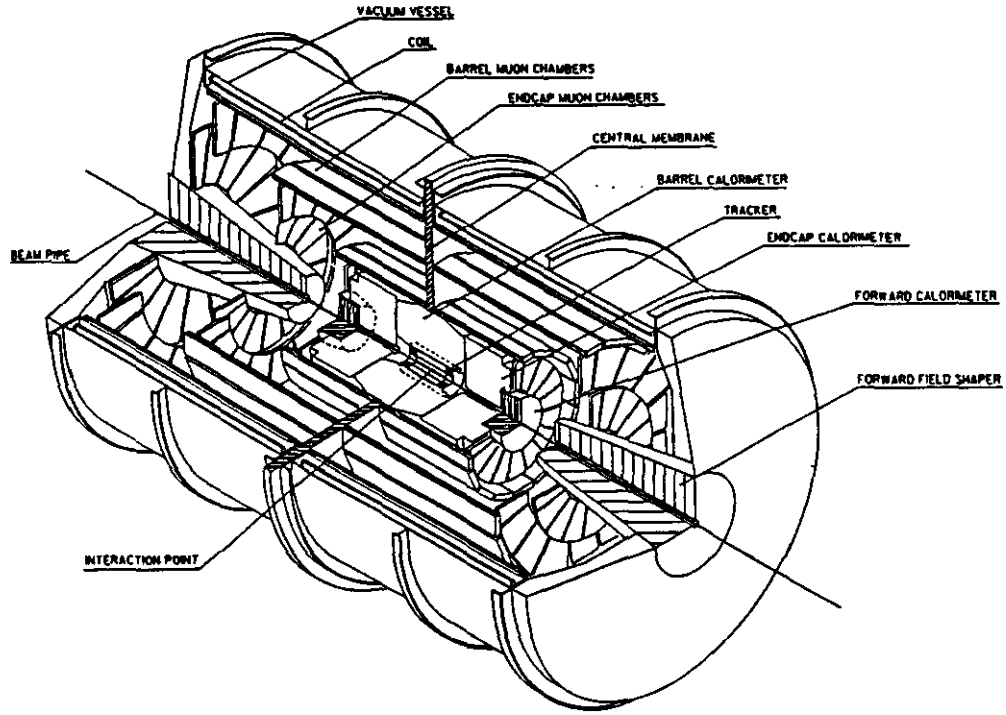

Figure 2-1 The baseline design of the GEM experiment.

The physics and engineering of a large solenoid coil, 30.8 m long with an 18 m diameter inner bore, leads to the selection of a superconducting solenoid with moderate field of about 0.8 Tesla. This can be achieved well within "state of the art" technology with a simple, single winding coil and satisfies all physics and technology needs. Higher field would require multilayer winding or other higher risk designs[5]. Resistive magnet technology was also considered and was found to be less cost effective than our baseline option. The resistive magnet requires a large iron return yoke and the associated cost (additional ~$100 M), construction schedule (additional ~1 year for iron installation) and power consumption (in excess of 20 MW) are unacceptable. Several of the alternative magnet concepts considered in the early design stages are listed in Table 2-1.

Table 2-1. Major Magnet Design Options

Option	Comments	Major Disadvantages
Resistive coil with iron flux return	low technical risk	high construction cost, high operating cost
Resistive coil without flux return	low technical risk, minimal construction cost	high operating cost, fringe field
superconducting coil with iron flux return	moderate technical risk, lower operating cost	high cost, schedule delay
superconducting coil with superconducting shield coil	high performance, high technical risk	technically risky, high cost, schedule delay
superconducting coil without iron flux return	low technical risk	fringe field and special shielding requirements

[5]GEM Magnet Technical Panel reports, R. Stefanski, ed., GEM GDT-16.

As a result of technical cost and schedule considerations, the GEM collaboration chose the superconducting solenoid without a flux return. Therefore, the GEM magnet does not have a return yoke[6,7]. The return yoke would require over 40,000 tons of iron, would increase the cost of the magnet by about $100 M and would require over one year longer installation schedule.

The baseline design satisfies the requirements of 5% momentum resolution for 500 GeV/c transverse momentum muons in the rapidity range of $0 < \eta < 1.5$. In an open field solenoid, the muon resolution in the forward direction, $1.5 < \eta < 2.5$, was found to be unacceptably low. The resolution in this region was relatively insensitive to the radius and length of the main solenoid, therefore, a variety of local forward field shaping options were studied (Table 2-2). From these options, we chose a simple, passive iron field shaper (see Fig. 2-2), which improves forward muon performance to meet our requirements. The iron forms a truncated cone around the beam axis in the region of 10 to 18 m from the beam intersection point. It introduces flux concentration and a large field gradient in the region of forward muon chambers allowing for 13% muon momentum resolution at $\eta = 2.5$.

Table 2-2. Forward Field Design Options Considered

Option	Design Objective	Performance	Disadvantage
longer superconducting solenoid	improved forward performance, lower cost, improved access	poor	
superconducting solenoid with end compensation	improved field uniformity	poor	high technical risk
forward pinch coils	improved forward performance	moderate to good	costly, complex
forward opposing field coils	improved forward performance	moderate to good	costly, complex
flat steel poles with coil windings	improved forward performance	moderate	costly, complex
conical steel field shaper with coil windings	improved forward performance	good	costly, complex
conical steel field shaper	improved forward performance	good	

[6]GEM Magnet Technical Panel Meeting, GEM GDT-5.

[7]R.Stroynowski, Considerations Leading to the Choice of Open Field Magnet, GEM TN-91-30.

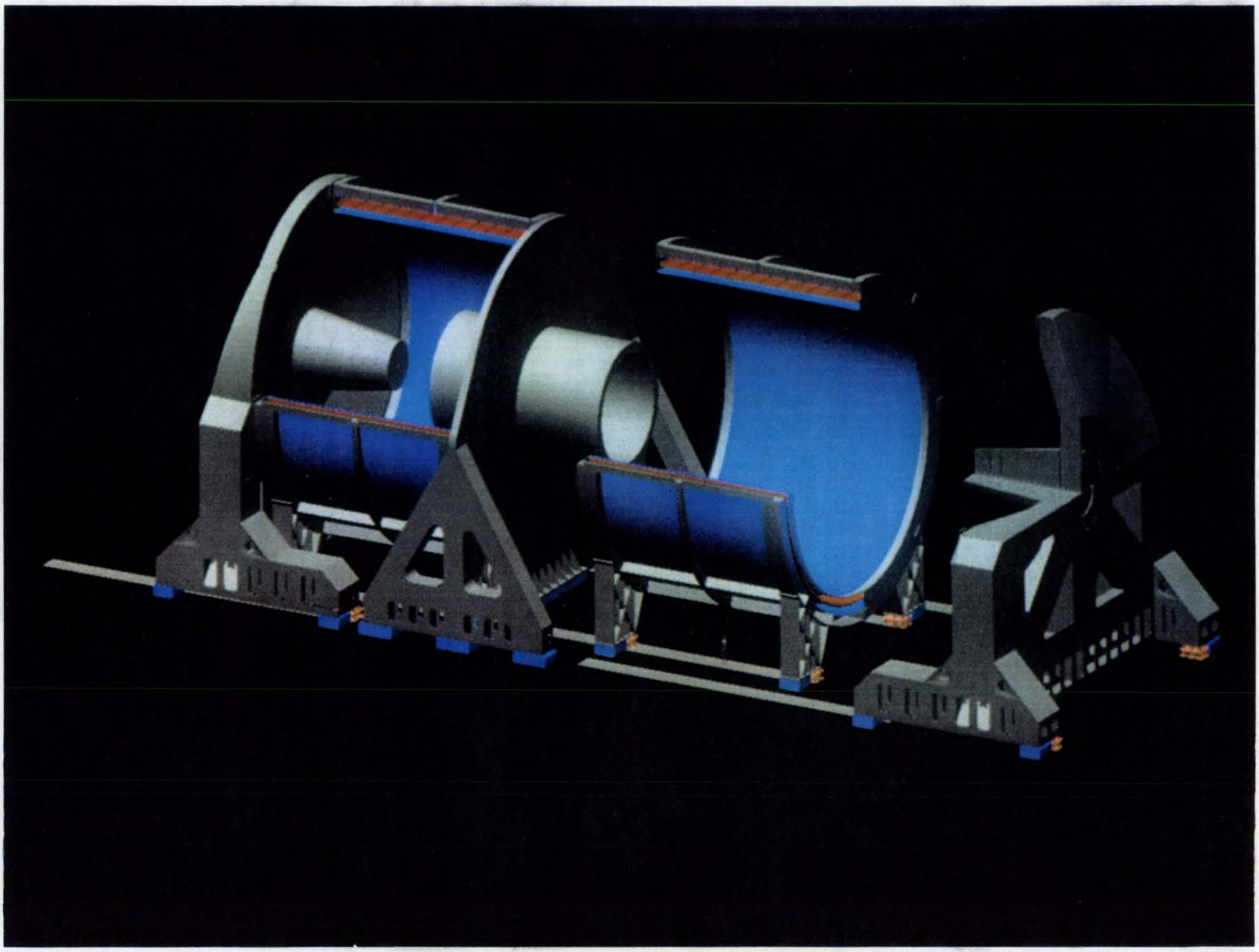

Figure 2-2 An artist's view of the GEM Magnet

The GEM magnet consists of two half-length coils each 14.44 m long, separated by a distance of 1.5 m. The central tracker and both electromagnetic and hadronic calorimeters are supported by a free-standing, fixed central membrane situated between the two coil halves. The decision to split the magnet into two coil-halves is dictated by the logistics of coil construction. The magnet is too long to be constructed and lowered from the surface into the experimental hall in one piece. Major parameters of the magnet are listed in Table 2-3.

Table 2-3: Major parameter list for the GEM magnet.

Central induction	0.8 T
Mean radius of windings	9.5 m
Inner radius of the cryostat	9.0 m
Overall outer radius, including structural ribs	10.9 m
Coil length, (per half)	14.44 m
Number of turns (per half)	228
Central gap between cryostats	1.5 m
Magnet axis height above floor level	13.0 m
Total magnet assembly weight (per half)	1300 t
Forward Field Shaper minimum z	10.0 m
Forward Field Shaper maximum z	18.0 m
Forward Field Shaper included angle	17.4 deg
Forward Field Shaper mass (each)	1265t
Operating current	50.2 kA
Stored energy	2.5 GJ
Inductance	1.98 H

The 1.5 m gap between the coil halves also allows for the installation of a support structure for the calorimeter and tracker and does not affect significantly the field uniformity in the central region. The gap is large enough to accommodate all signal cables and cryogenic and electrical services needed for the central detector.

The two coil halves are designed to be mobile along the beam axis allowing for their separation from the central detector support system during initial installation and allowing for the access to the calorimeters and the central tracker after the detector is put together by separating the magnet pieces during a major shut-down. The independent mobile support systems are necessary[8] for the initial installation of the magnet and the Forward Field Shapers.

Each coil half is constructed out of 12 identical segments. Each segment consists of 19 turns of conductor wound on the inside of the 7.6 cm thick and 1.2 m long cylindrical aluminum bobbin. The conductor for the GEM magnet is a NbTi "cable-in-conduit", which provides excellent stability against quench. This type of conductor has been studied extensively in the international fusion energy program, and its design is very similar to that used in the successfully-tested "Demonstration Poloidal Coil"[9]. We use 450 conventional NbTi:copper superconductor strands, cabled together, and surrounded by a 2.0 cm inner diameter stainless steel conduit filled with super critical helium at 4.5K which is in direct contact with the superconducting strands. This provides a large heat capacity, allowing the conductor to withstand substantial external heat input without quenching. With the modest magnetic field present at the conductor, less than 1.6 T even at the end windings, the operating current is less than 25% of the critical current, and the temperature margin is 3.4 K. The stainless steel conduit is surrounded by a rectangular aluminum sheath which provides hot-spot protection during the unlikely event of a quench.

[8] M.Harris, Magnet Mobility Considerations, GEM GGT-5.
[9] Steeves, M.M., et al, "US Demonstration Poloidal Coil", MIT ASC-90, (1990).

The large stability margin provided by this design allows relaxed requirements on winding and assembly, as appropriate for the large overall size of the coil. The present plan for winding and assembly of the coils calls for the conductor to be roll formed on the inside of the aluminum bobbin. Each conductor segment together with joint components at each end will be prefabricated and tested off-site. The on-site work on the coil segments will be performed in the South Assembly Building at IR-5. This will be limited to roll forming and insulating the conductor, and compacting the winding to a bobbin and end flange assembly. Twelve coil segments can be assembled with axes vertical to produce a coil half in the North Assembly Building. A special fixture to lift the stack of coils will be used so that successive segments can be inserted underneath. An alternative plan for assembly with axes oriented horizontally has also been developed. The baseline design of the electrical joints between the individual segments is a resistive coupling with a separate cooling system. It allows for the joints to be manufactured and tested off-site together on the conductor and it also minimizes the number of steps in the assembly procedure.

Cooling for the coil is provided by a natural-convection liquid helium thermosyphon system which is connected to the outside of the aluminum bobbin. This system removes the heat radiated or conducted to the 4.5K structure. A separate forced-flow of super critical helium removes heat from the resistive conductor joints and the cryogenic current leads. The super critical helium within the conductor is used only for stabilization of the conductor, and does not remove a significant amount of heat. All of the refrigeration for the GEM magnet is provided by a single refrigerator, similar to that used for the SSC Accelerator String System Test.

In order to reduce the heat load on the liquid helium system, each half coil is totally enclosed in a radiation shield consisting of multilayer insulation and panels cooled by liquid nitrogen. Both the conductor assembly and the radiation shield are enclosed in a vessel which provides insulating vacuum as well as structural support for the coil and the muon system. During assembly the completed half coil is inserted into the vacuum vessel still in the vertical axis orientation. The radial clearance between the cylindrical surfaces of the coil assembly and the vacuum vessel will be approximately 5 cm. The completed half coil will be then tested for vacuum and cryogenic leaks before rotating it into the horizontal orientation. Final cold leak testing follows this rotation. Completed half coil assemblies, Forward Field Shapers and the central detector support structure will be then lowered into the experimental hall for installation and full cold test of the magnet.

Knowledge of the magnetic field inside the detector will be needed for precise fitting of charged particles trajectories. It will be important also for local corrections for Lorentz angle effects in the muon chambers. A plan for measuring the field is under consideration. Options under discussion range from full field mapping of the empty volume of the magnet following its initial tests to placing sensors at strategic locations inside the muon tracking region and extrapolating the measurements to full volume. The process may become complicated if staging of the Forward Field Shaper components is necessary

In the absence of a return yoke, the static fringe field in the experimental hall will vary from about 2 T near the ends of the coil windings to about 50 gauss near the ends of the hall and in the access shafts. Precise knowledge of the field in the experimental hall will be needed to estimate and correct its influence on the beam, the final focus quadrupoles, and to mitigate or shield any mechanical or electrical component in the hall, electronic counting house and in the operations center. The forces[10] on structural I-beams and crane rails in the experimental hall will be small in comparison with normal gravitational and structural loads. Vital electrical and cryogenic equipment will be either shielded from the effects of the fringe field or selected to be insensitive to the field effects. Ample operational experience from existing facilities with such fringe field (mainly NMR facilities) has been accumulated and shows no substantial additional costs.

At the surface above the experimental hall, the fringe field will be approximately 44 gauss. This will decrease to the level of the normal earth's magnetic field at the SSC site boundary. An access and operations plan will be

[10] R. D. Pillsbury Jr., Fringe Field Dipole-dipole Force Interaction, GEM TN-91-35.

prepared, and when implemented the facility will comply with the current local and federal health and safety regulations.[11,12]

Electrical current from the 20 V/55 kA DC power supply, located in the surface utility building, is routed to the magnet using air-cooled resistive busses. This system is capable of charging or discharging the magnet in 8 hours. A 5 minute emergency discharge is also possible, and can be initiated by the quench detection system or by other safety interlock systems. The emergency discharge is accomplished by switching a large external dump resistor into the power circuit using large circuit breakers.

The magnet is on the early critical path of the overall GEM Detector schedule and thus the SSC itself. Installation and testing of the magnet must be completed before underground installation of any of the other subsystems can begin. After testing and field mapping, the magnet halves must be moved apart to permit access for installation of the central detectors and the muon subsystem. Magnet testing must be completed by March 1997 in order for GEM to be available for physics operation at SSC turn-on in June 1999. This aggressive schedule has led to our overall philosophy of prefabricating as many components as possible off-site. Using this approach, and assuming a two-shift operation for the winding, the desired overall magnet schedule can be achieved.

---

[11] R.P. Woolley, SSC GEM Magnetic Field SAfety & Health Effects, GEM TN-91-19.

[12] R. P. Woolley, Supplemental Environmental Analysis of the GEM Magnet, GEM IN-92-10.

3.0 MAGNET DESIGN AND GLOBAL PERFORMANCE REQUIREMENTS

The GEM detector must be capable of supporting in-depth exploration of the range of physics which will become available at the SSC, and must also maximize the physics discovery potential. These requirements drive the overall architecture of the detector and set specific performance goals for each of the detector components. Of particular importance to the magnet design are the requirements placed on the muon system, since the primary specification on the magnet is to provide a magnetic field necessary for the muon system to achieve a muon momentum resolution of 5% or better at $\eta = 0$ for muons with $p_t = 500\,\mathrm{GeV}$. This resolution should not be significantly degraded for rapidities up to $\eta = 1.5$. In the forward region, the resolution at $p_t = 500\,\mathrm{GeV}$ should be 13% or better, in the range of $\eta < 2.5$. These physics performance requirements, together with technology limitations within the muon detector systems, result in specific requirements on the size of the magnet and the magnitude and shape of the magnetic field.

The GEM detector must be operational during the entire SSC accelerator cycle, i.e., 4500 operating hours per calendar year. Specific reliability goals are set for each GEM system, to fulfill these requirements. For the magnet, the availability goal of 99% drives the overall design of the cryogenics, power protection, and controls systems and also dictates design features to allow access for maintenance and repair of key items such as cryogenic connections within the magnet assemblies. In addition to meeting these physics performance requirements, the GEM detector must also adhere to cost and schedule constraints. The overall schedule for GEM is based on availability for physics operation at the SSC turn-on in October 1999.

Finally, the design must also satisfy all applicable ES&H requirements at the SSCL including the Supplemental Environmental Impact Statement.

3.1 Magnet Design and Performance Requirements

The magnet performance requirement is to support the operation of other detector components. The detailed magnetic field requirements have been developed by a trade-off between physics needs and technology limits.

The magnet is constrained within definite cost and schedule limits. In order to achieve the total detector cost limit of $500M, the magnet together with all the support structures is required to cost less than $120M, assuming construction by a US industrial firm collaborating with national laboratories. This cost includes all costs associated with the magnet and includes R&D, conceptual, preliminary and final design, management, supervision, inspection, fabrication, assembly, installation, testing, and contingency. In order for GEM to meet its schedule of readiness for physics operation in October 1999, the magnet must be installed, tested, and the magnetic field must be mapped no later than June, 1997. At this time, installation of the calorimeters and muon subsystem must begin.

Overall Configuration

We have considered a wide range of magnet designs and made a number of choices regarding the overall configuration of the detector. Physics performance and economic constraints require that the GEM magnet be a large, open solenoid with field shaping iron in the forward regions. All detector components present at startup are placed inside the magnet. The magnet is "open", it is not surrounded by a local flux return. The flux return option was rejected for economic and schedule reasons[13]. The inner volume of the magnet available for other detector components is 9.0m inner radius, by 30.8m length measured between the ends of the magnet vacuum vessels. The overall length of the magnet system in the forward region is slightly longer.

In order to permit access to the muon, calorimeter and tracking systems, the magnet coil assembly is split at the axial midplane. The two halves have the capability to be moved apart along the beam line. This movement can

[13] R. Stroynowski, Considerations Leading to the Choice of Open Field Magnet; TN-91-30.

be accomplished during a normal SSC scheduled maintenance shutdown of 3-6 months. The central detectors i.e., calorimeters and the tracker, are supported by a structure which is independent of the magnet halves, and is capable of remaining in place and stable even when both magnet halves are moved away.

The magnet will also provide structural support for the muon system. The muon system will provide the space-frame structures necessary to support and align the arrays of the muon chambers to the necessary accuracy, and the magnet will provide discreet mounting points for these structures. The mounting points must be structurally stable, and capable of supporting and restraining the muon system. Finally, as a design goal, the magnet configuration should allow for possible future upgrade of the muon system. Specifically, an annular space around the outside of the magnet vessels should be reserved for the addition of an external superlayer of muon detectors.

Magnetic Field

The magnet will provide a solenoidal magnetic field with some shaping in the forward direction. At the interaction point, the magnitude of the field will be 0.8T. The field must be symmetrical about the beam axis to 0.5%. Since the field is provided by two separated coil halves, some non-uniformity will occur at large radii near the central membrane. In the forward region, the field required to provide acceptable muon momentum resolution is defined by the iron of the Forward Field Shaper.

The field magnitude and its distribution will be known at all times during GEM operation to an accuracy of 0.1%. This may be attained by a combination of one-time detailed field-mapping performed before inner detectors are installed and by continuous monitoring at discreet locations within the working volume of the experiment.

Duty Cycle and Lifetime

We presently require the magnet to operate continuously for at least 4500 hours which is the SSC running cycle. In order to facilitate access to the underground hall for maintenance and repair of the other detector systems, the magnet must be charged or discharged, under normal circumstances, in a maximum of 8 hours. At the end of such a normal discharge cycle, the magnet will be ready for immediate re-charging. This allows fringe field-free access to components outside the working volume of the magnet within one day turnaround. In an emergency situation, we require that the magnet be capable of a 5 minute discharge without sustaining damage. Following an emergency discharge, the magnet may require a cool-down period before charging.

The design lifetime of the magnet will be 20 years. During this time, the magnet will be capable of 100 thermal cycles from ambient to operating temperature and back and 1000 normal charge/discharge cycles. We require that the design be capable of withstanding an additional 100 emergency discharge cycles. These requirements will affect the components susceptible to fatigue or fracture. For economic analysis, we assume that there will be a total of 10 emergency full discharges during the lifetime of the magnet. This requirement is used to specify the design of the cryogenic system, and the handling of the boiled off helium by the recovery system.

Alignment

Alignment requirements for the magnet stem from four criteria. First, the magnet must not exert any influence on the SSC beams that would result in beam tune shift. Second, the major components of the magnet must be mutually aligned so that they do not produce unacceptable magnetic forces. Third, the alignment of the magnetic field with respect to the detector systems must be stable during the data collection. Fourth, the magnet structure must be sufficiently stable to satisfy the alignment requirements for the detector systems it supports. The specification of detailed requirements must await more simulation and analysis efforts. In the interim, the most stringent requirements are those involving the stability of the magnet structure. For instance, since the muon system is supported by the magnet vacuum vessel, it is vital that the support points on the vessel be stable during an SSC physics cycle. We presently assume that all magnet components must be placed in their ideal location within

25 mm, but after charging the stability of the position of all elements must be better than 0.5 mm during operation. Further definition of these global alignment requirements is in progress.

Codes and Standards

The magnet will be designed to the intent of the ASME Pressure-Vessel Code, but will not be code-stamped. The magnet will be subject to seismic design requirements, which are presently undefined. Since it is likely that seismic requirements will be developed for the SSCL in the near future, we have made a reasonable design assumption in this area. The Final Safety Analysis Report for the Comanche Peak Steam Electric Station provides the basis of this specification[14]. For a maximum seismic event at this station, the peak horizontal acceleration is specified as 0.12g, and the peak vertical acceleration is 0.08g. For simplicity, we adopt these specifications, which allow the use of the response curves in Ref. 14 for all preliminary analyses. For finite-element analyses, where a ground-motion history is required, we assume the standard history used at LLNL, with the peak acceleration scaled down to match the specifications from Comanche Peak. This provides a reasonable and easily-used procedure, until an SSC requirements are developed.

3.2 Interface Requirements

Specific interface control documents will be developed to detail the requirements for each of the interfaces between the magnet and the other systems. Consideration of these interface definitions is in progress and the main features of each of them are discussed below.

Magnet/Central Tracker Interface

The main requirements imposed on the magnet by the interface with the central tracker involve magnetic field, physical support, and access for installation and maintenance. The tracker requirements for the magnetic field are modest: the field should be as high as possible and nonuniformity of the filed should be less than 1.5%. The central tracker support must carry the tracker's weight, but it does this through the calorimeter. It also must provide stability and this requirement drives the mechanical design of the support. The magnet must allow access for installation and repair of the tracker, on a long (3-6 month) turn-around basis. This last requirement led to the design of the mobile magnet halves.

Magnet/Calorimeter Interface

The calorimeter interface provides requirements which primarily affect the design of the central detector support. Clearly, the weight of the calorimeter and the required stability are the key factors in this area. In addition, however, one of the potential fault modes for the LAr calorimeter is a cryogenic spill. This fault mode may affect the magnet inner vessel. The magnet is required to withstand this calorimeter fault without significant damage.

Magnet/Muon Interface

The requirements derived from the muon interface have been discussed above. This interface provides requirements on the magnetic field and the structural stability of the muon mounting points. Detailed specification of the muon mounts is in progress.

---

[14] "Final Safety Analysis Report, Comanche Peak Steam Electric Station", section 3.7b, Texas Utilities Generating Company.

Magnet/Facility Interface

The magnet interfaces extensively with the above ground and underground facilities at SSCL. Since design of the facilities is in progress, the magnet subsystem will be expected to accept most of the requirements as imposed on it by the facilities design. This will be the case particularly for the above ground assembly buildings. The magnet subsystem has provided rough requirements to the facilities design, and these are being incorporated.

3.3 Requirements Summary

A system-engineering approach is being followed in the design of the magnet. The requirements imposed on the magnet are naturally evolving as the design progresses, and we expect them to continue to evolve. However, changes in these requirements are expected mainly at the lower detailed levels, since the overall concept and performance of the detector and magnet are well understood. These requirements form the basis of the design discussed in the remaining sections.

4.0 MAGNETIC FIELD DESIGN

The design of the GEM magnet[15] is driven by the design of a detector that meets the requirements of the GEM physics program. These requirements include an 0.8 T central field with a homogeneity of 0.5% in the central tracker volume and, when combined with the muon detector design, a muon momentum resolution at a transverse momentum p_t=500 GeV of $\Delta p_t / p_t = 5\%$ at $\eta = 0.0(\theta = 90°)$ and $\Delta p_t / p_t = 13\%$ at $\eta = 2.5(\theta = 9.4°)$.[16]

Thus, the magnet design evolved together with the μ detector design. The design goals were met by the GEM baseline. The only magnetic structures in the baseline are the superconducting solenoidal coils and the forward field shapers. It should be noted that the *ideal* magnetic field shape for GEM is not homogeneous but exhibits extra curvature forward to enhance the μ resolution.

4.1 Basis for Design Evaluation

Homogeneity

The field homogeneity (over the central tracker volume) is defined as a fractional deviation of the field from that at the geometrical center of the magnet.

$$\left(B_z(\rho,z) - B_z(0,0)\right) / B_z(0,0).$$

Resolution

The momentum resolution is defined as

$$\Delta p / p = \Delta p_t / p_t \equiv \Delta\sigma(S) / S,$$

where the momentum $p = \left|\vec{p}\right|$, transverse momentum $p_t = \left|\vec{p}\right| \sin\theta$, and θ is the polar angle from the beam line. The momentum resolution is computed as a function of angle given $\vec{p}$. $S(\vec{p})$ is the sagitta, related to the curvature of the track, and $\Delta\sigma(S)$ is the total uncertainty including measurement error σ_{meas}, multiple scattering error σ_{MS}, and systematic error σ_{sys}. The uncertainty in the resolution depends on the actual track, because the path length varies and the angle relative to the magnetic field changes. Thus, to compute S and ΔS the muon detector geometry must be defined.

We start with the Lorentz force (the force on a moving charged particle),

$$d\vec{p} / dt = (Q / c)\vec{v} \times \vec{B},$$

and assume that the particle rigidity $\mathcal{R}(= p/Q$, where Q is the charge) is large enough so that $\rho \gg L$, where ρ is the radius of curvature $(= \mathcal{R} / B\perp)$ and L is the length of the track in the detector. Under this assumption, the osculating plane is fixed and small higher order corrections to the path may be neglected.

The first integral of the force equation is the impulse $\vec{\mathcal{I}}$:

$$\vec{\mathcal{I}} \equiv q/c \int_0^s \vec{B} \times d\vec{\ell}$$

[15] GEM Baseline 1 — GEM TN-92-76

[16] The symbol η is used for the pseudorapidity; $\eta \equiv -\ln\tan(\theta/2)$.

The impulse between two points is related to the angular change of a trajectory, as $\Delta \vec{p} = \vec{I}$ or $\Delta p_{\perp} = |\vec{I}|$. The second integral which we call $B\mathcal{L}^2$ s given by

$$B\mathcal{L}^2 \equiv 2\left|\int_0^L \int_0^s \vec{B} \times d\vec{\ell} ds\right| .$$

The factor of 2 in the definition of $B\mathcal{L}^2$ is included to agree with the results for a uniform field. $B\mathcal{L}^2$ is related to linear displacements, e.g., radius of curvature or sagitta S

$$S = \frac{0.3}{8\,|\vec{p}|} B\mathcal{L} = \frac{0.3 \sin\theta}{8\,p_t} B\mathcal{L}.$$

The sagitta of a track is sketched in Figure 4-1 where a muon trajectory is shown transversing three superlayers in a 4-8-4 chamber configuration; the sagitta is the indicated dimension. Thus, a figure of merit is

$$B\mathcal{L}^2/\sigma_{eff}$$

where σ_{eff} is the effective resolution of the GEM muon detector system, postulated to be 50 μm.

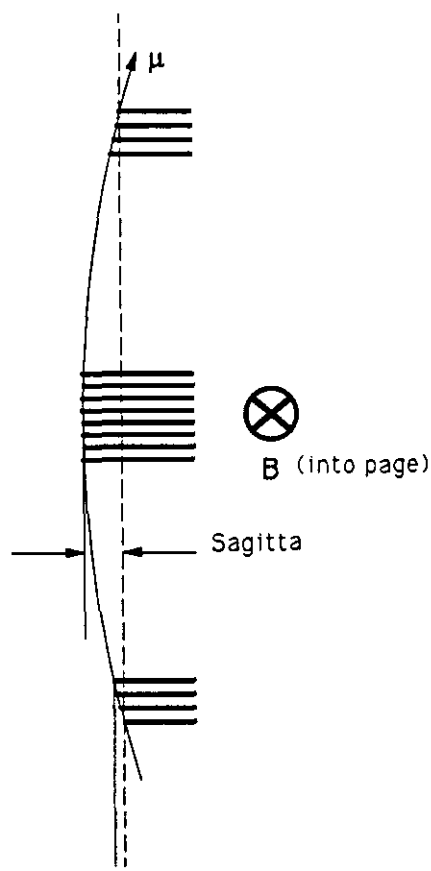

Figure 4-1 Sagitta measurement in one radial module of the central detector (B is the magnetic field).

4.2 Magnetic Field and Force Analysis

Field Plots

Figure 4-2 shows an elevation view of the experimental hall with the magnet and the forward field shaper shown. Also shown are the positions of the crane rail, the two assembly shafts and the two access shafts. Flux lines are overlaid. The magnetic field vectors are parallel to these lines and the field magnitude is inversely proportional to the spacing.

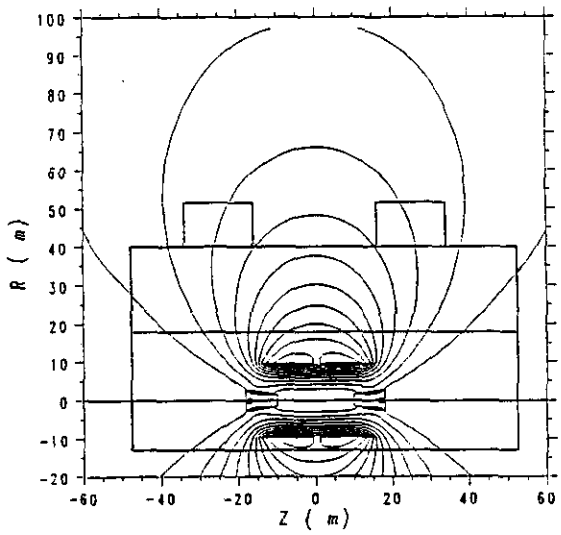

Figure 4-2 Contours of constant flux in the X=0 plane (labeled in gauss) overlaid on an elevation view of the experimental hall and the assembly and end shafts.

Figure 4-3 shows the same elevation view as in Figure 4-2 but with contours of constant flux density. As can be seen, the surface flux density is about 40 G. The flux density in the two end elevator shafts and utility shafts is between 100 and 200 G. The magnitude of the flux density in the electronics shaft before shielding is between 50 and 200 G.

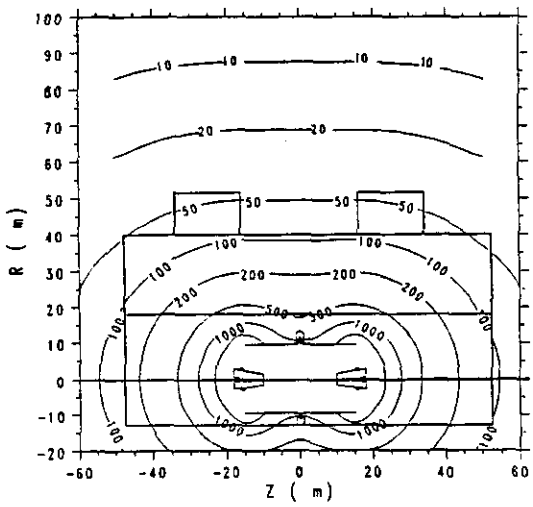

Figure 4-3 Contours of magnetic flux density for the baseline design for GEM in the X=0 plane overlaid on an elevation view of the experimental hall and the assembly and end shafts.

The shape of the magnetic field within GEM may be more easily seen in Figure 4-4 and the magnitude at different scales in Figures 4-5 through 4-9.

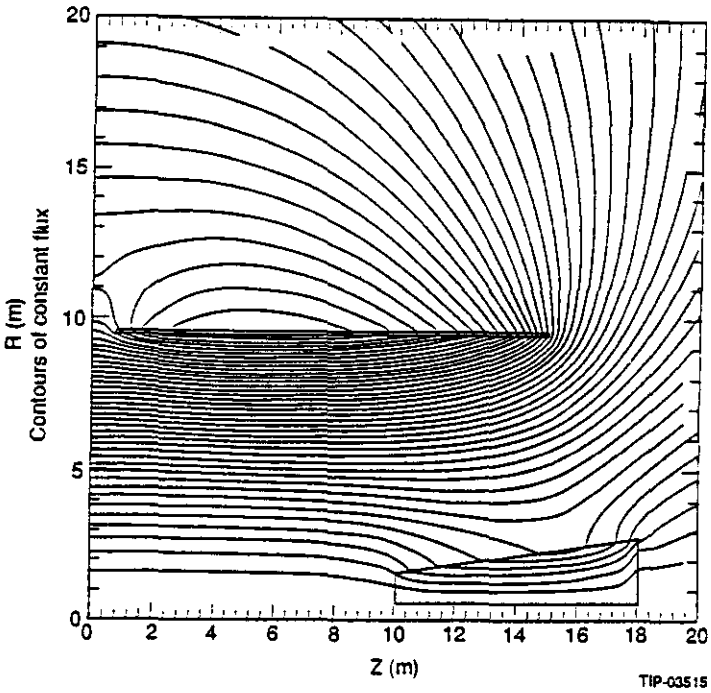

Figure 4-4 Contours of constant flux.[17]

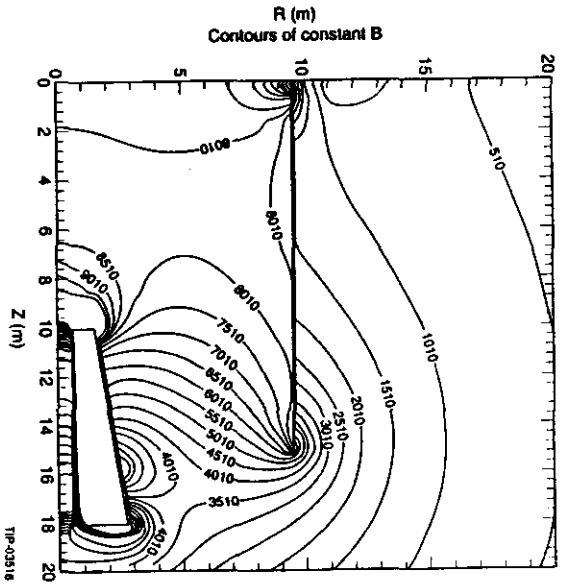

Figure 4-5 Contours of constant *B* labeled in gauss. (See Footnote 17)

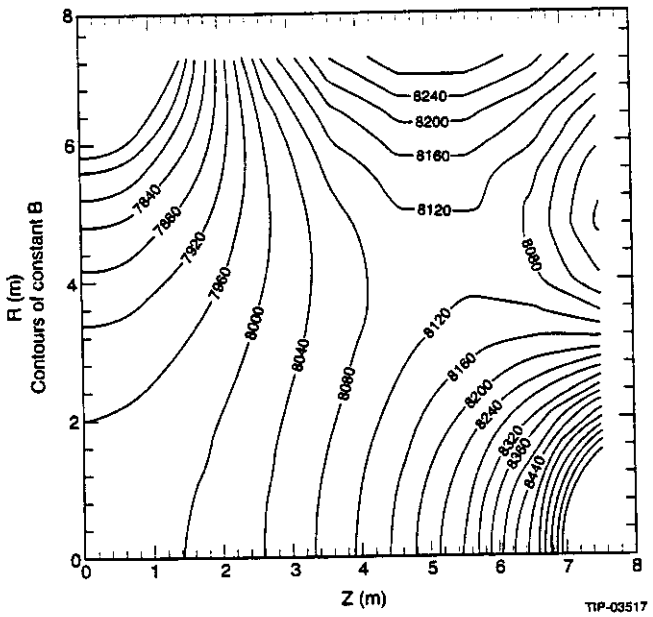

Figure 4-6 Contours of constant B for the central tracker labeled in gauss; the contours are increments of 40 G apart.

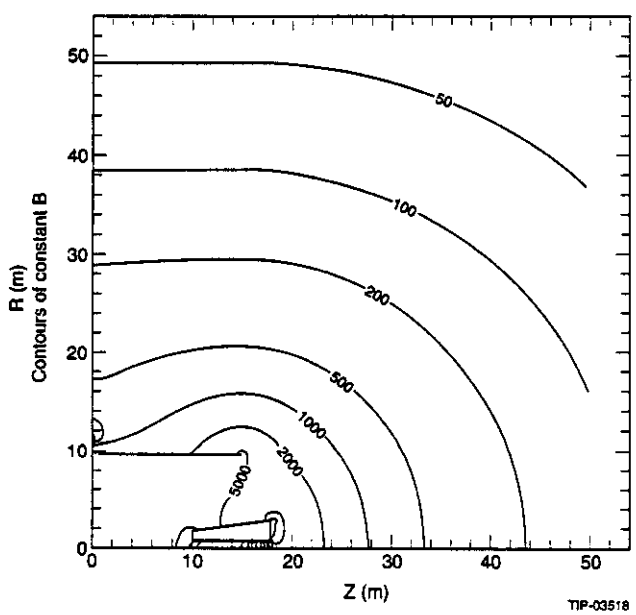

Figure 4-7 Contours of constant B out to 55 m labeled in gauss.

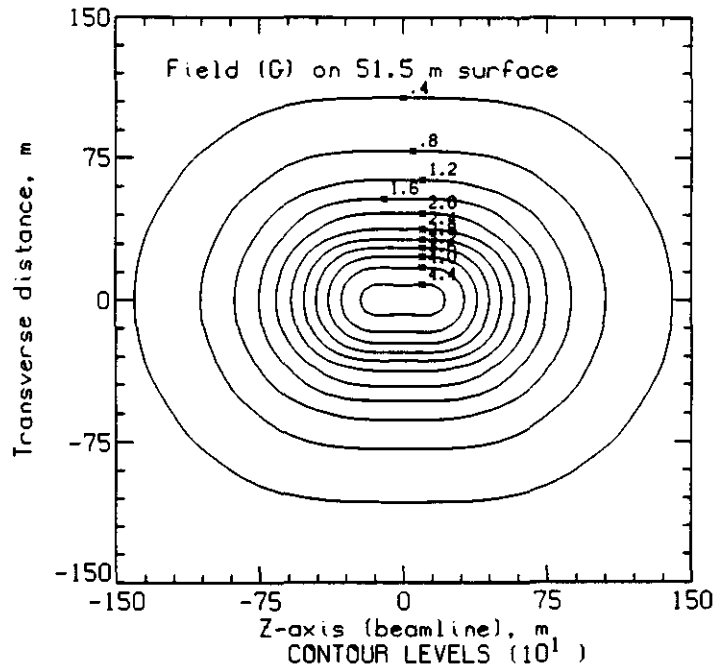

Figure 4-8 Contours of constant B on the surface labeled in gauss.

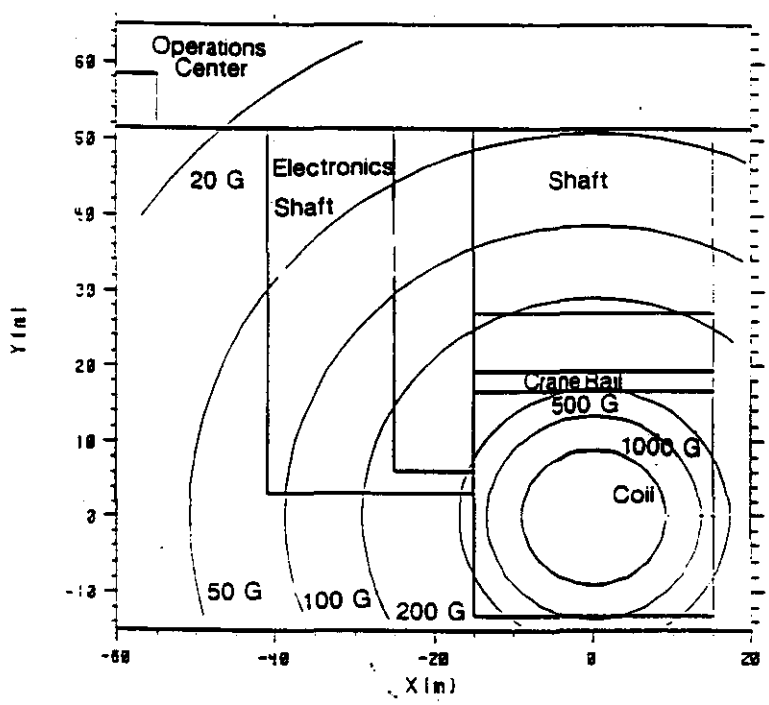

Figure 4-9 Contours of constant B in the midplane (labeled in gauss); contours (from the outside in) are at 20, 50, 100, 200, 500, and 1000 G. The innermost ring represents the coil at 9.5 m.

For μ momentum resolution, it is clear that the forward field shaper provides significant additional radial field component at small angles.

The homogeneity in the central tracker varies by less than 0.4%; this is shown explicitly in Figure 4-10.

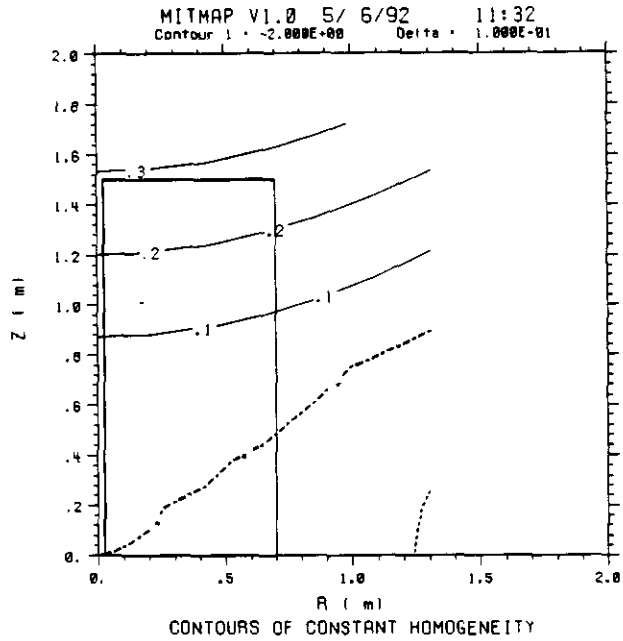

Figure 4-10 Plan view of the field homogeneity in percent in the central tracker volume (the contours are space at 0.1% intervals); the central tracker is delineated by heavy lines.

The momentum resolution for the baseline geometry is shown in Figure 4-11.

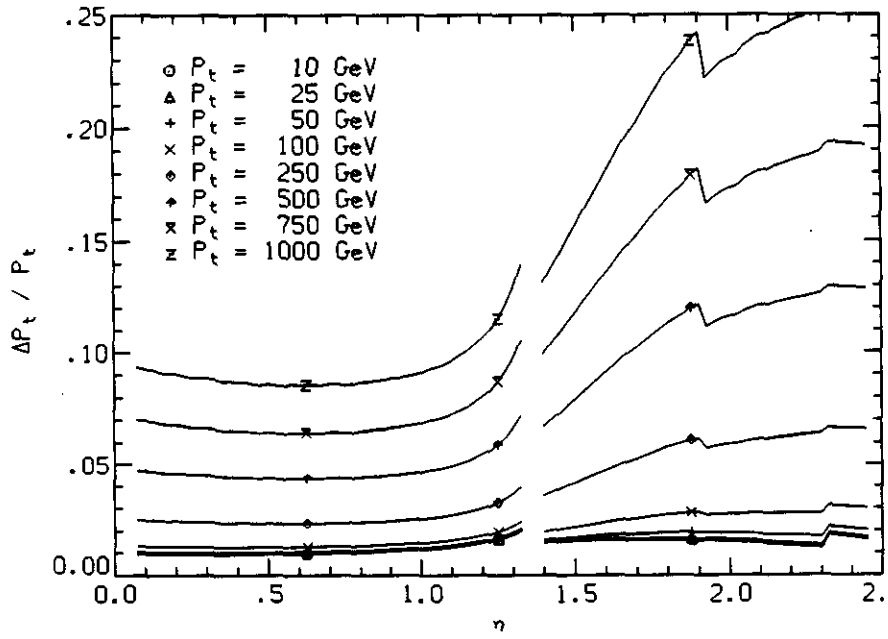

Figure 4-11 Momentum resolution versus pseudorapidity at constant p_t These curves correspond to the mean position of the endcap muon chambers. The gap at η 1.35 corresponds to the transition between the barrel and endcap chambers.

Fringe Field Environment

The decision not to provide a flux return to shield the fringe field is a common one for large magnet systems. Large air core electromagnets without flux returns are common in superconducting magnetic energy storage, MHD and MRI devices and in the large magnetic fusion machines such as JET, TFTR and MFTF. The cost of providing enough iron or a bucking solenoid to capture all of the flux lines of these machines is prohibitive. A less costly alternative is to shield only required volumes. The economics of this decision for GEM is influenced by the significant depth of the detector hall. The distance alone provides sufficient reduction of the fringe field on the surface that the effects can be easily managed[18].

The technology to operate satisfactorily in the fringe field of the detector hall and in the ancillary access shafts is well understood. There are several significant operational aspects to the fringe field environment created by a large high-intensity magnet. Forces and torques[19] act on ferromagnetic bodies and current carrying elements, electric currents may be induced by time varying fields (particularly in the case of a quench), and susceptible components may require shielding to operate properly.

Forces and Torques

If the volume of ferromagnetic material is small so that its influence on the local field is negligible, the body force density can be expressed as:

$$\vec{F} = (\vec{M} \cdot \vec{\nabla})\vec{B}$$

where $\vec{M}$ is the magnetization in the material (i.e., the dipole moment per unit volume) and $\vec{B}$ is a magnetic flux density. For a current carrying element with current $\vec{I}$, the force per unit length is the familiar $\vec{I} \times \vec{B}$. For ferromagnetic bodies, the force is most easily computed from the Maxwell stress tensor over a closed surface.

If the material magnetization vector is unable to align with the local magnetic field direction, the volume of magnetizable material will also experience a torque that tends to align the magnetization direction and the ambient field directions. This torque is given by:

$$\vec{T} = \vec{M} \times \vec{B}$$

If the material is saturated then the magnitude of the magnetization can be written as:

$$M = B_{sat} / \mu_0$$

where B_{sat} is the saturation flux density for the material and μ_0 is the permeability of free space. Typical values of the saturation flux density for iron range from 1.2 to 2.0 T.

On the basis of these equations, the body force density experienced by a small magnetized body that can rotate so that its magnetization direction is aligned with the ambient magnetic field can be written as:

$$\vec{F} = B_{sat} / \mu_0 (\vec{B} / |\vec{B}| \cdot \vec{\nabla})\vec{B}$$

[18] R. Woolley, SSC GEM Magnetic field Safety and Health Effects, GEM TN-91-19.
[19] MIT-GEM-EM-01 and MIT-GEM-EM-06

The magnitude and direction of the force density at various points in the experimental area are estimated using this equation and assuming a saturation flux density of 1.5 T.

Contours of constant body force density are shown overlaid on the hall in Figure 4-12. A small body of magnetizable material aligned with the local field line on one of these contours will experience that body force density shown. As can be seen, regions near the end of the coil and the end of flux concentrator experience the largest magnitude of the force and the direction is toward the coil or iron. For example, the crane rail above the magnet end sees a body force density of approximately $8\,kN\,m^{-3}$.

Figure 4-13 shows an end view of the magnet and hall at the midplane of the magnet system. Shown is an outline of the hall, the crane rail, the tunnel and electronics shaft and the operations center at the surface. Overlaid are contours of constant body force density. In this view all forces are directed radially inward toward the axis of the magnet represented by the circle. The vertical I-beams that support the crane rails see a maximum loading of 30 $kN\,m^{-3}$ with the load falling off as a function of vertical position to 5 $kN\,m^{-3}$.

Figure 4-14 shows the dipole-dipole force contours in a plane $Z = 18\,m$ which corresponds to the axial position of the end of the flux concentrator.

Induced currents – Time varying fields

Changes in the magnetic flux Φ threading a surface will induce an EMF and potentially drive currents. That is

$$EMF = d\Phi/dt$$

and this will give rise to eddy currents which will be manifest in conductive loops, coupled conductive plates, and circulating currents (induced dipoles). Responses of conducting material in the time varying field are to be evaluated.

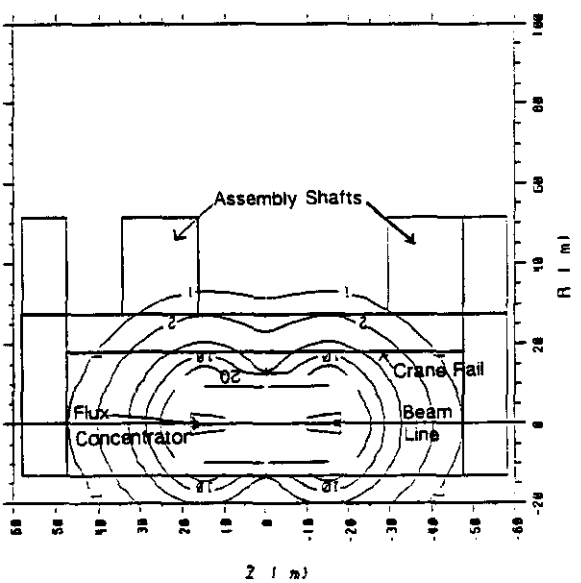

Figure 4-12 Contours of constant body force density in $kN\,m^{-3}$ for the baseline design for GEM. A small magnetizable body at any point along a contour will experience a body force density of the magnitude indicated.[20]

[20] For iron at 7800 kg m^{-3} 1 kN m^{-3} of body force density translates to an acceleration 0.013 galileo.

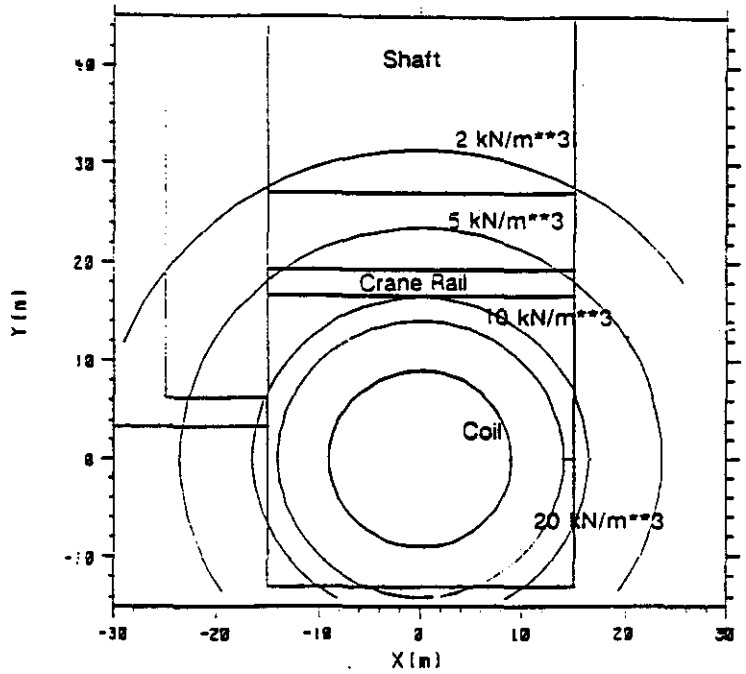

Figure 4-13 Contours of constant body force density in kN m^3 for the baseline design for GEM in the plane of the coil center at Z = 0. Contours at values of 2, 5, 10, 20, kNm^{-3} G are shown surrounding the superconducting coil at 9.5 m. The shaft and crane rails are also sketched in. A small magnetizable body at any point along a contour will experience a body force density of the magnitude indicated.

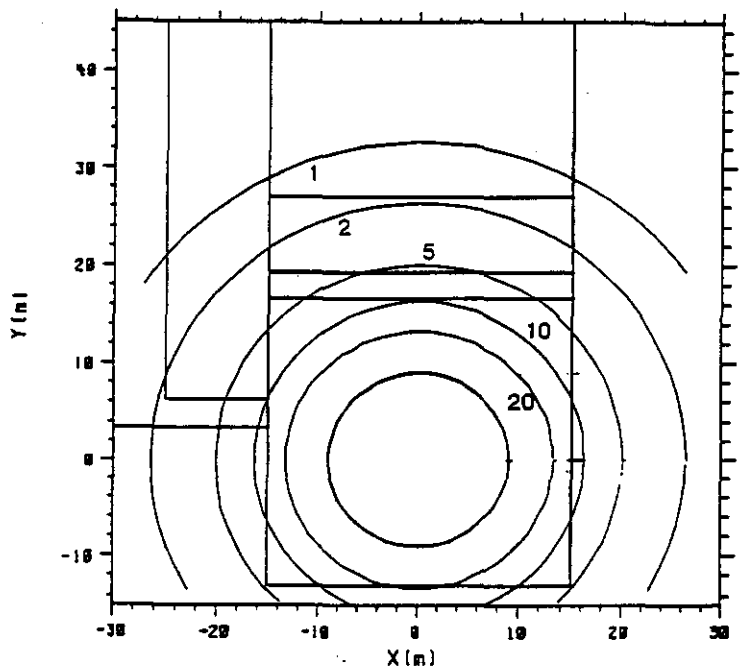

Figure 4-14 Contours of constant body force density in kN m^3 for the baseline design for GEM in the plane through the end of the flux concentrator at Z = 18 m. The superconducting coil is shown surrounded by circular contours at isopleths of 20, 10, 5, 2, and 1kNm^{-3}. The shaft and crane rails are also sketched in. A small magnetizable body at any point along a contour will experience a body force density of the magnitude indicated.

Shielding

The magnitude of the flux density in the Cable Electronic Shaft is between 50 and 200 G. The analyses indicate that if the shielding of this room is required to reduce the field to 50 gauss, about 300 tons of iron plate stock will be needed. The position and thickness of the shielding material is critical in minimizing material costs while achieving the 50 G design limit. The following shielding configuration with total mass 307 tons results in a peak field of 46 G:

Table 4-1 Shielding Requirements for Cable Electronics Shaft

Surface	Thickness, in
Easterly facing wall.	2.5
Westerly facing wall.	1
North and south facing walls	1
Cable Electronic Shaft bottom floor	2.5
Cable Electronic Shaft Room Level 1 Ceiling	2

The effect of the shielding material's characteristic B-H curve is that a reduction in the relative permeability from 4000 to 1708 (mild carbon steel) indicates a minor deterioration in the shielding effectiveness. In one configuration the peak field in the room increases from 46 G to 52 G, while the average Level 1 field increases from 28 G to 32 G. Tradeoffs between material cost and shielding effectiveness are yet to be done.

Table 4-2 shows the fringe field limits for typical susceptible electronic components developed for the High Field Test Facility (HFTF) and PHENIX experiments at LLNL[21]. Shielding these components in a few hundred gauss fields is common practice in the magnetic fusion experiments[22], [23],[24]. Shielding of the small susceptible volumes such as those of electronic components is typically carried out by completely enclosing the volume with close-fitting shields composed of an outer layer of steel and inner layers of highly permeable material if necessary.

Table 4-2 Typical electronic components tested for HFTF for the effect of DC magnetic fields on operation. (The worst orientation and lowest field values are quoted here.)

Component	Minimum Field (gauss)
Solenoid valve	1460
Linear power supply	750
1.5 Hp electric motor	640
Switching power supply	210
Octal relay	175
Turbomolecular pump	75
Computer monitor	20

[21] Personal correspondence with M. Chaplain, LLNL.

[22] Albrecht Mager, "Magnetic Shields", *IEEE Trans of Magnetics*, Vol. Mag 6, 1970, pp 67-75.

[23] *Neutral Beam Conceptual Design Proposals for ITER from Euratom, Japan, Soviet Union, United States*,,ITER-IL-HD-4-0-33, Nov 1990, pp 56-64.

[24] Thome and Tarrh, *MHD and Fusion Magnets Field and Force Design Concepts*, Wylie and Co., 1980, pp 69-96.

5.0 COLD MASS DESIGN DESCRIPTION

The cold mass for the GEM magnet consists of the modular coil windings, module-to-module joints, and the bobbins and end flanges which provide radial and axial structural support. Twelve identical superconducting solenoidal coil modules are each mechanically and electrically joined together to form symmetric coil halves. The cross section of the coil is shown together with the cryostat, the Forward Field Shaper and the muon chambers in Figure 5-1. Parameters for the cold mass subassemblies and related magnet parameters are summarized in Table 5.1.

The conductor is cable-in-conduit NbTi superconductor which is permeated with low-flow supercritical helium. Each coil half has its own set of current leads which operate nominally at 50,200 A. The center line radius of the windings is 9.5 m, and the active winding length for the twelve modules comprising one magnet half is 14.25 m. The coil modules are housed inside a cryostat which includes sets of inner and outer liquid nitrogen thermal shields and vacuum vessels. The cryostat components and current leads are described in other sections of this report.

The coil turns are formed against an aluminum bobbin which provides structural containment for the radial magnetic force. The axial magnetic loads accumulate through the turns to the end of each module, where they then are distributed, through the module end flanges, into a parallel load path comprised of the adjacent module winding and bobbin. The cumulative axial load of the modules is reacted through a set of axial cold mass supports which are connected between the structural end rings of the vacuum vessel and the bobbin interface structure located at the magnet half axial center. These load paths are discussed in more detail in the cold mass support analysis section of this report.

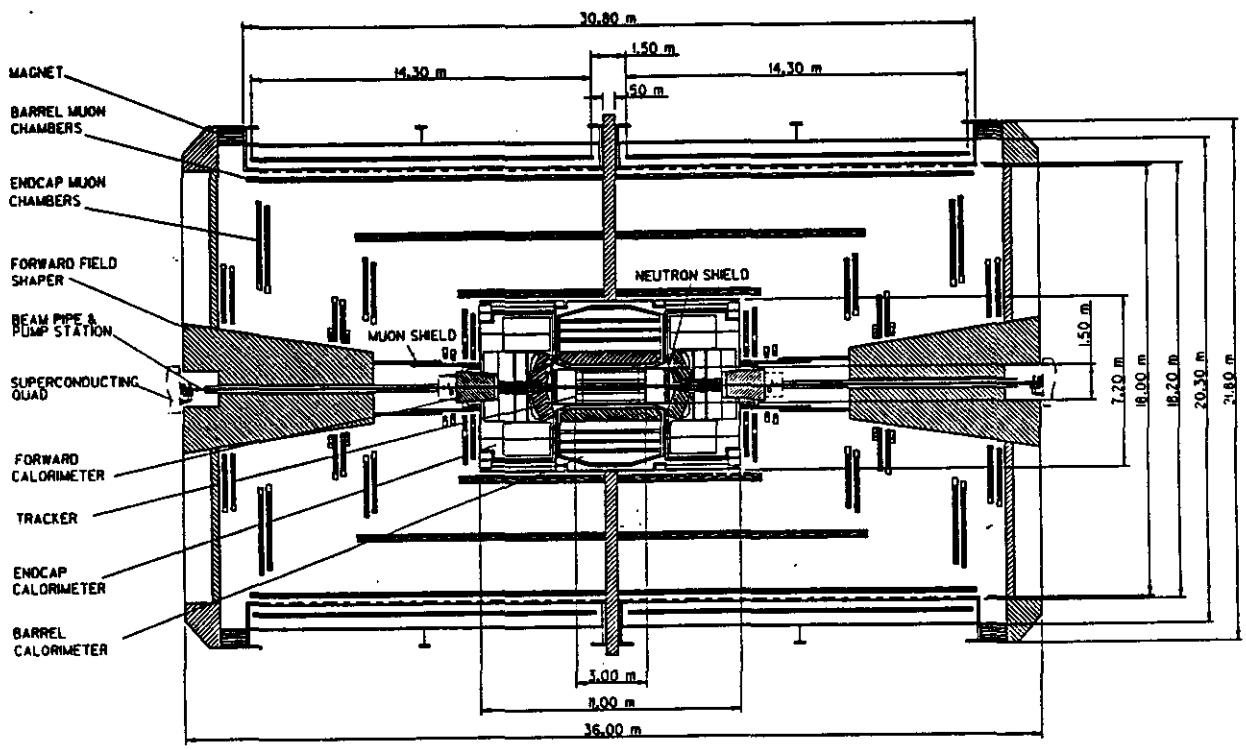

Figure 5-1 GEM Detector Layout

Table 5-1 Magnet Cold Mass Parameters

Mean radius of windings	9.5 m
Cold mass length end-to-end (per half)	14.25 m
Finished Conductor length (total)	27,219 m
Total mass of conductor and insulations (per half)	158,000 kg
Total mass cold 4 K structure (per half)	525,000 kg
Operating current	50,200 A
Stored energy	2.5 GJ
Inductance	1.98 H
Total number of turns	456
Inner radius conductor	9.466 m
Outer radius conductor	9.534 m
Inner radius of conductor inner ground wrap	9.456 m
Axial force on flux concentrator	12 MN
Axial force on conductor (per half)	52 MN
Bobbin inner radius	9.544 m
Bobbin outer radius	9.620 m

5.1 Coil Design

A cross section of the coil module is shown in Figure 5-2. The left end of the module cross-section shows the module-to-module interface typical throughout most of the azimuthal extent. The right end of the module cross-section shown in Figure 5-2 has been rotated into view from a region of the module-to-module interface where the electrical joint is made. The joint design is discussed in more detail in section 5.3.

Each coil module is comprised of 19 conductor turns which are wound in a single layer on the ID of the module bobbin and captured axially by the module-end compression flanges. The compression flange bolts are tightened during the module construction phase to apply an axial precompression to the coil stack. This precompression is sized to provide an initial axial winding displacement which is greater than that which would arise from the electromagnetic force generated by the radial component of the magnetic field. Axial precompression of the winding stack minimizes conductor motion when the magnet is powered.

A cross-section of the conductor is shown in Figure 5-3. It consists of 450 NbTi-copper/superconducting strands which are cabled in a 3x5x5x6 pattern. The copper-to-superconductor ratio is 3:1. The cable is compacted inside of a stainless steel tube leaving a helium void fraction of about 37%. The cable-in-conduit is enclosed in a continuous extrusion of aluminum which provides quench protection for the conductor. The conductor will be assembled in the factory in full-module finished lengths of 1134 m. The conductor design is discussed in more detail in Section 5.4.

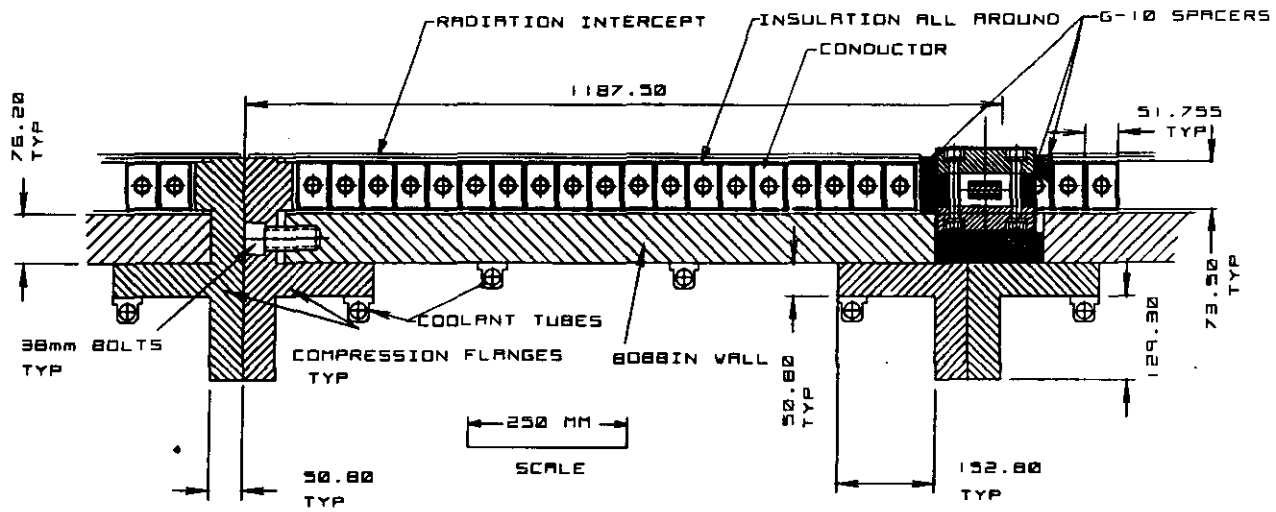

Fig 5.2 Coil Model Cross Section

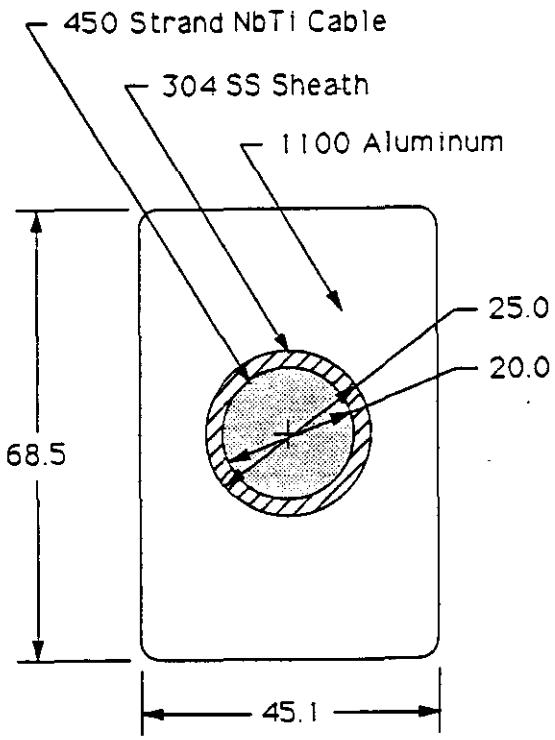

Fig 5-3 GEM Magnet Conductor

Each coil turn is wrapped with 3mm thick turn insulation. A layer of 6 mm ground insulation is applied at both the ID and OD of the winding. The ground insulation insulates the winding from the aluminum bobbin at the OD and from the radiation intercept at the ID. The radiation intercept receives the radiation heat load from

the warm bore of the magnet and shunts it around the winding, through the module-end compression flanges, and into the coolant tubes which contain helium from the thermosiphon loop. The bobbin is similarly cooled at its OD by coolant tubes with helium from the thermosiphon loop. The bobbin cooling removes the radiation heat load from the outside of the magnet and also those small amounts of heat which may be generated inside the bobbin due to small conductor motions relative to the bobbin.

A helium flow schematic for the cold mass is included as Figure 5-4. The present plan is to provide three separate cooling loops to the coil modules, one for the thermosiphon loop around the bobbin OD, one for the conductor conduit, and one for the joints. Alternative cooling schemes are being evaluated which could potentially reduce the number of loops and/or the number of insulating breaks required.

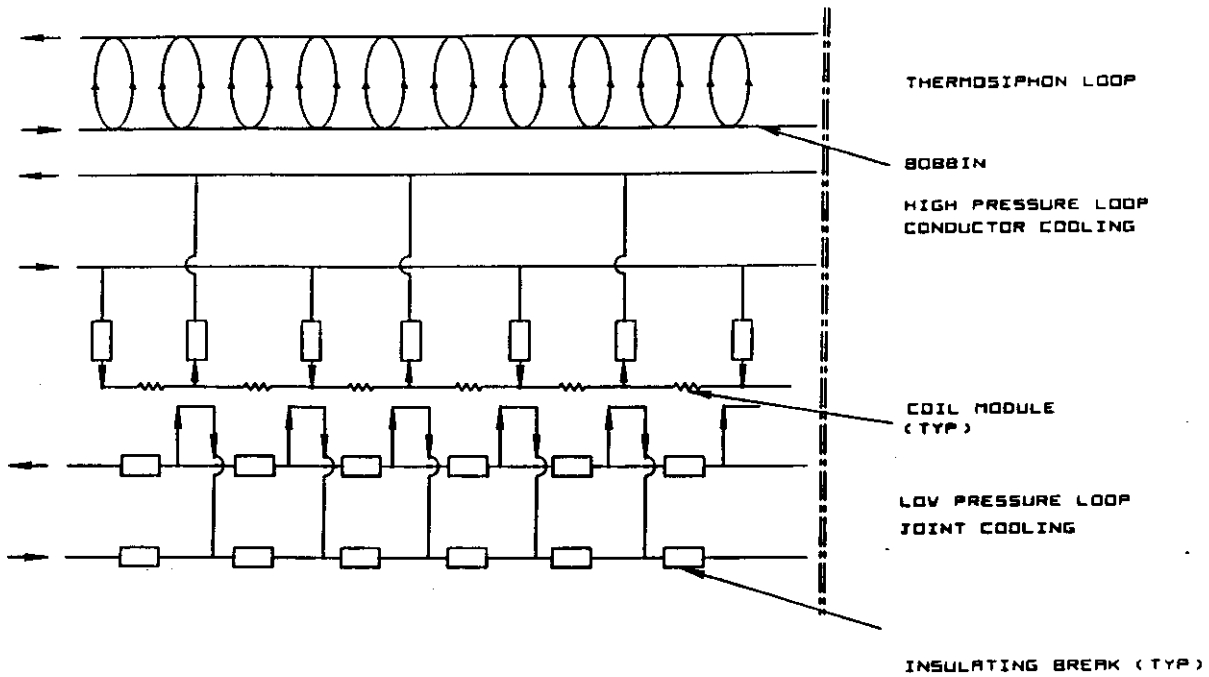

Fig 5-4 Magnetic Helium Flow Schematic

5.2 Module Structural Support

The bobbin provides support for the coil hoop stress, shares in carrying the cumulative axial load, provides indirect cooling to the winding through the thermosiphon loop, and shields the winding from the external thermal radiation load.

The coil bobbin for each module is made of 76 mm thick 6061-T6 aluminum plates which are rolled or stretch formed to a nominal inner radius of 9.544 m. In the baseline design each bobbin is comprised of four arced segments and four tensioning joints which also provide azimuthal insulating breaks. The tensioning joint provides a means of adjusting the bobbin diameter to the final coil diameter after winding, and of compressing the conductor in the hoop direction to ensure good radial contact between the winding and the bobbin. This adjustment is accomplished through a set of bolts whose ends are opposite-hand threaded, providing a turnbuckle action. The insulating breaks in the bobbin minimize the eddy current losses in the bobbin during magnet charge and discharge. Without insulating breaks, the eddy current heating in the bobbin during emergency discharge is sufficient to quench the coil. Recharging the magnet must then await cooldown which could take several days. For this reason, insulated bobbin quadrants are desirable. The insulated tensioning joint is shown in Figure 5-5. Alternate tensioning joint designs are under study.

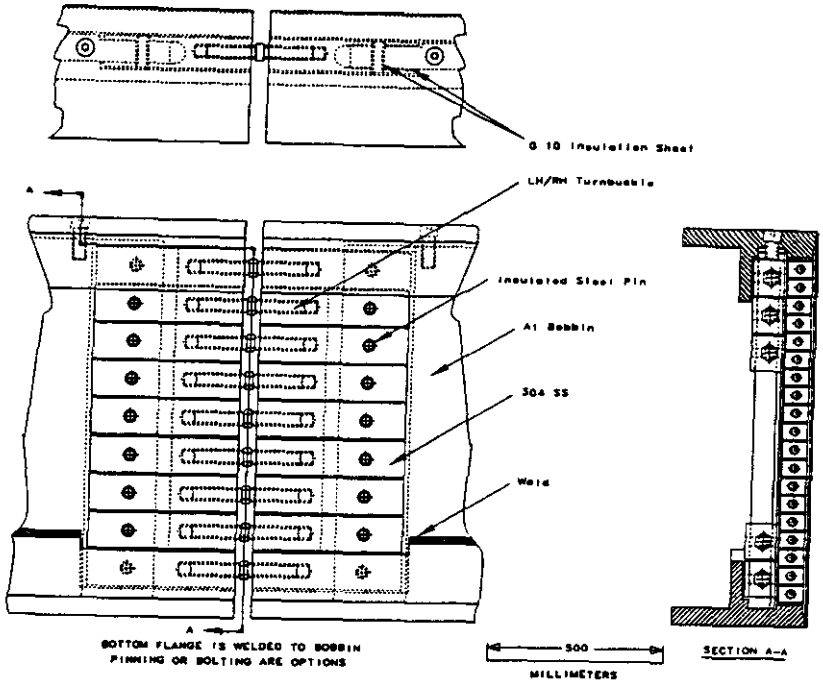

FIG 5-5 Insulated Bobbin Hoop Tensioning Joint

The axial compression flange segments are also of 6061-T6 as shown in Figure 5-6. These flanges induce the axial prestress in the winding, provide for module-to-module mechanical bolting, interface with the axial and radial tie rods which carry coil module loads to the vacuum vessel, and transmit heat from the radiation intercept at the ID of the winding to the thermosyphon system. The bolting ring in the compression flange segments have alternating bolt holes and slots so that adjacent module flanges are mated with a bolt through a hole/slot pair, enabling small azimuthal alignment adjustments between coil modules.

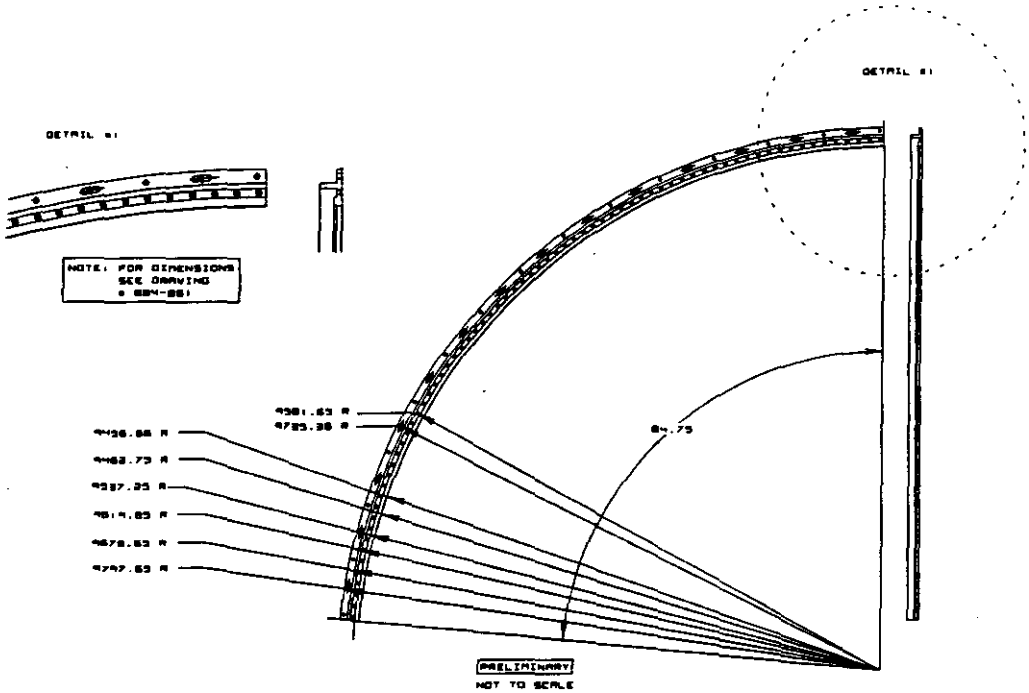

FIG 5-6 Axial Compression flange

Preliminary evaluations of the radial field component at the windings were made based initially on a simple model which does not include the smaller contribution to the radial field from the saturated iron of the forward field shaper. The forces on this solenoid act somewhat differently than a simple solenoid model would predict due to the space between conductor windings at module joints and between coil halves. The radial field at the winding due to current in the coil modules alone is shown in Figure 5.7. The radial field at the winding peaks at the end of the coil to a value of 1.1 T at the centroid of the last turn, but is also significant near the axial center of the magnet due to the 1.5 m spacing, centered about z=0, between the winding halves. The radial field crossed with the azimuthal current produces axial forces on the winding. The accumulation of these axial forces within each module is shown in Figure 5-8, assuming the bobbin and end flanges are infinitely stiff, meaning all of the load is removed between modules by the structure. This is not actually the case, but the assumption enables an estimate of the magnitude of the axial precompression that must be applied to each winding to offset the axial electromagnetic load and minimize conductor motion. Maximum precompression is required in the outside end module near z=15 m where 27 MN of electromagnetic load accumulates. This corresponds to 452,000 N/m (2600 lb/in) of bolt load around the circumference.

The same simplified model was used to estimate the hoop load on the conductor. The axial field on the windings generates the highest total hoop force in the third coil module near z=3.6 m of 0.365 T. This generates a local hoop force on one conductor of 174,000 N (39,500 lb). The net area available to carry this hoop load is the conductor width (45.1 mm) times the conductor plus bobbin thickness (68.5 mm +76.2 mm) or 6.53 $X10^{-3}$ m^2 (10.1 in^2). The average hoop stress in the conductor plus bobbin is then 26.7 MPa (3900 psi). More detailed finite element calculations have been completed and the results are summarized in the cold mass structural analysis section.

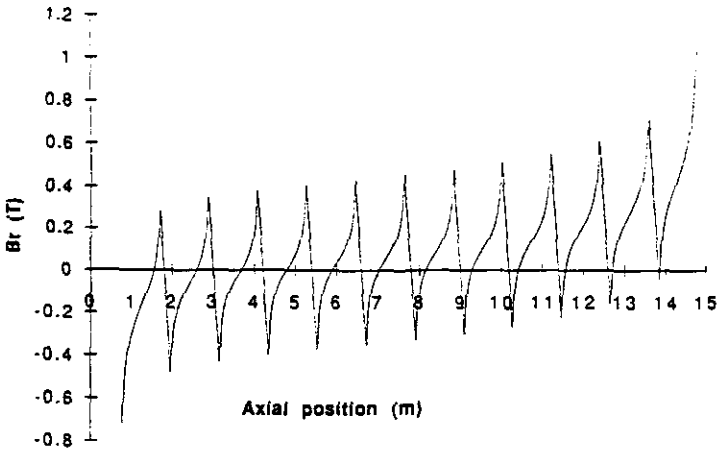

Fig 5-7 Radial Field Component at the Winding Due to Coil Alone

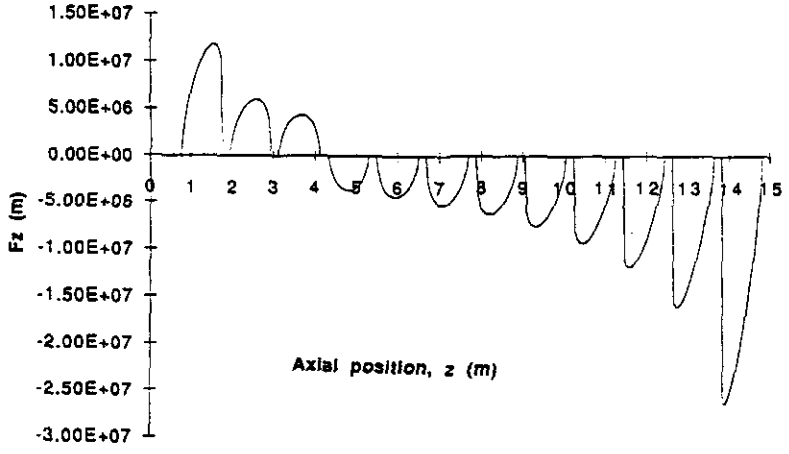

Fig 5-8: Cumulative Axial Force within Each Coil Module Due to Coil Alone (Assumes Infinitely Stiff Flange/Bobbin)

5.3 Coil Joints

The baseline joint design provides a low resistance electrical interface between two mating conductor ends on adjacent coil modules. There are a total of 11 module-to-module joints and 2 end-module-to-lead joints per magnet half. The joint halves are fabricated, attached to the conductor ends of each coil module and leak tested in the conductor assembly factory, remote from the winding site. This enables a complete coil module length of conductor, with factory preterminated ends, to be shipped to the coil winding facility on site, and eliminates the need to make helium-tight welds to the conductor conduit in the field. During the magnet assembly process on site, the mating joint halves are simply soldered and clamped together. Helium tubing from the cryogenic system is welded to pre-fitted pipe nipples on the joint halves. Each joint is separately cooled. The conduit of each module conductor supplies helium at one end of the 1134 m length and is vented at the other. The fittings are integral to the joint design and are also leak tested at the factory.

The joint is depicted in Figures 5-9 through 5-12. During joint fabrication, the cable-in-conduit conductor end is machined to accept the joint components. The stainless steel conduit is cut away from the superconducting cable. A stainless steel reinforcing block and a transition block, prefitted with a pipe nipple for conduit helium supply or venting, is then slipped over the cable and welded to the conduit (see Figure 5-9). A length of copper tubing is pulled over the cable and welded to the stainless steel transition block. The cable is rolled flat inside the copper tube and filled with solder. A copper block, shown in Figure 5-10, is machined with cooling grooves which are sealed with an electron-beam welded copper plate. Pipe nipples, which communicate with the cooling grooves in the copper block through drilled holes, are welded to the side of the copper block and leak tested. The conductor end shown in Figure 5-9 is then soldered into the machined groove in the copper block. A copper cover block is then bolted over the transition block. All helium joints are then leak tested, and the factory preassembly is complete.

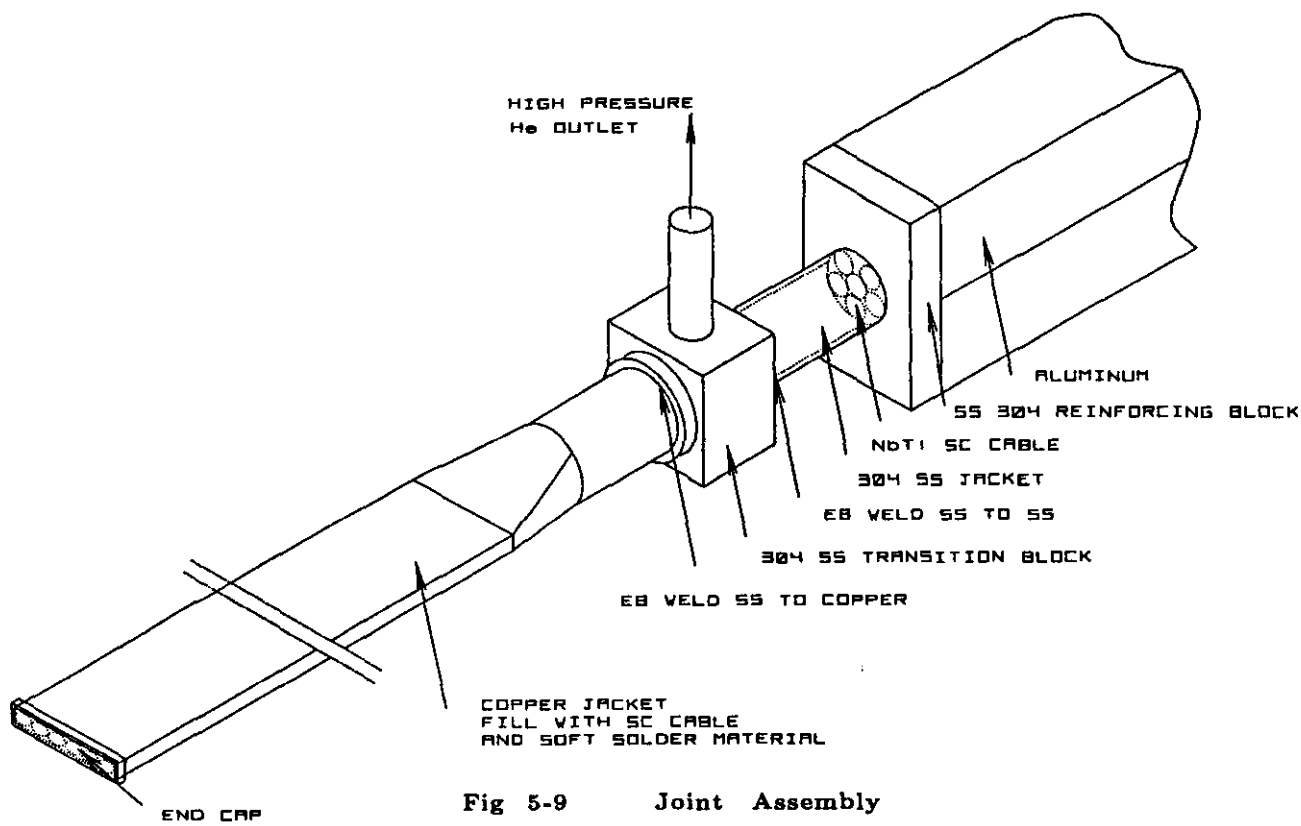

Fig 5-9 Joint Assembly

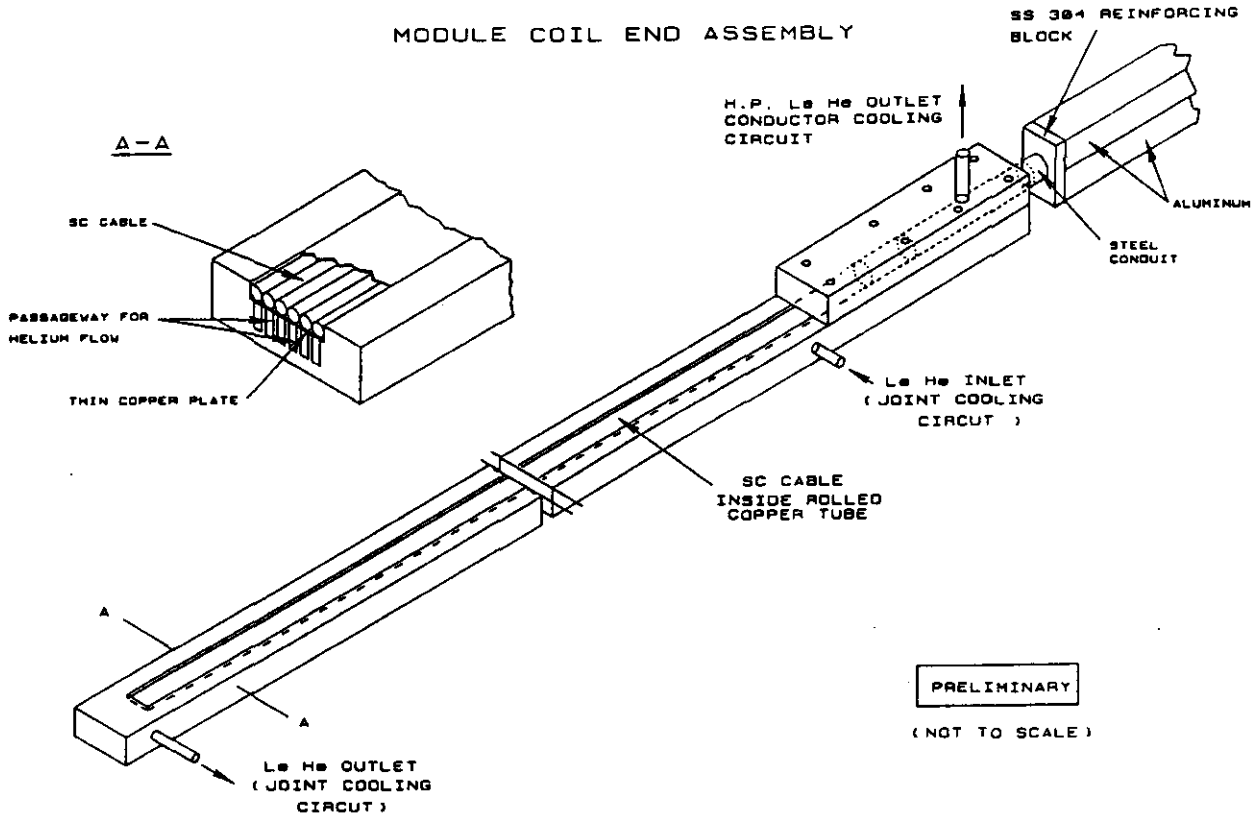

Fig 5-10 Joint half. The aluminum clamp bridging the two coil sections is not shown.

After module winding on site, the joint half is lapped with and soldered to its mate from the adjacent coil module, and the entire assembly is bolted together with aluminum clamping plates. The clamped joint cross-section is shown in Figure 5-11. The aluminum clamping plates are welded to the aluminum sheath on either side of the joint. This passes the hoop tension from module to module without stressing the joints. The amount of overlap in the joint is designed to accommodate the small differences in position of the joint from one module to the next, so all joints will be nominally in the same azimuthal location on the assembled magnet. An isometric view of the joint region between two coil modules is shown in Figure 5-12. The joints are designed to be fully cryostable and are based on a similar proven design which was part of the US Demonstration Poloidal Coil (DPC) program. The US DPC joints underwent stringent testing which included field ramp rates of 5 T/s without quenching.

GEM CONNECTION

PRELIMINARY

NOT TO SCALE

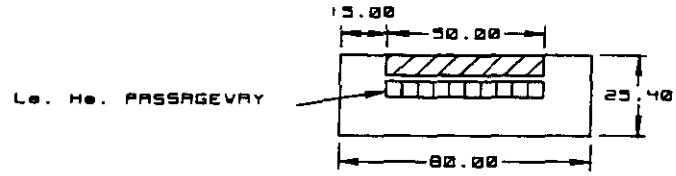

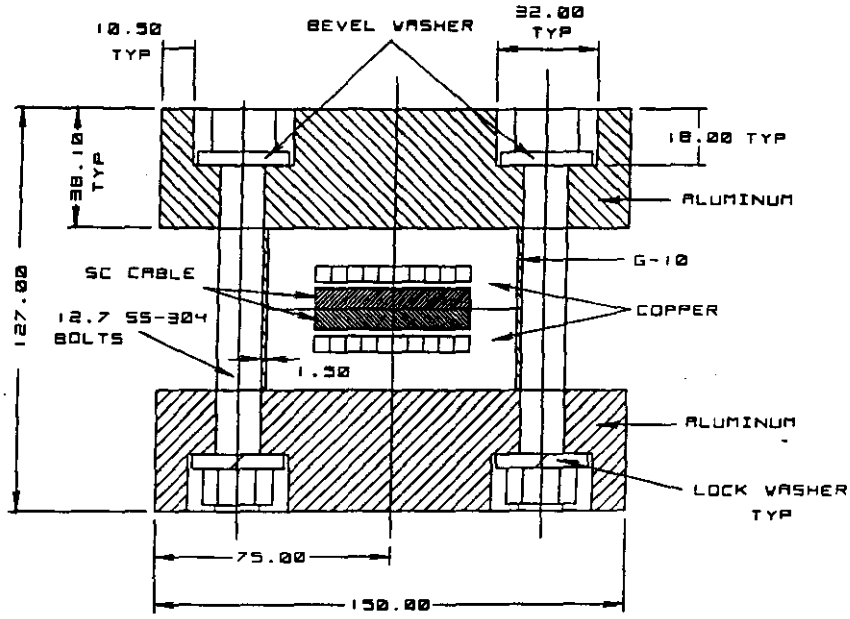

Fig 5-11 Joint Clamp

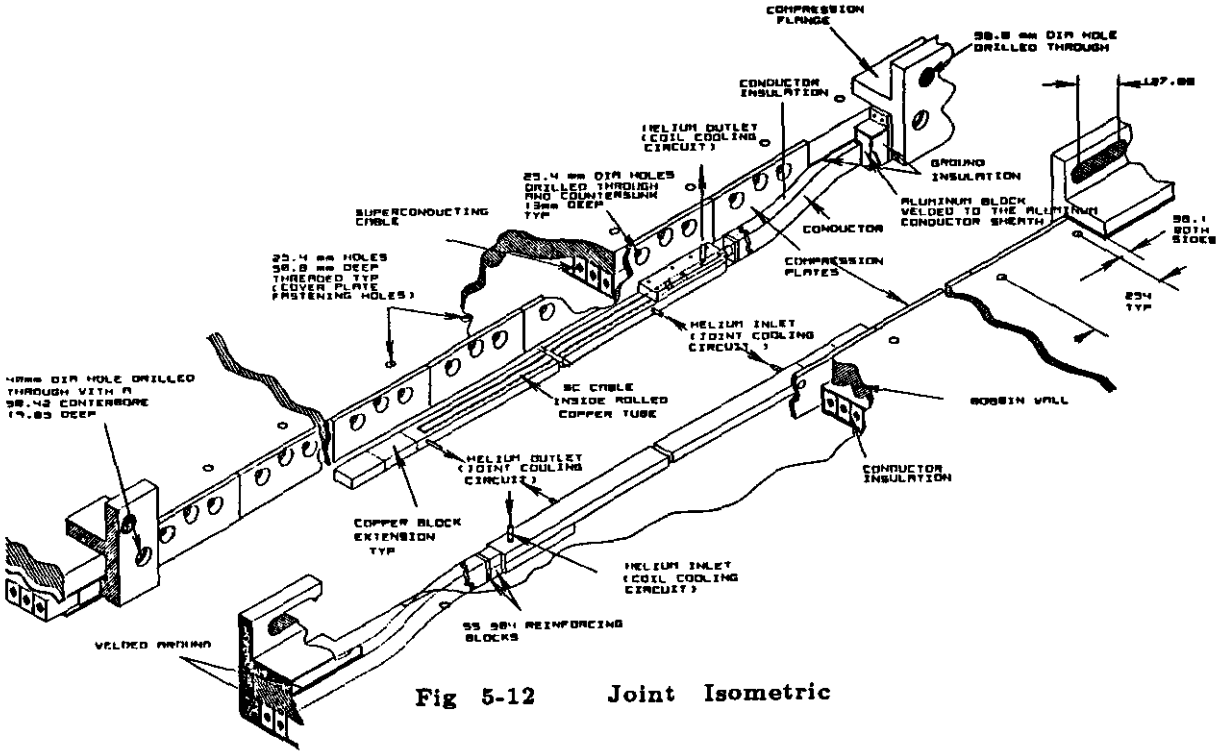

Fig 5-12 Joint Isometric

5.4 Conductor Design & Manufacture

Introduction

The GEM Detector Magnet must be designed to operate with the highest level of stability and reliability to insure maximum availability of the detector system. This requires a conservative conductor and coil design which allows for substantial operating margins, yet one that can be manufactured and operated with reasonable costs. A conductor and coil design based on the cable-in-conduit (CIC) conductor concept fulfills these requirements and therefore was chosen for the GEM Magnet. This type of conductor has had the benefit of many years of development by the U.S. and international magnetic fusion programs. This conductor type will both simplify the on-site winding required for GEM and minimize the risks of operating instabilities. It is specifically designed to maximize the use of proven manufacturing processes, tooling and operating experience gained from previous CIC conductors. The selection of this conductor was based on detailed comparative assessment and collaboration review of several options.

Conductor Requirements

The conductor must provide a uniform DC magnetic field in the bore of an extremely large, thin solenoid. Although the nominal central field requirement of 0.8T and the resulting electromagnetic loads are not high, the huge dimensions of the magnet require on-site coil winding and magnet assembly. This requires a robust conductor and coil design which minimize the risk inherent in the on site construction of such enormous winding and is consistent with the level of cleanliness and assembly tolerances achievable in the anticipated fabrication facility.

The main dimensional requirements of the coil are given in Table 5-1. The main operating requirements are summarized in Table 5-2.

Table 5-2 Conductor Requirements

Central Field (T)	0.8
Nominal Field at Winding (T)	1.1
Peak Field at Winding (T)	1.6
Operating Temperature (K)	4.5
Operating Current (kA)	52
Maximum Hotspot Temp. (K)	100
Maximum Dump Voltage to ground (V)	500
Number Charge/Discharge Cycles	200
Charging Time (Hr)	8
Maximum Number of Quenches	100
Number Thermal Cycles RT/4.5	100

Conductor Description

The conductor is based on a cable-in-conduit design using strands of multifilamentary NbTi-copper composite wires in a multistage cable enclosed by a stainless steel conduit. This circular CIC is surrounded by a rectangular sheath of aluminum. In this design the stabilizer function for fast transient stability is provided by the local copper in the multifilamentary strand, while the aluminum sheath provides the low resistance current shunt for hotspot protection during a quench. The conductor, which is sized for a nominal operating current of 52kA, is shown in Fig. 5-3, and the conductor configuration is summarized in Table 5-3. The main conductor parameters are summarized in Table 5-4.

Table 5-3 Conductor Configuration

Strand
Diameter = 0.73 mm
Cu:SC = 3:1
Superconductor = NbTi
RRR = 150-200
Filament size: <40 μm
Twist pitch = 25 mm or less
Total length = 13,000 km
Total weight = 45,400 kg

Cable
4 Stage, twisted
3 x 5 x 5 x 6
450 strands
0.05 mm x 11 mm wide type 304 SS tape - spiral wrap/50% overlaps

Stage	Element	Strands	Twist Pitch (mm)	Diameter (mm)
1	Triplet	3	50	1.46
2	(5 x 3)	15	100	3.6
3	(5 x 5 x 3)	45	200	8.05
4	(6 x 5 x 5 x 3)	450	400	19.7

Total winding length = 24 x 1134 m piece length (27.2 km)
Cable weight/piece = 1890 kg

Conduit
Material = Type 304 L stainless steel
ID = 20.0 mm
OD = 25.0 mm
Manufactured by continuous seam weld by TIG on tube-mill or by butt welding seamless tube sections.
Conduit weight = 42,400 kg total = 1770 kg/conductor length

Sheath
Material = Type 1100 Aluminum
RRR = 14 minimum after assembly
Dimensions = 45.1 mm x 68.5 mm in two halves (2 x 22.55 mm)
Manufactured by continuous conform extrusion
Piece length = 2 x 1134 m/coil
Total length = 2 x 27,200 m
Total weight = 190,000 kg, 7920 / module

Table 5-4 Conductor Parameters

Sheath Material	Aluminum Alloy 1100
RRR	14
Hole Diameter	25.0
Width W_o (mm)	45.10
Height H_o (mm)	68.50
Corner Radii R_o (mm)	3.0
Conduit Material	Type 304 L SS
Outer Diameter (mm)	25.0
Inner Diameter (mm)	20.0
Cable	
Cable Pattern	3x5x5x6
Strand Diameter D_s (mm)	0.73
Cu:Non-Cu	3
Number strands	450
Cabling Factor	1.05
I_{op}	50,200
Strand Area (mm^2)*	188.3
Copper Area (mm^2)*	141.3
Superconductor Area (mm^2)*	47.1
Wetted Perimeter (mm)	860.0
Cabling Factor*Strand Area	197.8
Helium Area (mm^2)	116.4
Cable Space Area (mm^2)	314.2
Void Fraction	0.371
Overall Cond. Area (mm^2)	3081.6
Al Sheath Area (mm^2)	2590.8
SS Conduit Area (mm^2)	176.7
Hydraulic Diameter (mm)	0.541
Fraction of Al	0.841
Fraction of SS	0.057
Fraction of Helium	0.038
Fraction of Cable	0.064
Fraction of Copper	0.046
Fraction of NbTi	0.015
$J_{superconductor}$ (A/mm^2)	1066
J_{copper} (A/mm^2)	355
J_{strand} (A/mm^2)	267
$J_{aluminum}$ (A/mm^2)	19.38
$J_{cable\ space}$ (A/mm^2)	159.8
$J_{conductor}$ (A/mm^2)	16.3

* Area normal to strand cross section

The magnet is composed of two coil halves with two independent sets of current leads. There are 12 coil modules per magnet half, 24 in total. At a coil diameter of 19 m with 19 turns per coil module, conductor must be produced in finished lengths of 1134 m. The 24 coil modules will be joined electrically and mechanically with resistive joints and helium from the conductor in each module will be vented at these joint locations. The baseline design calls for the joints to be cooled with an independent supercritical helium circuit, but other options are also being explored. The number of modules and unit conductor length is determined primarily by conductor manufacturing considerations which are discussed later.

Conductor Performance

The conductor is designed to operate at 50.2 kA generating a central field of 0.8 T. The average magnetic field over most of the conductor is approximately 1.1 T, but the field peaks up at the ends of the coil halves to a maximum of 1.6 T. The performance calculations were made for a magnetic field of 1.1 T. Performance at a peak field of 1.6 T can be handled in several ways. One is to increase the NbTi content in the strand and slightly lower the overall current density. This will maintain good margins at the peak field turns, but it will also result in an inefficient use of superconductor in the bulk of the coil where the field is much lower. An alternative is to use two slightly different strands, the one described above for the bulk of the coil and a higher field strand at the coil end modules. The baseline permits somewhat smaller stability margins near the coil ends. The final decision will be based on detailed credible fault analysis and performance test data.

DC Operation

The coil is designed to operate with stagnant supercritical helium at a nominal temperature of 4.5 K and a pressure of 3.5 atm. Since the coil is operated DC the only heat loads are expected to be thermal radiation and conduction. These heat loads are removed continuously by conduction to the aluminum coil bobbin which is in turn cooled by the thermal-siphon loop. There is no need to flow the helium through the cable space to enhance stability, even during coil charge or discharge. This would only result in increased pumping losses without significant increase in stability margin.

The nominal DC operating margins on critical current and current sharing temperature are quite large, e.g. $I/I_C = 0.225$ with a temperature margin of 3.4 K, as illustrated in Fig. 5-13. The superconducting strand requires a critical current carrying capability which is easily achievable by standard materials and wire production methods.

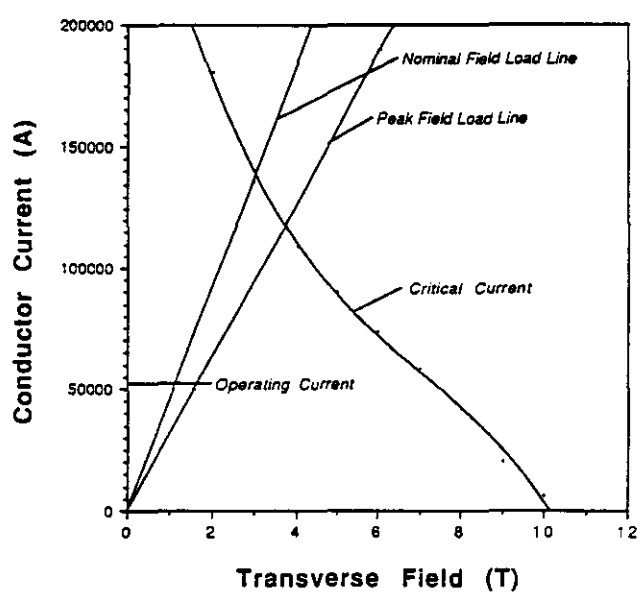

Fig. 5-13 Conductor critical current versus magnetic field and operating point.

Stability

The CIC conductor is well known for its excellent stability to sudden disturbances. Coils made with CIC conductors are distinguished by the lack of training often found in coils made with other conductor types. This high stability is due to a) the high heat capacity of the helium which is in intimate contact with the superconducting wires, and b) the very large heat transfer surface area from the wire to the helium. The most likely source of disturbance in the GEM magnet is due to some mechanical event occurring external to the CIC. In this case the superconducting strands are buffered from this disturbance energy by the helium in the conduit. The energy margin then is given by the enthalpy of the helium and the wire between the operating temperature of 4.5 K and the current sharing temperature. This is dominated by the helium enthalpy which is 1-2 orders of magnitude greater than all the other conductor components. For such an external perturbation event, the time scale is practically irrelevant since all the helium must be brought up to the current sharing temperature before a quench will occur.

Other types of disturbances internal to the cable can also occur, although these are very much less likely in the GEM operation. One of these could be AC loss, but only during coil charge or discharge. Since the nominal charge time is 8 hours, the loss energy will be removed on a quasi-steady state basis by the thermal-siphon loop. Another possible disturbance source could be sudden wire motion within the cable. Measurements of the mechanical hysteresis have been performed at 4.2 K on a large, similar cable. Those results[25] indicate that, even if all this energy was deposited suddenly in the cable, the energy margin is at least one order of magnitude greater.

For internal disturbances the stability margin is defined as the largest sudden energy deposition to the conductor from which it can still recover the superconducting state. The stability margin is not necessarily equal to the enthalpy margin of the helium because the helium is only effective if the energy dissipated directly in the cable can be effectively transferred to the fluid. This depends on the power balance between heat generation, due primarily to Joule heating in the strand, and the convective heat flux to the supercritical helium. The GEM conductor is designed to insure that this energy balance is always satisfied, i.e., at normal operating conditions the helium enthalpy is used to maximum advantage. This is accomplished by insuring that the limiting current between being well-cooled or ill-cooled is above the operating current. The limiting current is defined as I_{lim} where,

$$I_{\lim} = \sqrt{\frac{hpA_{cu}(T_c - T_b)}{\rho_{cu}}}$$

where,

h = heat transfer coefficient (W/m^2-K)
p = cooled perimeter (m)
A_{cu} = area of copper stabilizer in cable
ρ_{cu} = copper stabilizer resistivity (Ω-m)
T_c = critical temperature (K)
T_b = initial helium temperature (K).

The stability results for the main coil modules are summarized as follows:

Energy margin for external disturbances	315 J/m
Energy margin for internal disturbances	250 J/m.

By comparison the energy margins of indirectly cooled, high purity aluminum conductors typical of those used for other large solenoidal detector magnets (eg., CDF, ALEPH, DELPHI) is between one and two orders of magnitude

[25] Bruzzone, P., et.al. "Mechanical Properties of the Prototype Cable-in-Conduit conductors for NET", IEEE Transactions on Magnetics, Vol. 28, No.1, January 1992.

lower than that of the CIC. This implies that conductor motion of ~ 1 mm would quench the indirectly cooled magnet. There is a reasonable risk of such mechanical imperfection in the "on-site" wound coils of the proportions required for GEM.

The joints between the coil modules have been designed to be cryostable. This is done primarily by using large copper blocks with integral cooling channels to lower the Joule heating below the steady state heat flux. With a cryostable joint design, this normally resistive portion of the coil circuit is not a weak link , but actually more stable than the bulk of the coil. This can be achieved with a moderate flow of 0.5 g/s of supercritical helium at 4.5 K to independently remove the 1.25 W generated at each joint.

Strand

The superconducting strand that has been specified requires no special development in terms of the required critical current, superconductor or copper content. The requirements on the GEM conductor stands are significantly less severe than on those of the SSC dipole strands. The production of such a wire is straightforward, and thus the full production run should require only a good quality assurance program and acceptance testing. Manufacture of this wire by a vendor may be divided into material procurement, material outside processing, material inside processing, and QC steps. This scheme is similar to that of the conductor for the dipole and other magnets of the SSC. The quality of the wire will be gauged throughout the manufacturing process. Documentation will be supplied and signed off at every inspection point. Vendor audits will be at specific points in the manufacturing program.

Quench

The GEM magnet should not quench under any conceivable operating conditions, however allowances must be made for safe removal of the coil energy if any unforeseen event occurs. The coil modules must be simultaneously and continuously monitored by compensated voltage taps whenever the coil is energized, no matter the current level. Quenches are detected by use of a suitable quench voltage monitoring and triggering circuit which senses growing normal regions in the coil and triggers the dump circuit. This requires opening a room temperature switch to insert a large dump resistor into the circuit to safely dissipate the coil energy at room temperature and above. The dump time constants are determined by the L/R time constant of the coil-resistor circuit. Values are chosen consistent with the maximum allowable voltage-to-ground in the coil.

A series of calculations have been performed for the case of a coil quench in order to choose the appropriate dimensions of the aluminum sheath for quench protection, and to determine the time dependent and maximum values of the conductor temperature and helium temperature and pressure. All calculations were made based on the following parameters:

Coil Energy (GJ)	2.5
Coil Inductance (H)	1.98
Maximum Allowable Hot Spot Temperature (K)	100
Maximum Allowable Coil Voltage (V) to ground	500
Quench Detection and Dump Delay Time (s)	1.0

These numbers result in a dump circuit time constant of 99.6 seconds.

Hot Spot

The hot spot calculation is based on the assumption that the hottest position in the coil is the center of the normal zone where the quench began. This is because Joule heating occurs for the longest time at this location, and because it is assumed that there is no heat removed from this region either by conduction along the conductor or to adjacent turns and structure, or by convection to a flowing helium stream. This is a worst case calculation. For this

basically adiabatic calculation it is further assumed that current is shared between the cable and the aluminum sheath. The temperature dependent specific heats of copper, superconductor, helium, steel and aluminum are all included. For the CIC and aluminum sheath dimensions and properties described in this report the maximum temperature is 100 K for both the helium and conductor. The pressure will increase, at constant density, to 445 atm (6700 psi) at this temperature. Some energy will be transferred by thermal conduction and electro-magnetic induction to the coil bobbin which will result in a further reduction of the hot spot temperature.

One-Dimensional Quench

The time-dependent propagation of the quench was studied in one dimension by use of the computer code SARUMAN. This code was also developed by L. Bottura of the NET Team. The code is capable of solving the 3-dimensional problem, but this was deemed not necessary for purposes of the conceptual design. The result of this analysis for a quench that is located in the center of the 1140 m coil module and initially 20 m long (about a third of a turn) indicated a maximum conductor temperature of 100 K and a maximum pressure of 340 atm (5000 psi). The final temperature was not significantly different than for the hot spot case because the heat removed from the normal zone by conduction and convection, was compensated by the increase in temperature due to less helium mass remaining in the center of the conductor. The reduction of the maximum helium pressure was also due to the significant helium mass flux at the coil vents.

Both of these calculations indicate that the coil temperature will not exceed the maximum value of 100 K. The maximum pressure that can be achieved is 445 atm, even if the coil vents are closed off. This is quite safe for the steel conduit stresses. The actual peak temperature and pressures will be significantly less than these maxima when account is taken for the current and energy transfer to the bobbin during the coil discharge. Further analysis will include three-dimensional effects and parametric variations of the initial normal zone distribution.

Cable Manufacture

The cable will be made up by twisting wires in the cabling pattern as defined in Table 5-3. This pattern is rather standard and superconducting cables of similar size (i.e. the 486 strand Westinghouse LCP cable and the 225 strand U.S.-DPC cable) have been produced in multiple kilometer lengths.

The wire will be supplied in spooled lengths to the cabling facility in the longest possible lengths. These will be mapped and cabled in the most efficient manner into a fully-transposed 3x5x5x6 configuration, starting from triplets composed of three strands, to yield a 450-strand cable of 20 mm diameter.

The first operation of the cabling phase will be to twist the triplets in a direction that is the same as the strand twist to obtain the best wire lays. All other cabling operations will likewise proceed in the same twist direction of the triplets. The second operation will be to twist a group of five triplets to make 15-strand subcables; the third to twist a group of five 15-strand subcables to make 75-strand subcables; the last to twist a group of six 75-strand subcables to make the final 450-strand cable. The cable will be wrapped with a thin stainless steel tape, with 50% overlays, to prevent "bird caging" of the strands and possible interference with the weld arc in the tube mill operation. If deemed necessary, the cable will be ultrasonically cleaned in a bath of solvent to remove lubricants or contamination from the cabling process.

It should be noted that the 1134 m cabled lengths needed for the GEM magnet weigh approximately 1890 kg and therefore the last subcable stage exceeds the spool capacity of most cabling machines. Preliminary efforts have located a final-stage machine with at least six 30" (762 mm) diameter spools that are capable of holding the 75-strand subcables.

Cable-in-Conduit Manufacture

Fabrication of the GEM conductor conduit could be essentially the same as the process used for the Westinghouse Large Coil Program conductor and more recently for the US - Demonstration Poloidal Coil Conductor[26],[27],[28]. Alternatively, the cable could be pulled through an 1150 m length of conduit formed by butt welding lengths of seamless tube. Only the tube mill process will be described here. In this process, the conduit will be placed around the cable using a tube mill. The function of the mill is to shape a flat strip into a tube, autogenously weld the seam, and compact the tube to final dimensions. Seam welding is a critical process since the conduit is the primary mechanical structure and helium cryostat. Therefore, the tube mill operator will be qualified to the standards of the ASME Boiler and Pressure Vessel Code, Section 9. Welding procedure specifications will be developed according to the code for all welds and will be strictly adhered to during the entire conduit fabrication process. Weld quality will be checked by direct visual, fiber-optic visual, eddy current, and, if necessary, dye penetrant inspection. Helium leak tests both at room temperature and at 77 K will be performed on each finished length.

A modified tube mill and tooling now exist to form an 80.8 mm wide x 2.5 mm thick strip into a circular tube into which a cable can be placed. The inner diameter of the tube will be 22.6 mm at the weld box, yielding a gap between the tube inner diameter and cable outer diameter of 22.6 - 20 = 2.6 mm. This is sufficient to protect both the weld arc from contamination and the cable from heating damage. The gap is closed after weld cooling in the compaction section of the mill.

Since dwell time in the arc is short and multiple weld passes are not required, the use of type 304 L stainless steel is recommended for the conduit. This is a very good, widely available, low cost allow with a history of successful use at cryogenic temperatures and a relatively large data base of mechanical and physical properties. Should it be determined that higher yield strength is needed, a switch to the nitrogen strengthened 304 N or 304 LN could be made. There will be no sensitization of the welds in this process due to precipitation of chrome carbides to grain boundaries, because the exposure of the stainless steel to high temperatures is very short. The weld puddle will be quenched immediately by thermal conduction and upon exit from the weld box by passage through a manifold that vents vapor from liquid nitrogen onto the conductor. Weld quenching also assures that the NbTi superconductor will have minimal exposure to higher temperatures. There is adequate demonstration of this manufacturing process to assure that weld heat does not measurably effect the superconducting properties of the conductor.

After welding, the conductor will be rolled to a compaction that yields a nominal cable-space void fraction of 37%. The conductor will then be reeled in a single-layer onto a take-up spool with the weld seam in a radially outward position. It will be pressurized, bubble leak tested and helium-mass-spectrometer leak tested. Any leaks will be repaired by grinding out the weld seam and rewelding according to the appropriate welding procedure specification using an appropriate filler metal. Weld heat during the leak repair process will be monitored and minimized. Each conductor length will then be pressurized in a proof pressure test to at least 400 atm gauge (6,000 psig) and leak checked again. Note that this is greater than the maximum anticipated quench pressure. The final leak test will be at 77 K; this will be performed by immersion of conductor reels in a liquid nitrogen bath with the conductor pressurized with helium to at least 30 atm gauge.

Aluminum Sheath

The last component of the conductor is the 1100 "0" aluminum sheath. The two current designs are shown in figures 5-3 (baseline) and 5-14 (alternate). The aluminum sheath will be extruded on to a 3.65 m (12 foot)

---

[26] Steeves, M.M., et al, "Progress in the Manufacture of the US-DPC Test Coil", MIT ASC88, (1988).
[27] Steeves, M.M., et al, "Further Progress in the Manufacture of the US-DPC Test Coil", MIT-11, (19888).
[28] Steeves, M.M., et al, "US Demonstration Poloidal Coil", MIT ASC-90, (1990).

diameter take-up spool in a continuous length of approximately 1134 m. The aluminum is then transported by truck to the conductor vendor for assembly.

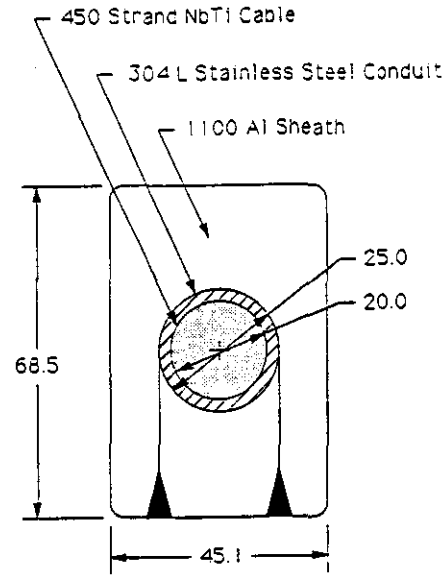

Figure 5-14 Alternate design option for aluminum sheath

The manufacturing methods of extruding large lengths of aluminum under evaluation are tandem extrusion (die-stop) and conform extrusion. Figure 5-15 a & b illustrate the processes. The con-form extrusion method is a process in which a one-inch aluminum stock rod is fed into a groove of a rotating cylinder which placticizes the material and feeds it into a chamber with an extrusion die. This process is continuous and does not require any welding. The other method is the tandem or die-stop method. This method is identical to the typical method of extruding material with the difference that the butt and head of the billits are machined in a mating fashion. This process creates a fusion weld during the plastic deformation at the die and thus a continuous extruded product.

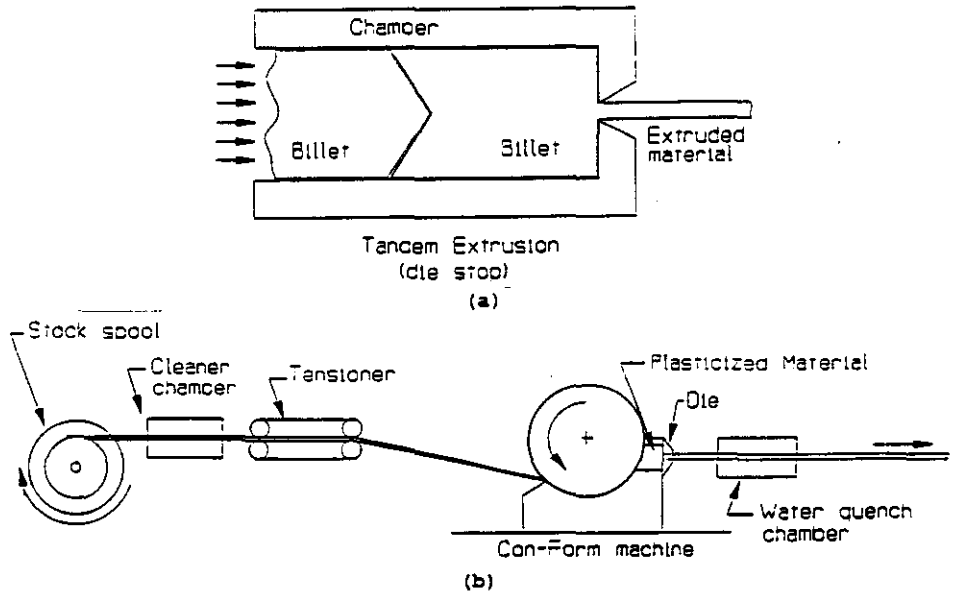

Figure 5-15 Aluminum sheath manufacturing options; a) tandem extrusion method, b) conform extrusion method

Ongoing discussions with vendors regarding manufacturing of the aluminum sheath and the required take-up spool equipment have been positive and encouraging. Two companies have already been identified as possible candidates for the manufacturing of the aluminum sheath. Methods for the conductor vendor to insert the cable-in-conduit into the two candidate sheath designs are being evaluated in the R&D program.

5.5 Coil Module Assembly

5.5.1 Bobbin Preassembly

Adjacent to the two winding stations there will be an assembly station to pre-assemble the bobbin. The assembly station is composed of a disc shape foundation plate fastened to the floor. A ring with aligned dowel pins and tapered in thickness (spiral) at the winding helix angle serves as the interface plate for the bottom bobbin flanges.

The bobbins are made up with four quadrants which are held together with a mechanical joint. Each quadrant is made up of a bobbin shell, and an upper and lower set of bobbin flanges.

Assembly starts with the lower bobbin flanges. The flange's circular bolt hole pattern is mated with the dowel pins of the interface spiral ring for alignment. The exposed top surface of the flange has a groove into which the bobbin shell segments are placed. An alternative approach that is currently being evaluated, is to have the bobbin shells already welded to the bottom flanges. The foundation plate will also have vertical support and alignment posts with adjustable jack screws which will hold and position the bobbin shell. The four bobbin shells are joined and the bottom flanges are welded to bobbin shells.

The final operation is to bond the ground insulation on the inner wall of the bobbin. For the case where the bobbin shells are already welded to the bobbin shells, the insulation could also already be installed. The lifting spider is attached to the bobbin and used to transfer the pre-assembled bobbin to the winding station.

5.5.2 Winding Process

The winding station is composed of a box beam ring turntable driven by cable and powered by a 20 HP motor (see Figure 5-16). Secured to the top plate of the turntable is a spiral ring, identical to the one in the pre-assembly station, with its dowel pins aligned and permanently secured to the turntable. The bolt hole pattern on the bottom bobbin flange mates with the spiral plate dowel pins to align the pre-assembled bobbin on the turntable. The turntable also has alignment support posts with adjustable jack-screws which will hold and position the bobbin as shown in Figure 5-17. At this point the bobbin is aligned and secured to the turntable, the conductor transport spool is in place and secured, plus all of the necessary equipment such as the roll forming, tractor drive (only if found necessary in the winding R&D program), cleaning station, insulation wrap, and the turn length control machines are in place and secure. To insure that the roll forming machines are set correctly, a conductor sample is roll formed and checked against the bobbin for final radius.

A curved draw bar is bolted to the conductor end termination (half joint) to begin to pull the conductor through the 1st set of guide rolls and into the 1st roll-former. This allows the conductor the be fed through the winding mechanism. The joint half is attached to the bottom of the bobbin at the flange joint opening, and the winding process begins. To monitor the winding process, a measuring device is placed after the insulation station and set of fiducial marks are automatically scribed every 45^0 (arc length of 7461 mm (24.5 feet)). At the end of the winding process, the joint half is secured to the bobbin at the top joint opening. A HiPoT and a turn-to-turn electrical insulation test is performed. The top flanges are then installed along with the joint compression plates. The inner radiation shield is bolted to the bottom and top flange. The bolt holes at the top of the shield are slotted to compensate for movement of the top flange. The shield is installed with its insulation pre-assembled. In addition the radiation shield doubles as the winding buckling stabilizer during pre-load. The pre-load is accomplished by the hydraulic press cylinders installed on the turntable support posts. The winding presses contain load cells which

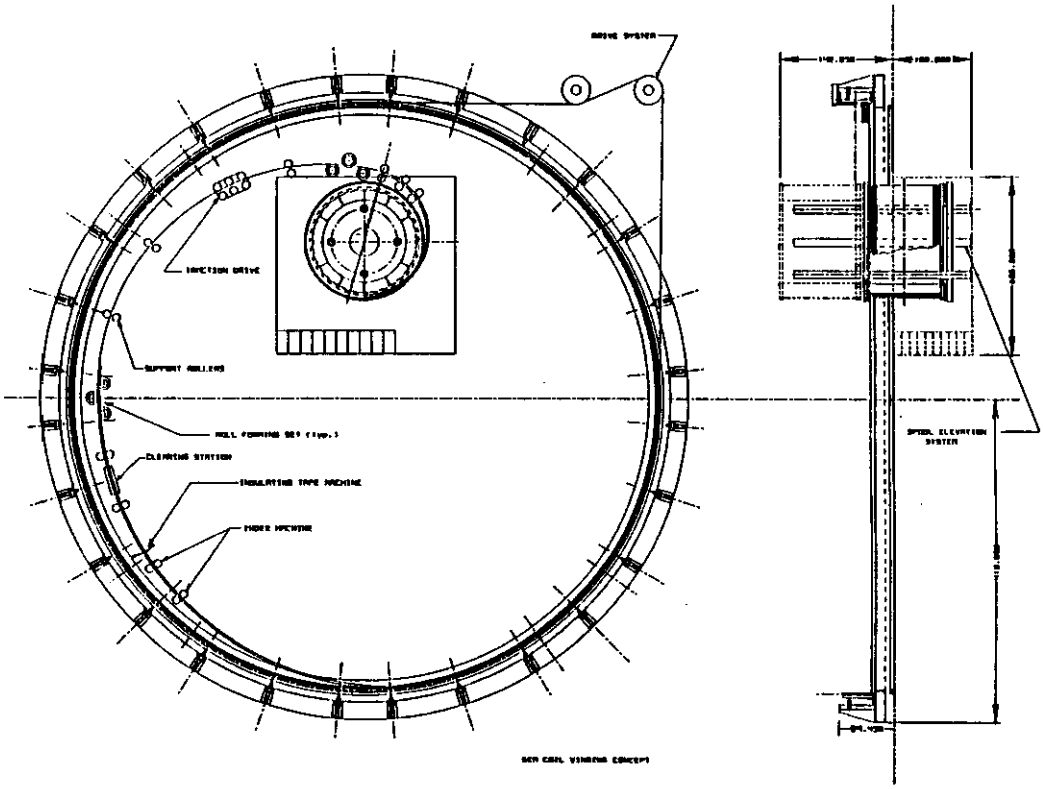

Figure 5-16 Winding Assembly

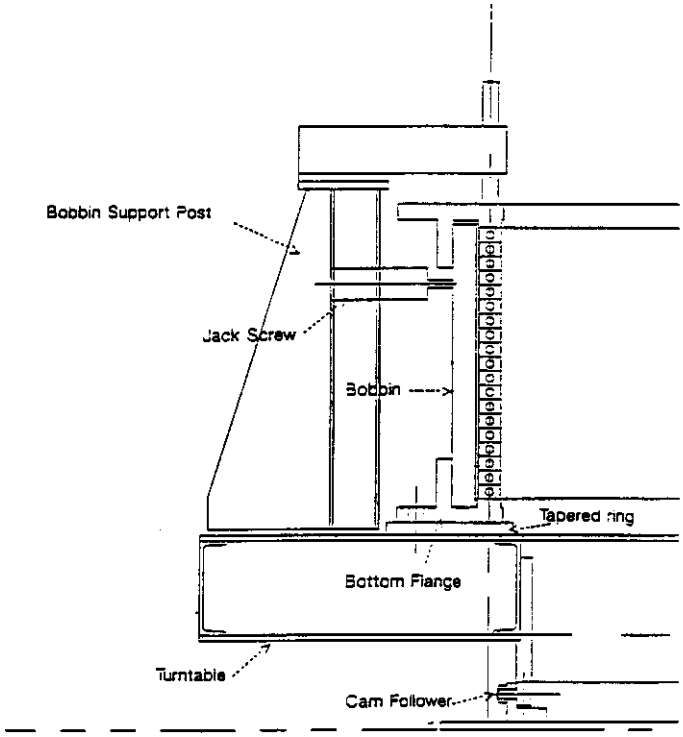

Figure 5-17 Winding Alignment Assembly

indicate the load applied. The winding is first compressed with an oversize shim between the winding and the press. The bobbin-to-press gap at full preload is measured. Compression is then relaxed and the correctly sized shim is inserted. The winding is re-compressed with the flange in place on the bobbin. The flange bolts are then tightened to retain the pre-load. Once the winding is pre-loaded a HiPot and turn-to-turn test is performed again. The last step is to install the lifting spider to transport the wound coil module to the magnet assembly building.

5.6 Structural Analysis Introduction and Summary

The GEM magnet must sustain mechanical, thermal and electromagnetic loads. Bobbins are used as primary structural members, supporting the radially outward Lorentz forces from the coil winding. The resulting bobbin stresses are well below the allowable, even if the structural contribution from the conductor is neglected. Service is low cycle, and fatigue is not limiting to the design. Other performance criteria are more important than stresses.

5.6.1 Conductor Stress Analysis

While much less strain sensitive than other conductors, the cable-in-conduit-conductor (CICC) must be protected from excessive strain and slippage of components of the winding. Preload of the coil winding and use of thick aluminum bobbin shells help minimize strains. The conductor uses stainless steel in the conduit, and a high conductivity aluminum sheath is used for additional quench protection. Ideally this sheath should remain in intimate electrical contact with the conductor conduit throughout the life of the magnet. Differential contractions produce large contact pressures at cooldown which slightly yield the sheath. Subsequent quench pressurization further strains the sheath, however analysis shows adequate contact pressure remains at 4K.

These local interactions between the conduit and sheath have been investigated with a model of a single conductor and associated bobbin section. Elastic-plastic analysis is done for a sequence of load steps which includes cooldown, Lorentz force application, quench, reduction in Lorentz force, and heat-up to room temperature. This sequence is repeated three times to ensure the plastic response of the sheath has shaken down. Figure 5-18 shows selected model plots. Figure 5-19 is a plot of the gap forces around the conduit. Forces are compressive for points in the load cycle for which contact is needed. The Lorentz force remains significant in the early phases of the quench event, and adds about 250 lbs per inch of contact loading. Contact is lost at about 120K. This has no effect on the quench current transfer behavior because this temperature is reached well after the quench event is over. Contact which existed after manufacture is permanently lost, making mechanical restraint of the conduit a design requirement for the conductor terminations. Yielding of the sheath can effect the electrical properties. Figure 5-20 is a plot of the equivalent, radial(x), and axial(y) plastic strains. They "shake-down" after the first load cycle and their magnitude is much smaller than the winding strains, for which electrical property degradation has been found acceptable. Figure 5-21 shows a contour plot of the equivalent strain after plastic strains have stabilized.

Yielding of the sheath effects the global behavior of the coil as well. Plastic strains tend to relax all applied loads. Thermal contraction mismatch contact pressure between sheath and conduit is relieved by radial strains. Lorentz force hoop tension is shed to the bobbin. Figure 5-21 shows a hoop stress history. The element chosen to represent the sheath is in the region where most of the plastic strains are occurring. The sheath hoop tension increases with the first Lorentz force application, but as the quench pressure is applied, hoop tension is relaxed and compression develops due to the radial compressive stress imposed by the expanding sheath. Compressive stresses remain locked-in for subsequent cycles, and effectively sheds some of the Lorentz forces to the bobbin.

5.6.2 Global Stress Analysis

The global behavior of the coil is modeled with a variety of axisymmetric and 3D models. Conductors and bobbin shells and flanges all share hoop and axial loads. There are slip surfaces at the bobbin/conductor interface and this as well as the sheath plasticity represent significant non-linearities in the model. These effect global behavior and because of the size of the magnet they have to be addressed in a combination of the small non-linear and large

linear models. Figure 5-23 shows two simple axisymmetric models of the coil with axial load support points at a mid-coil flexure support and at the central membrane. The current design basis uses the mid coil tierod support concept. Figure 5-24 shows a three dimensional model developed by sweeping the axisymmetric model around 180 degrees. This model is used to consider the effects of the discrete cold mass support attachment points. Figure 5-25 shows the single bobbin model used in the evaluation of the differential cooldown contraction and preload effects.

Figure 5-26 shows the Lorentz force distribution in the coil. The most significant loading is the radially outward load which is resisted by the bobbin and conductor hoop tension. Hoop stress for the 3 inch thick bobbin is plotted in Figure 5-27. This includes a contribution from the strength of the sheath. Three to four ksi is not a problem for the bobbin shell which is 6061-T6 aluminum (which yields at 40 ksi), but the sheath of the conductor yields at 5 ksi, and thermal and quench effects add to the global stresses to yield the sheath. To minimize the effects of sheath yielding a 3 inch bobbin has been selected. With the effect of the plasticity in the sheath, the bobbin stress goes up to 4.9 ksi. The 3 in thickness was also chosen to provide margin for design details such as tapped holes and attachments. The 3 in. Bobbin Stress is 7.1 ksi, if it alone must resist all the Lorentz forces. This would peak around the bobbin segment joint hardware to 9.3 ksi, which is still below the allowable.

Substantial axial loading is evident at the ends of the coil. Axial loads also exist within the interior of the coil, due to the separation at the bobbin flanges. The axially segmented bobbin design is intended to force accumulation of axial loading in both the bobbin shell as well as the conductor. Accumulated axial loads are periodically transferred into the bobbin shell through the bobbin flanges. In the outer bobbins there is minimal accumulation of axial load in the bobbin. The conductor stack may compress more than its bobbin leading to separation at the flange. Figure 5-28 shows the results of an analysis of just 2 of the end bobbins. Other models approximated the conductors and bobbin as a bonded media. This smaller model of the two outer bobbins uses low friction gap elements at the conductor/bobbin boundary. Under load a small gap opens and would produce some small frictional energy to be added to the coil. To avoid this, axial precompression is added to the bobbins at assembly. The intent of the precompression is to avoid this gap.

5.6.3 Joint Stress Analysis

The baseline joint is contained in a cavity made from a cutout in the bobbins. Radial Lorentz loads are directly transmitted to a cover plate on the outside of the cavity. The body of the joint consists of copper bars that clamp over the flattened copper tube extensions of the conductor conduit. Aluminum covers are used to clamp the copper bars closed. As in the conductor, differential strains result from the cooldown. Aluminum shrinks more than the copper, is placed in tension and produces compression in the copper. The copper compression is directly transferred to the conductor sheath end face via reinforcing blocks which also serve to restrain conduit motion resulting from differential thermal strains. Large internal loads must be reacted within the joint. An alternate all-aluminum joint eliminates these loads. The joint assembly strains both thermally and under load differently than the bobbin which surrounds the joint. The differential strains are absorbed in the curved conductor extension at either end of the joint. The joints near the end of the coil are exposed to large axial loads. The joint body is supported by g-10 fillers which transfer the loads to the cavity sidewall. The curved conductor extensions are loaded in bending and must be partially supported to control bend stress while still allowing absorption of axial strain differentials. Figure 5-29 shows the model of the joint used to evaluate these phenomena.

5.6.4 Cold Mass Support Analyses

The coil is supported by a system of radius and axial straps, or flexures. The radius rods at the ends of the coil resist loading normal to the axis of the coil, and maintain the circularity of the coil. The axial flexures resist the axial loads, both magnetic and during handling. The flexures connect the center of the coil to the end cryostat support by the forward field shaper support. Local attachment moments were previously discussed in the context of the axisymmetric model. The eight discrete attachment points are analyzed using the large 3D model of the coil shown in Figure 5-30. Earlier designs transferred the rather large tierod cooldown tension loads through conventional lugs attached to the outside of the bobbin. These had large local moments. The flexure design brings

the large axial load to the surface of the bobbin shell, reducing the local offset moment. The bobbin shell displacement contours result from the small offset moment and the eight radially outward load components, the latter being most important for the flexure support concept.

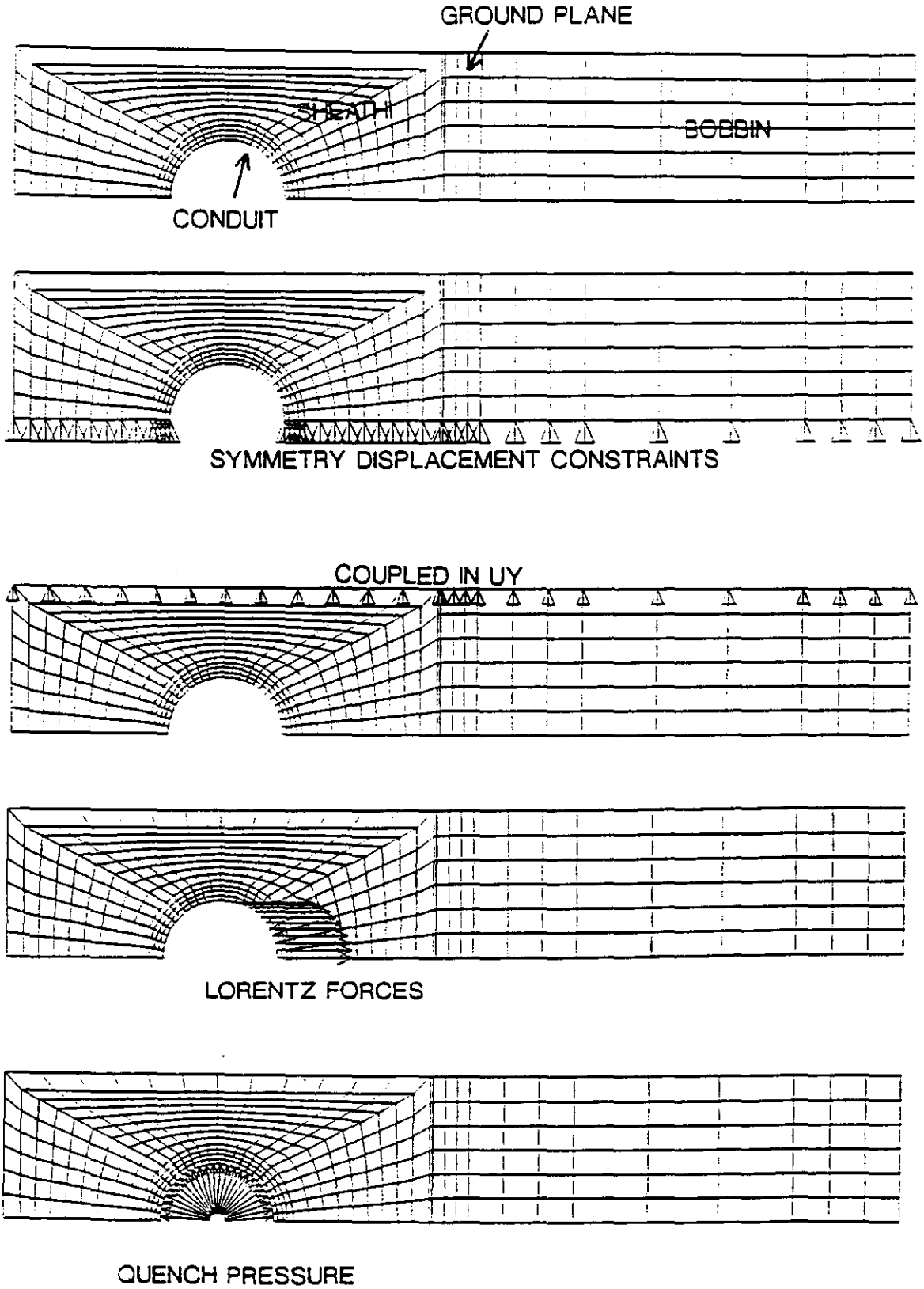

Fig 5-18 Baseline GEM Detector Magnet Conductor Elastic-Plastic Stress Analysis

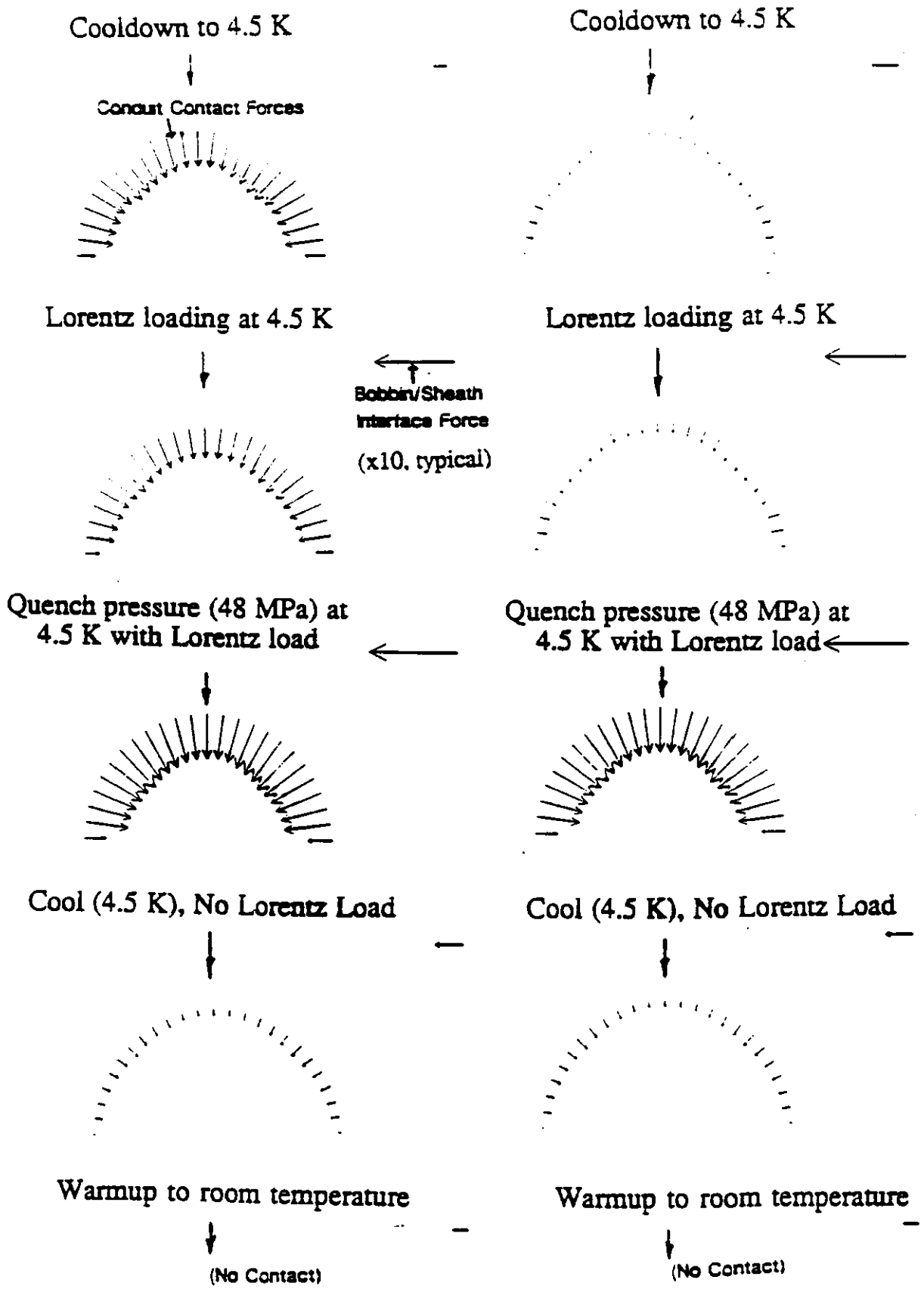

Fig 5-19 Sheath/Bobbin Contact Force Vectors for Each Load Step

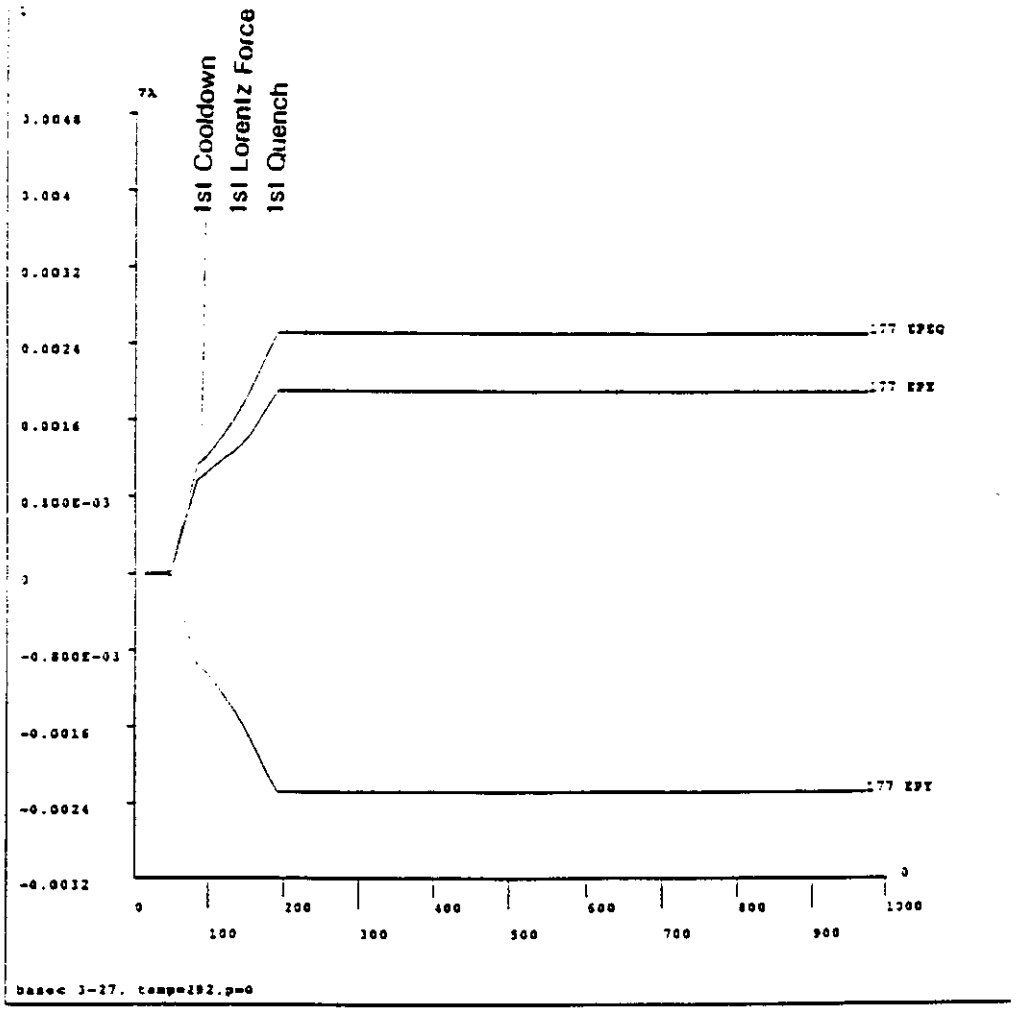

Figure 5-20 Baseline conductor plastic strains

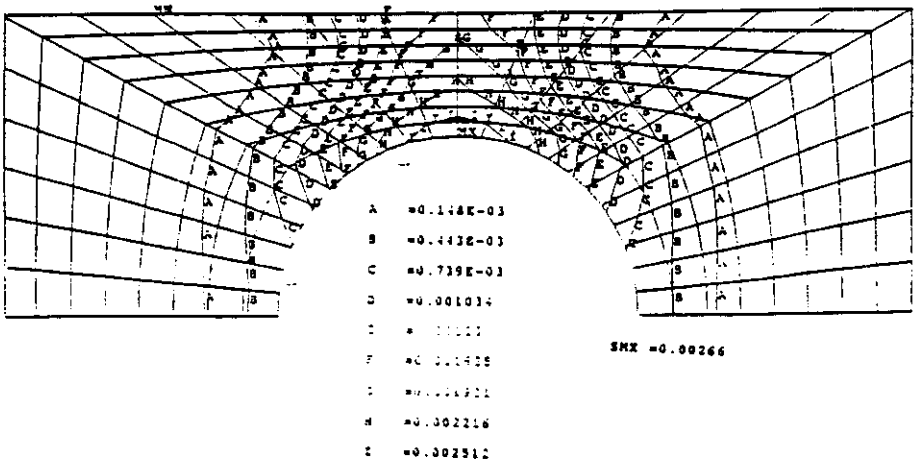

Figure 5-21 Plastic strains after "shake-down"

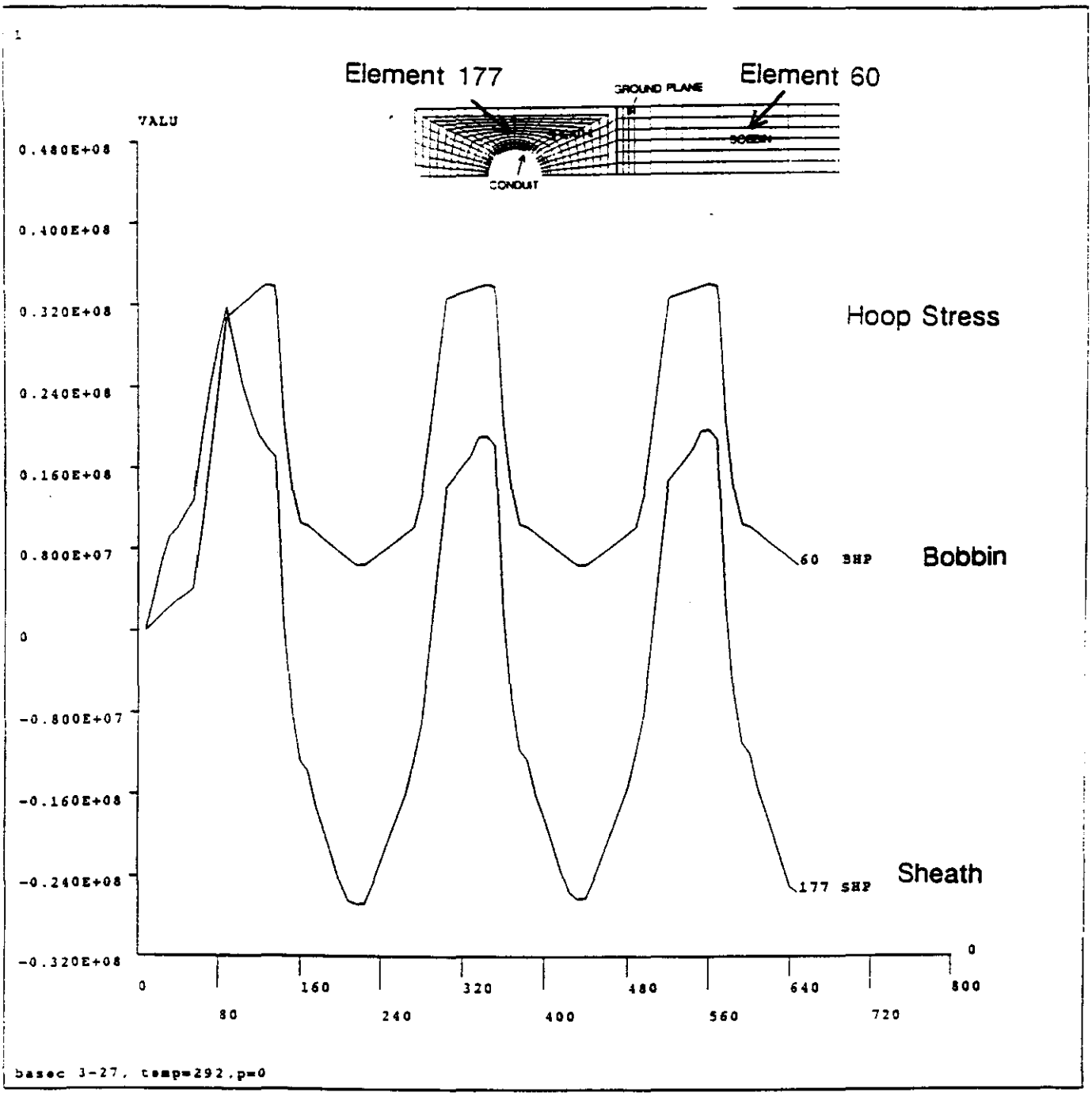

Figure 5-22 Hoop stress history

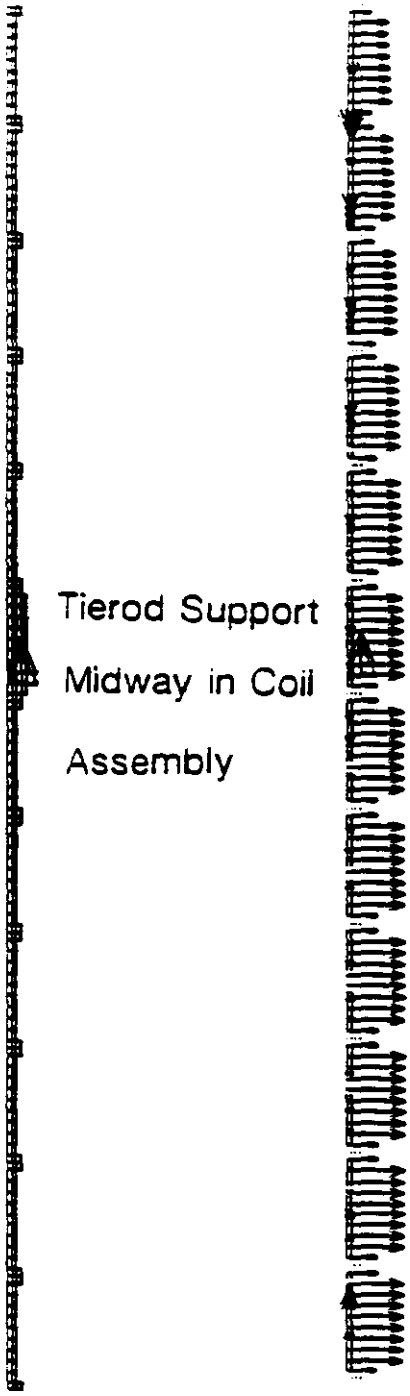

Figure 5-23 Coil stress analysis

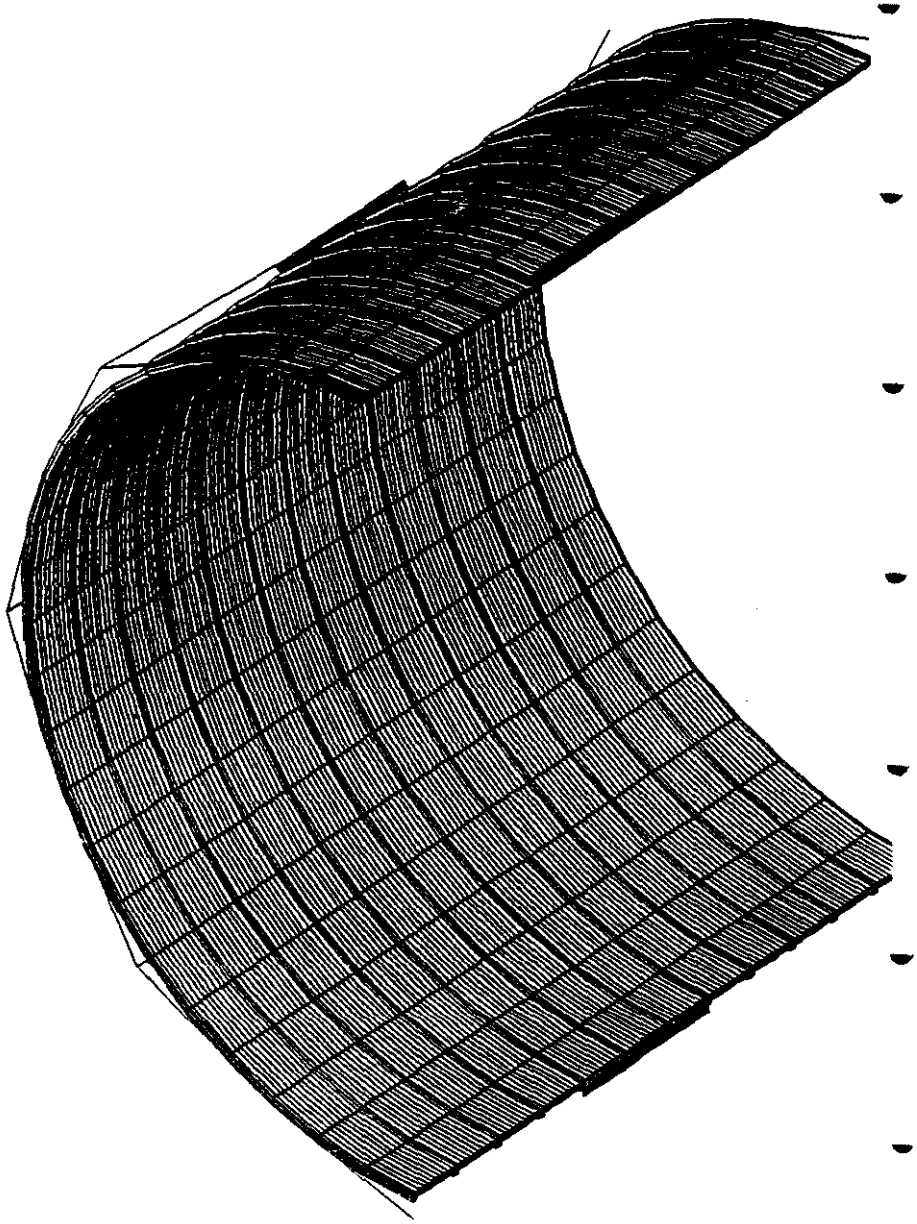

Figure 5-24 Global stress analysis model

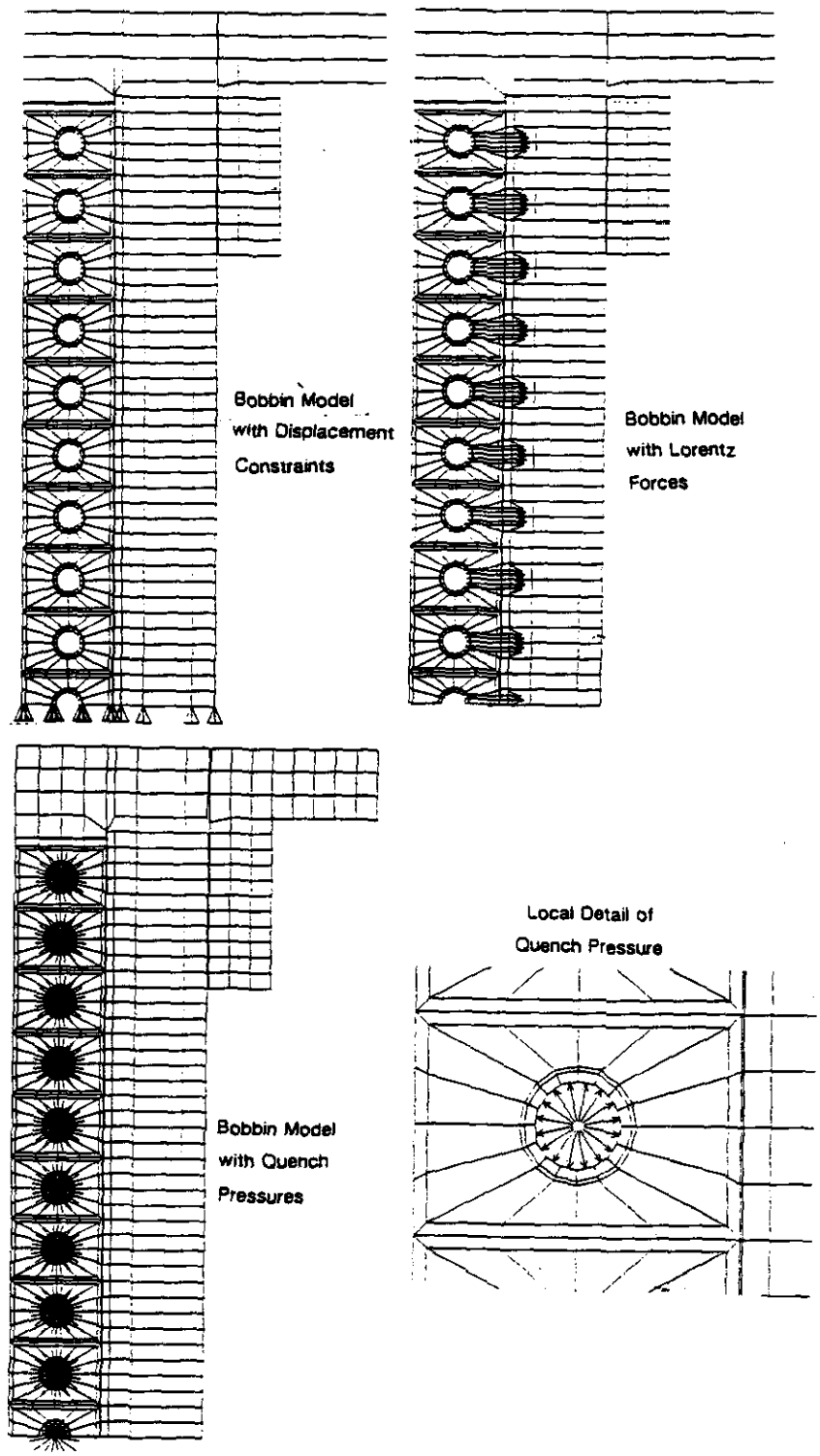

Figure 5-25 Single bobbin model for global stress analysis

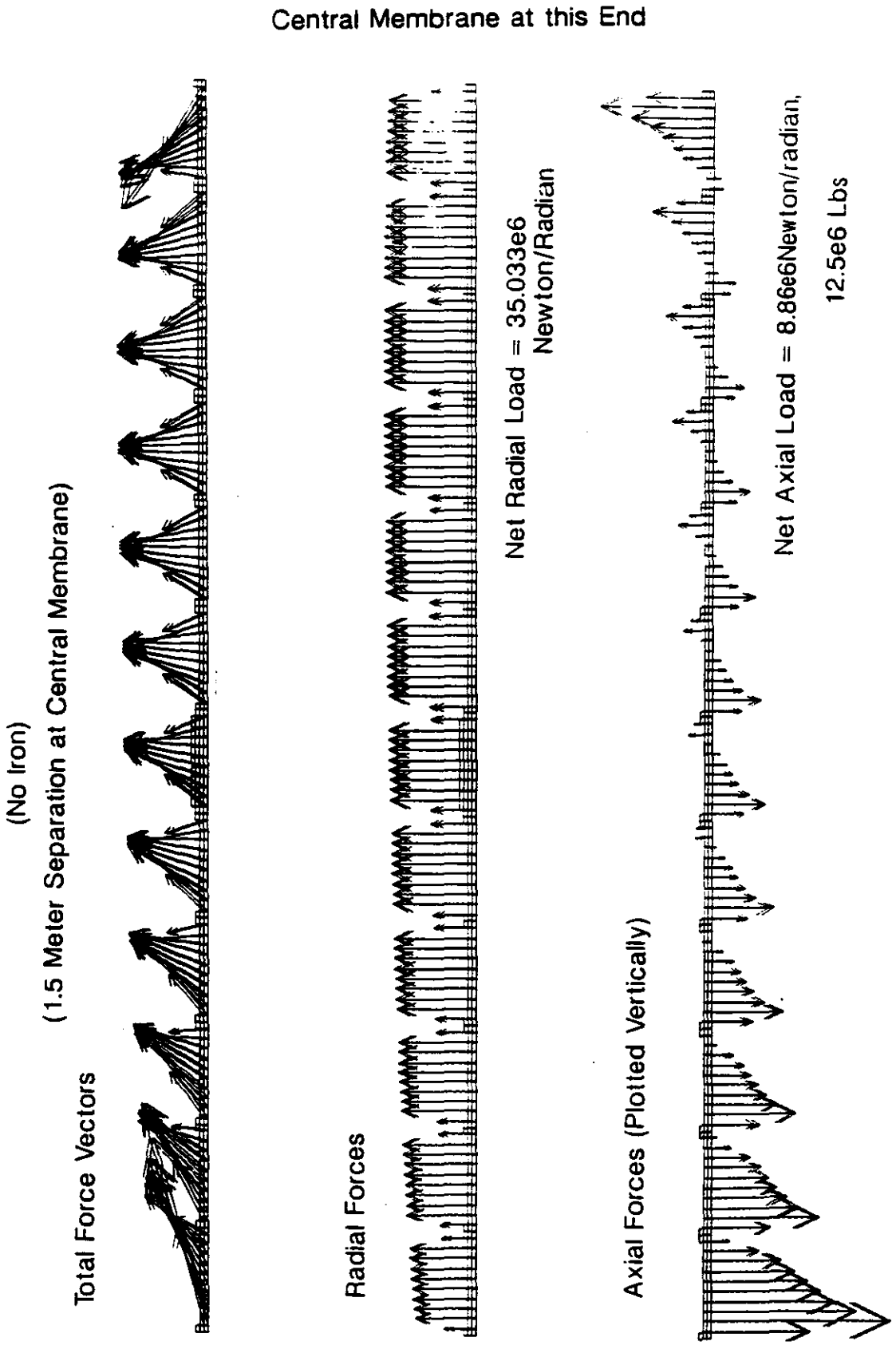

Figure 5-26 GEM detector magnet Lorentz forces

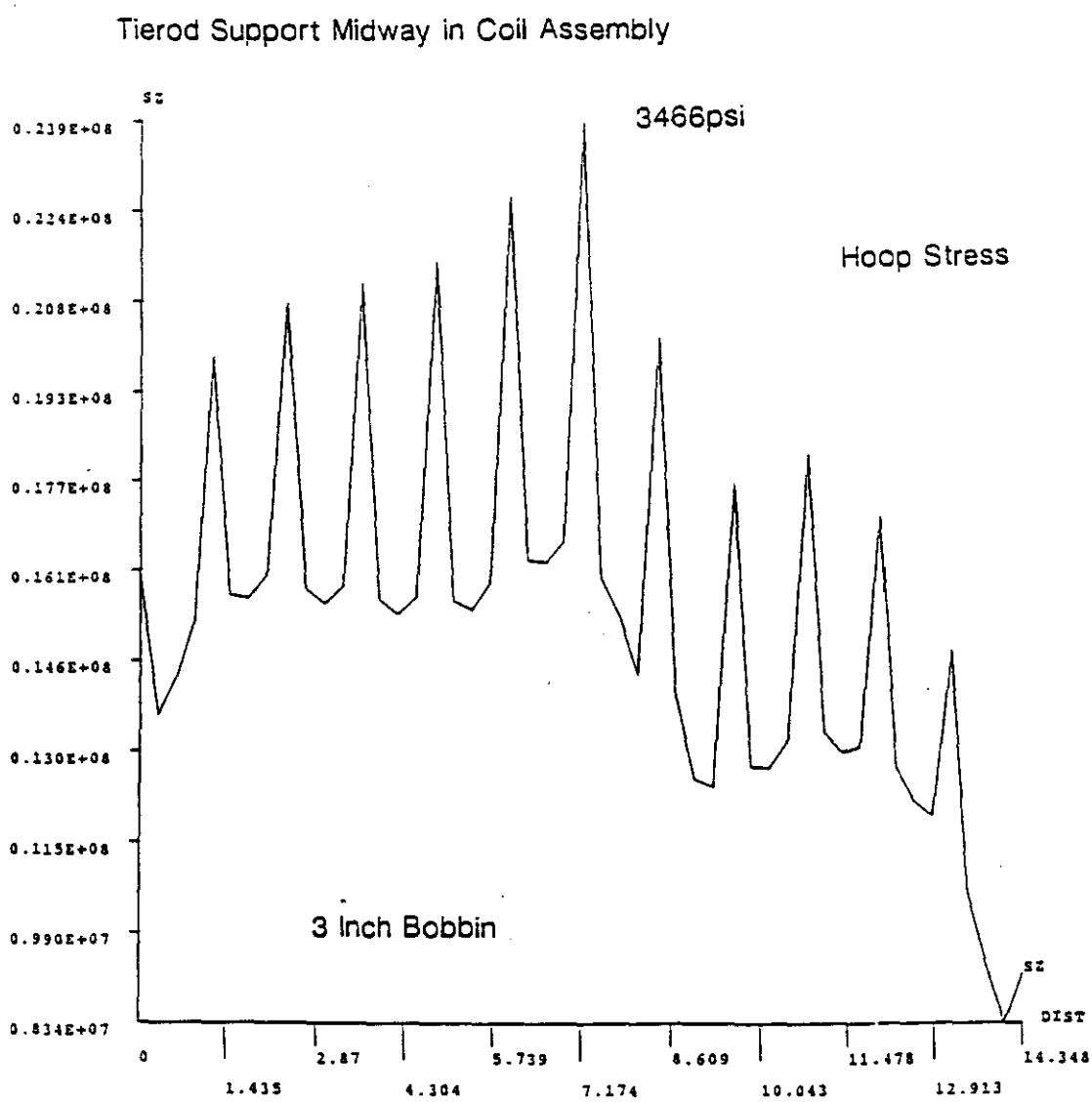

Figure 5-27 Hoop Stress

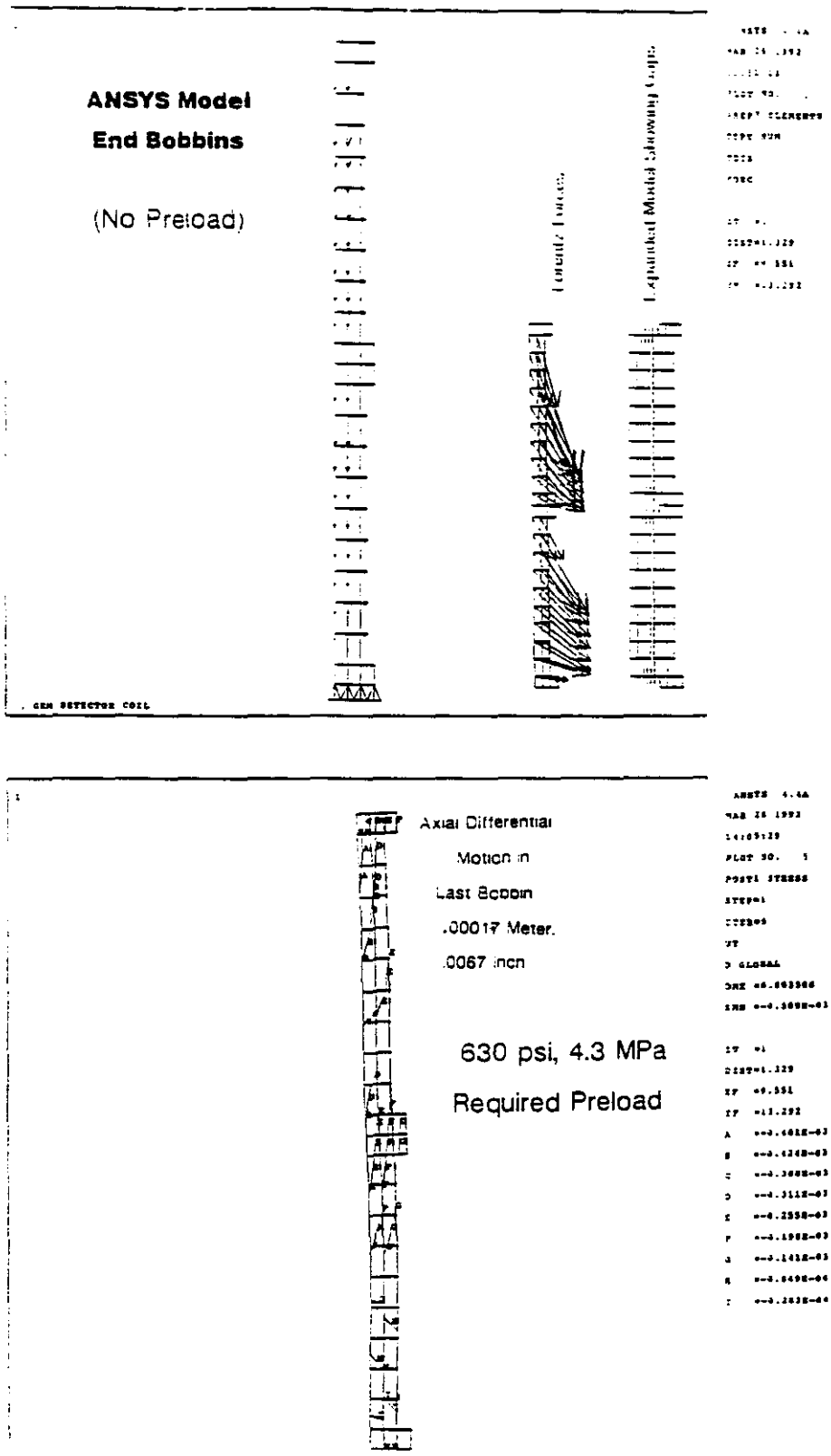

Figure 5-28 Stress analysis of two end bobbins

GEM JOINT

Finite Element Model

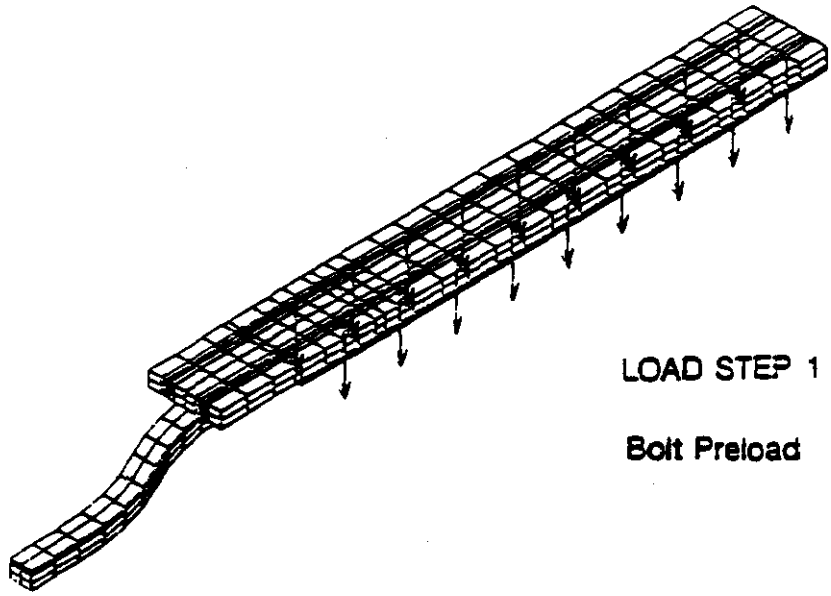

Boundary Conditions

UX=0

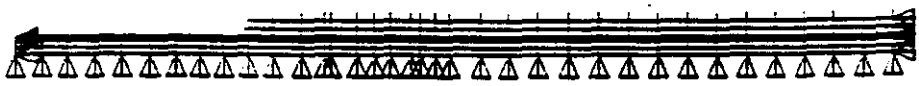

Δx=0.24" ---->

UY=0

UZ=0 @ Centerline Nodes along compression plate

LOAD STEP 2

Add:

Thermal Load: 294K to 4K

End Displacement Δx=0.268" ---->

LOAD STEP 3

Add: Lorentz Displacement Δx=0.2364" ---->

8/17/92

Figure 5-29 Joint finite element model

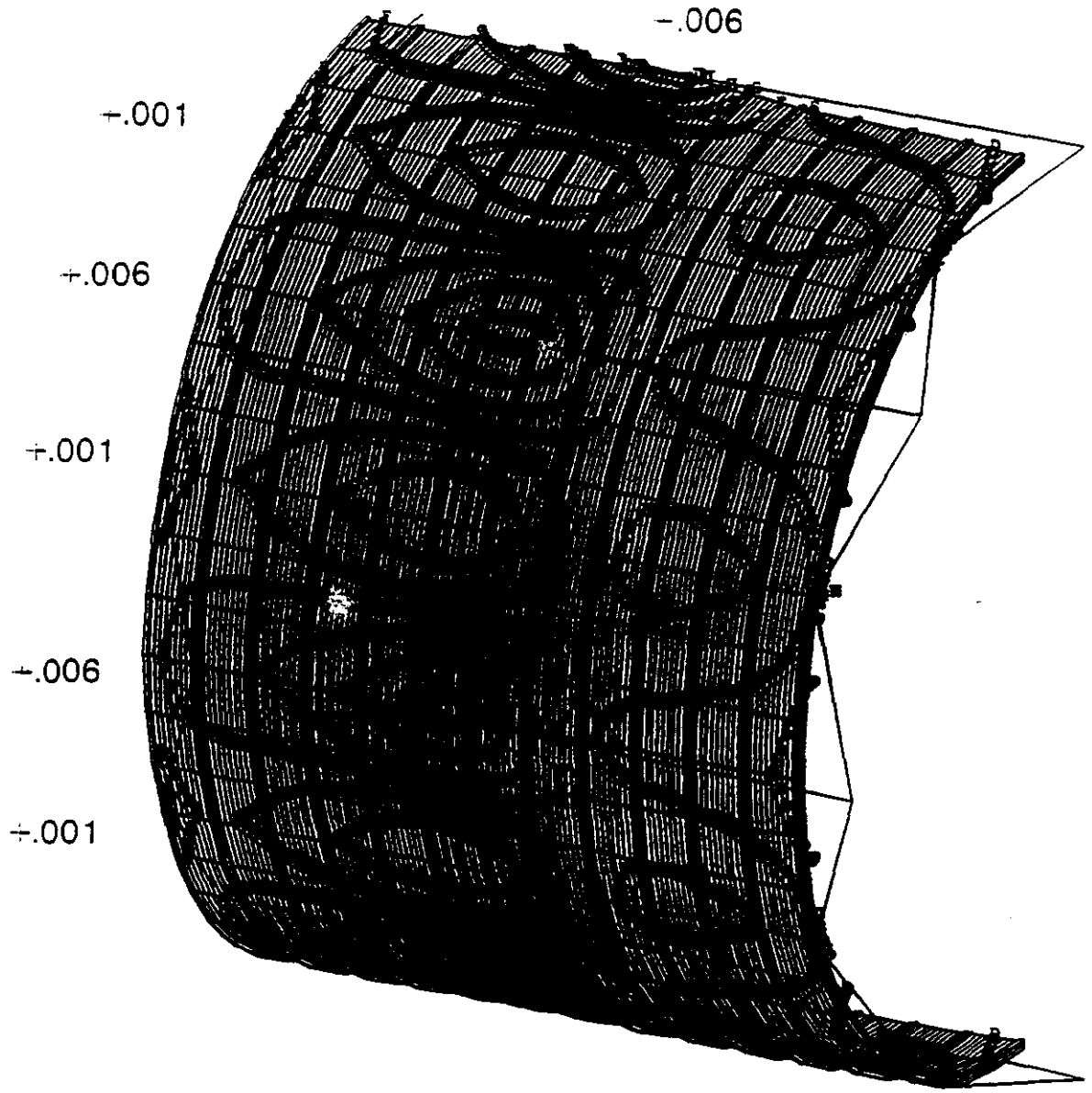

Cold Mass Support Flexure Displacements

Superimposed on the Lorentz Force Hoop Expansion

(in Meters)

Lorentz Forces

Figure 5-30 Radial Displacement Contours

6.0 COIL ASSEMBLY DESIGN

Two coil assemblies consist of coil subassemblies (the cold mass), thermal radiation shields, cold mass supports, cryogenic current leads, vacuum vessels, and cryogenic piping inside the vacuum vessel. The coil assemblies are stand-alone objects, capable of supporting themselves against gravity, seismic loads, holding vacuum, and moving in limited ways. With the addition of the vacuum, cryogenics, and power systems, the coil assemblies can be operated as magnets. The following sections discuss the various components within the coil assemblies, and the design, construction, and testing approaches.

6.1 Vacuum Vessel

The vacuum vessel is an integral part of the GEM detector, providing the main structural support for many of its internal components and insulating the cryogenically cooled, superconducting magnets (see Figure 6-1). Each of the two identical vessels weighs approximately 900 tons, excluding the weight of the cold mass or nitrogen cooled shields inside. Individual vessel dimensions are 15.1 meters long and 21.8 meters in diameter. Each vessel is independently mounted to the floor of the underground hall, at specially reinforced mounting locations. For initial installation, ongoing maintenance, and repair, the vessels can be lifted off their mounts and transported to the ends of the experimental hall. Each vacuum vessel can be evacuated independently of the other. The cold masses are suspended in each vessel's annular space on titanium rods. Inner and outer cylindrical shells form an evacuated annulus enclosing the cylindrical magnet. Anular rings provide structural support at the ends of the vacuum vessel.. In addition, each vessel must support the dead load of 16 muon barrel sectors weighing approximately 10 tons each. These sectors are roughly pie shaped and are supported by the vessel end rings.

The two vacuum vessels butt end to end at the midplane of the GEM detector and are separated by the central detector support structure. A total of 64.2MN of compressive force results from the magnetic forces on the coils and on the Forward Field Shapers when the magnet is energized. These forces are transmitted from outer ends of the vessels to the midplane through eight structural columns (longerons) on the outer shell of each vessel. Loads from the coil (52MN) are transmitted from the coil through eight axial restraint rods which fasten to the vessel at the eight longerons. Loads from the FFS (12.2MN) bear directly on the longerons through shim blocks (see figure 6.1).

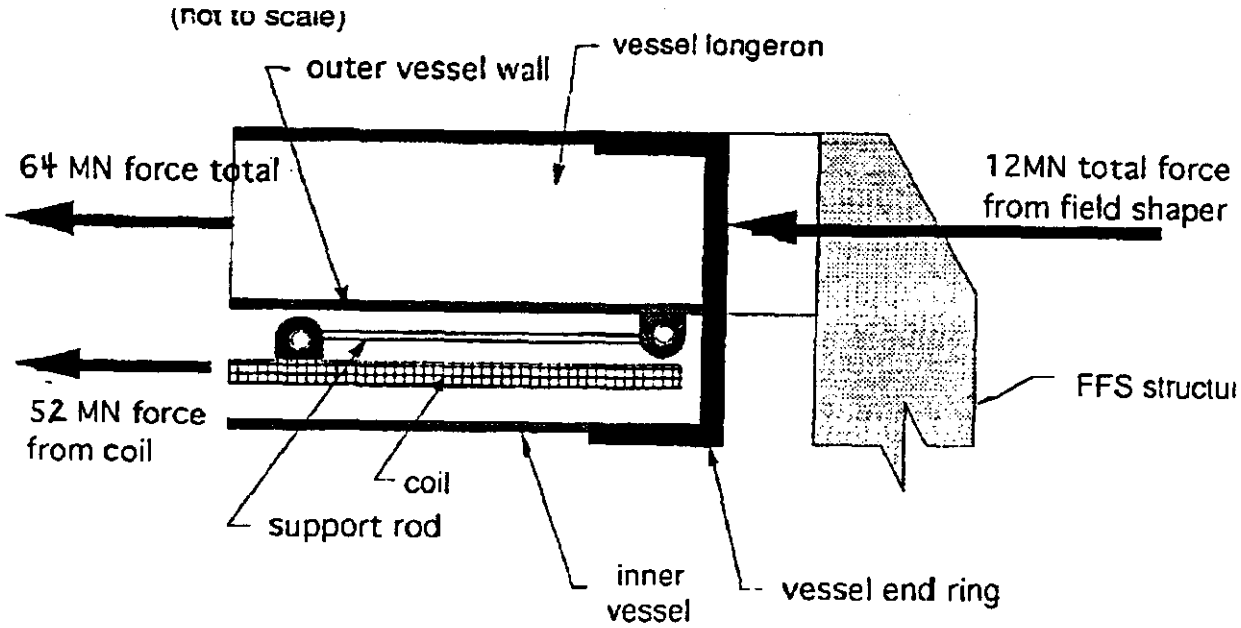

Fig. 6-1. Magnetic forces on restraint rods.

The required base pressure of 10^{-5}torr, inside the vacuum vessel, will be achieved with a combination of mechanical pumps, roots blowers, and diffusion pumps. Feed through ports are provided at various locations for relief valves, vacuum lines, cryogenic lines, power cables, sensor cables, and access for magnet coil support rod tensioning. Stainless steel (304 L) is used for all structures which need to be non magnetic. The selection for the vessel shell material is under review. All structural elements other than the vessel will be constructed from A36 low carbon steel. The vessel will normally operate in room temperature environment at about 70 F. The temperature variation in the vessel during coil cool down will not impose significant stresses in the vessel or support structure.

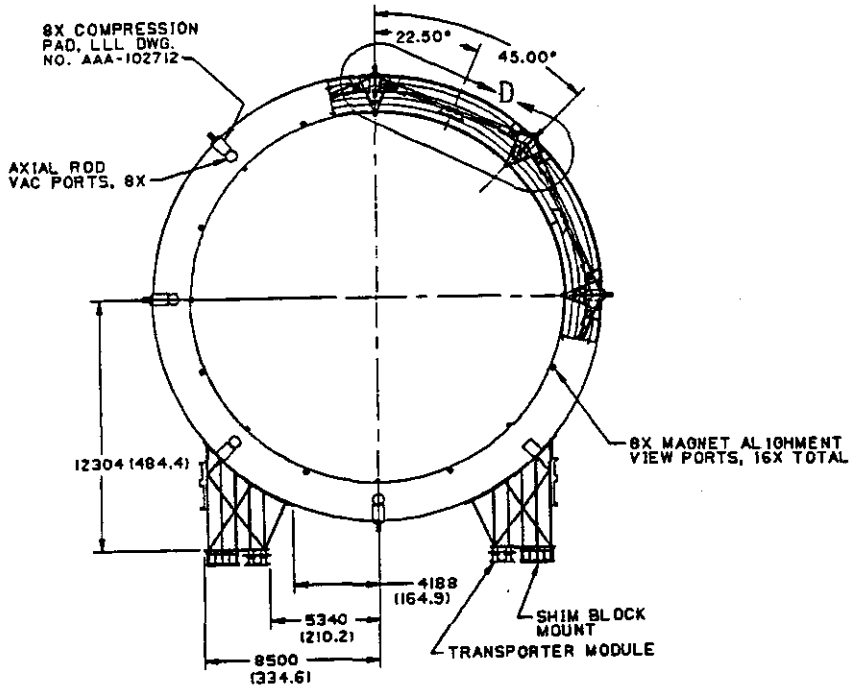

Figure 6-2a Vacuum Vessel End-View

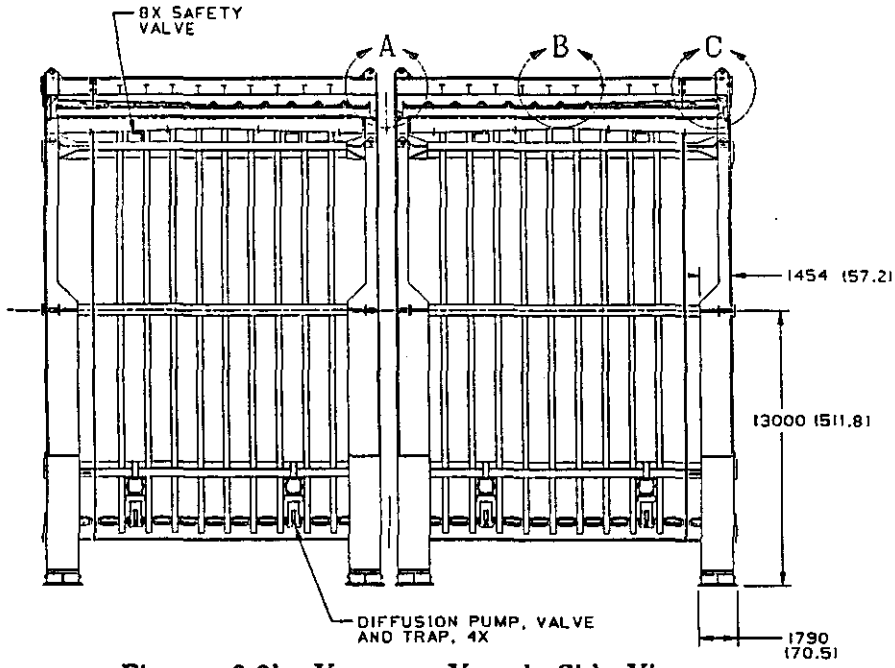

Figure 6-2b Vacuum Vessel Side-View

Vacuum Considerations

Under normal conditions, the outer vacuum shell experiences external pressure equal to the ambient pressure in the hall. The inner shell is normally an internal pressure vessel, with atmosphere on its inside and vacuum on its outside. The annular end caps are designed for vacuum loads and other structural loads described below. The nominal level of vacuum required before magnet cooling is approximately 10^{-5} torr in order to provide sufficient thermal insulation for the cold mass.

There are several potential sources of gas in the vacuum vessel. These include vessel wall leaks from external pressure, virtual leaks from long path lengths in the cold mass insulation, outgassing from the vessel walls, outgassing from the cold mass insulation, and cryogen leaks from the cold mass. The gas load in the cold mass insulation is difficult to estimate because of the complex conductance path between the layers of insulation. One can calculate total potential outgassing from published data for the insulating material, but this outgassing rate into the vessel will be mitigated by the long conductance paths. This geometry will most likely behave like a virtual leak.

The extent of actual leaks is determined by the effectiveness of the leak checking procedure during construction and assembly. The threshold of acceptance for leak checking will be set by the expected rate of outgassing and virtual leaks from within the vessel. In other words, it is not necessary to check for extremely small leaks if other gas sources in the vessel are orders of magnitude larger. However, leak rates must be kept low enough so that the cold mass does not accumulate significant amounts of cryopumped gas and water vapor. Leaks from joints in the cryogenic piping may inject some amount of helium or nitrogen into the vessel.

The vacuum system for each vessel consists of rough and high vacuum systems. The rough vacuum system, which is shared by the two vessels, consists of two 4000 CFM roots blowers each backed by a 300 CFM mechanical pump. Mechanical pump oil contamination is isolated from the vacuum lines using refrigerated traps. The roughing header diameter is 12 inches. The high vacuum system for each vessel consists of four 24" diffusion pumps backed by a single 300 CFM mechanical pump. Refrigerated traps isolate the vessel from diffusion pump oil contamination. A control system monitors interlocks, crossover pressure, trap functions and backing pressures.

Pressure considerations

Internal pressure within the annular vessels is not a normal operating condition. However, a cryogen pipe failure could result in a rapid pressure rise inside the vessel, due to the boiling and subsequent expansion of cryogenic fluids interacting with the warm vessel walls. Although this rise would be partially mitigated by the vacuum system, pressure relief is provided to prevent failure of the inner vessel. Relief valves, set at 1 psig, will be sized to handle the maximum potential gas volume that could be generated when the cryogenic fluids gasify.

The internal pressure scenario would turn the inner vessel into an external pressure vessel and the outer vessel into an internal pressure vessel. Under this condition, the weak link in the vacuum vessel structure would be the inner vessel. Using ASME Boiler and Pressure Vessel Code section VIII guidelines, the wall thickness required for 15 psi of internal pressure results in a vessel design that meets requirements for an external pressure of 1 psi without any additional structure. The 1 psi relief valve specification is a result of structural capacity already designed into the vessel for normal operation.

Cold mass support rods

The cold mass is supported by long, relatively slender rods at each end. Radial rods, oriented in a vertical plane, support the weight of the coil. Axial rods, oriented parallel to the axis of the vessel, are distributed about the circumference of the coil. These rods transfer the coil's axial magnet forces into the vessel.

Axial support rods are tied to the vessel end rings, as shown in Figure 6-3. The rods on each coil assembly are arranged in eight pairs around the circumference. Each of 8 axial rods, connected to the cold mass at its center

plane, imposes about 1.5 million pounds of force on the end ring when the coil is energized. This load is resisted by longeron stiffeners outside the vessel shell, which act as columns. Each axial rod is located directly under a vessel longeron stiffener.

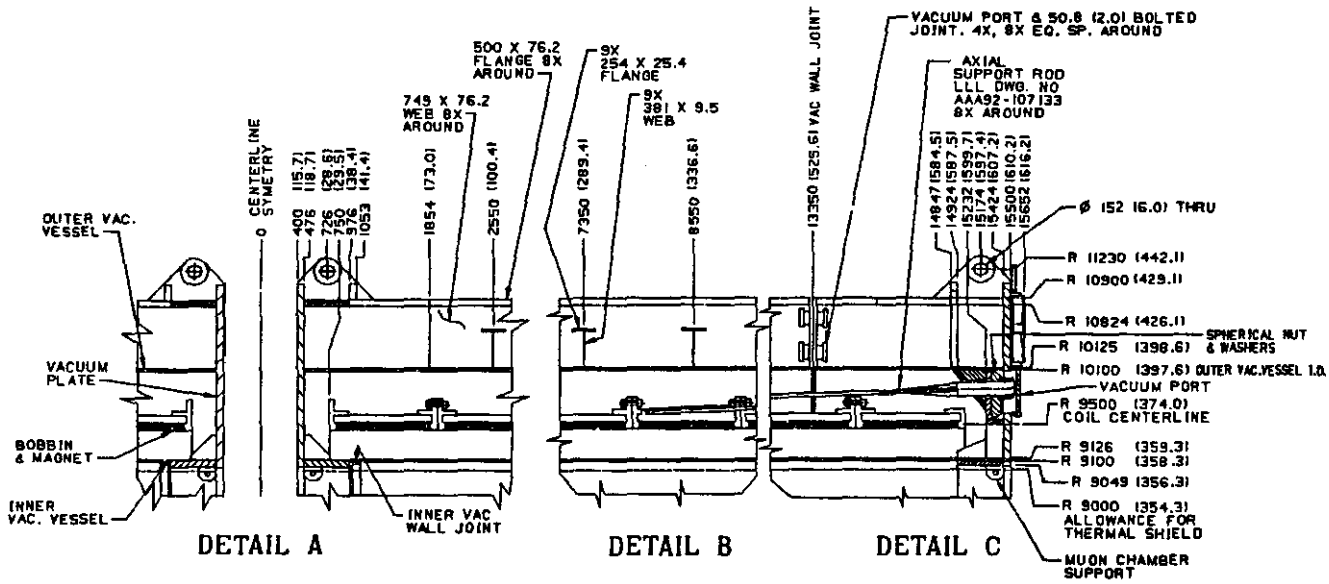

Figure 6-3 Detail of the Vacuum Vessel Design

Radial support rods support the weight of the coil. A total of eight pairs of radial rods transfer the coil dead load to the vessel at each end-ring. Figure 6-4 shows the gussets in the end-ring designed to react these loads. The rod ends are fastened to the vessel end ring with rod end nuts on spherical washers, identical to those used on the axial rods. ISO type vacuum ports cap off the rod ends to seal the vessel. Radial rod pairs are pretensioned using commercially available hydraulic tensioners, as shown in Figure 6-4. To perform the tensioning, the end-nut vacuum closure is removed. A coupling nut is added to the radial rod end above the rod end-nut, and an additional tensioning rod is assembled to the coupling nut. The hydraulic cylinder pushes on this secondary rod to tension the radial rod in the vessel. When the proper tension and alignment is achieved in opposing rods, the rod end nuts are tightened, and the hydraulic cylinder is depressurized. This procedure is repeated for each pair of rods on each end of each cold mass.

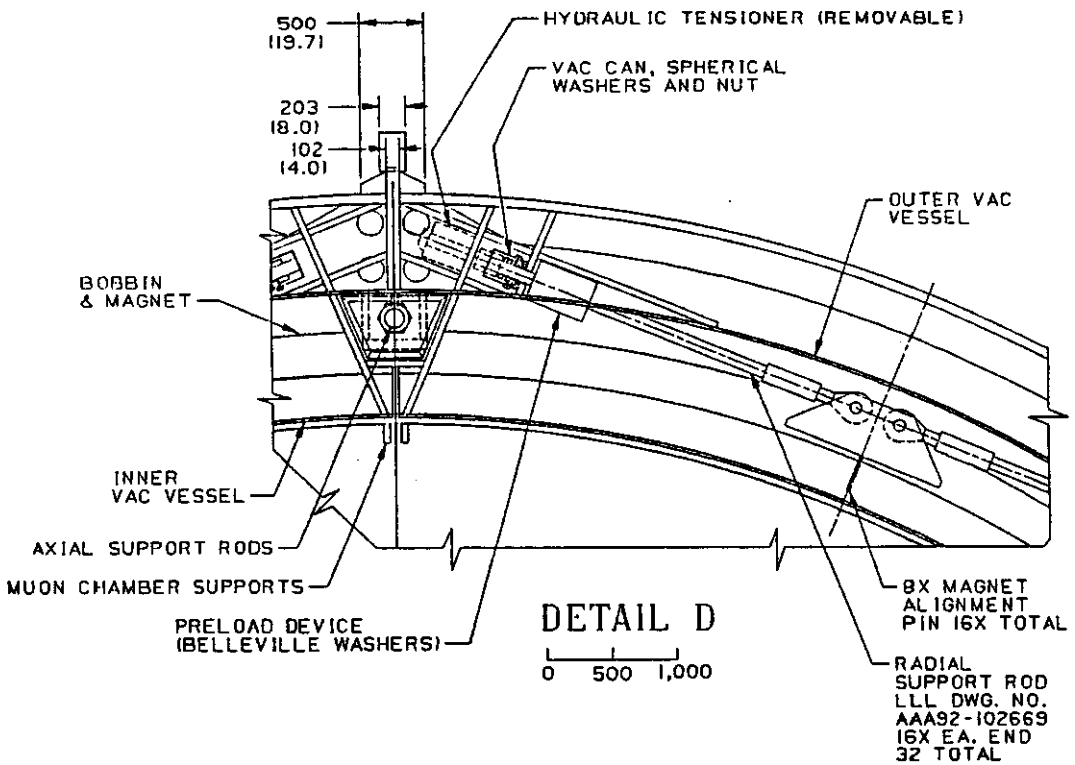

Figure 6-4 Detail of the Vacuum Vessel Support Rod Design

Forward Field Shaper Interface

The Forward Field Shaper support structures, large circular weldments that contact the vessel ends, exert an axial force on the ends of the vessel due to the magnetic field. The load bears on the ends of the eight longerons on each vessel, through shims and cylindrical bearing pads. These bearing pads allow the forward field shaper to deflect under magnetic load without transmitting moments into the end of the vacuum vessel, giving the field shaper structure a hinged support. This eliminates moment loadings on the vessel which can misalign the muon sectors mounted to its end rings.

Vessel Support Saddles

Each vessel is supported by end saddles consistent with conventional pressure vessel design. Four saddle legs attach to each vessel at the end rings where the vessel is stiffest. Each saddle is a plate girder weldment designed for vertical dead loads and horizontal seismic loads.

When mounted in its operational position, each vessel rests on support blocks which mount on the floor of the experiment hall. During vessel lifting and transport, the weight of the vessel rests on four transporters. Each vessel support saddle is designed to be supported at either of two bottom surfaces to accommodate the two support conditions. The load transfer occurs during lifting onto the transporters, when the vessel load moves from the support block interface to the transporter interface.

Saddle Support Blocks

Each vessel support saddle is supported by a saddle support block as shown in Figure 6-5. The function of the block is to provide a simple, inexpensive, disposable structure which can be replaced if the floor of the

underground hall heaves excessively. The saddle support block can be viewed as a long term shim element, rarely or never replaced. Scenarios have been postulated in which the floor moves up or down over time. Downward motion would be caused by settling of the vessel mass on its foundation floor. Heaving would be caused by reaction to the removal of the large volumes of earth in creating the underground hall.

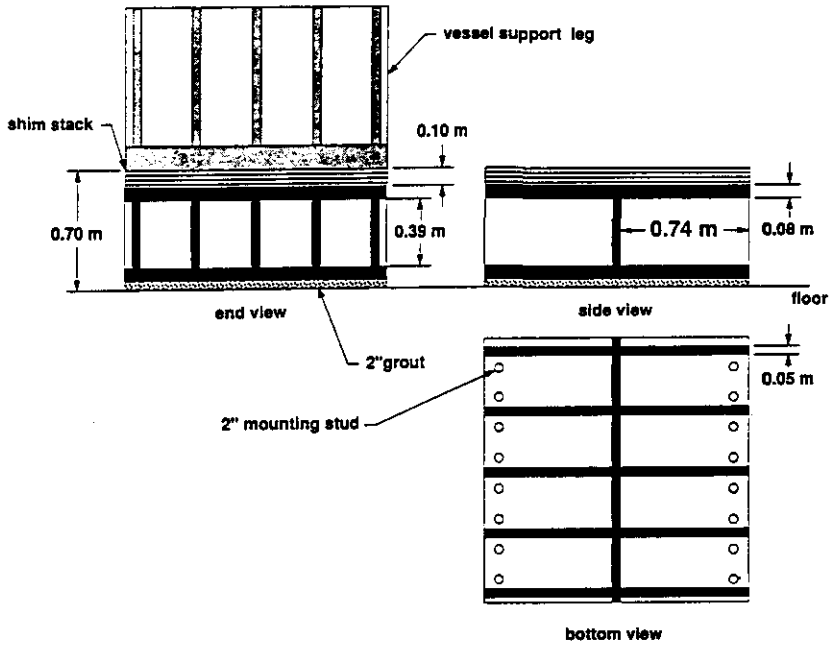

Figure 6-5 Vacuum Vessel Structure Mounting Block (see Figure 6-2 for location of these blocks.)

Initial setup of the saddle support blocks would consist of surveying, v leveling with floor studs, and grouting. Up to two inches of grout may be required due to variations in the floor level, and four inches of sheet metal shims will be supplied for final vessel alignment.

If the floor sinks over time beyond the alignment tolerances of the vessel, shims will be added to the existing shim stacks where necessary. To do this, the vessels will be lifted slightly using the transporters, new shims will be added, and the vessel will be lowered back onto the support blocks. If the floor heaves upward beyond alignment tolerances, the same alignment procedure will be used to remove shims from the shim stack. However, if the floor rises more than the shim thickness, and no shims are left to remove, the support block will simply be replaced with a shorter one.

Transporter

Each vessel is designed to be mobile to allow access for maintenance and repair of the detector subsystems inside. To move the vessels, they must first be lifted slightly to transfer the weight onto the four transporter modules. The actual amount of lift will be limited by the clearance between the sixteen muon sectors supported by the vessel end rings and the central detector supported by the central membrane. Once lifted off the vessel mounting pads, the vessel can be moved on tracks embedded in the experimental hall floor.

A modular transporter unit provides the lifting and horizontal motion functions for the vessel. Four transporters are required to lift each vessel. Each of these transporters consist of hydraulic jacks connected in parallel to the pressure source, nominally providing 900 tons of lifting force. Under each jack is a bearing element for horizontal motion. The bearing element will be either a pressurized grease pad array or roller with 900 ton capacity. The jacks and bearing elements are tied together onto a common mounting structure which can be removed when the vessel is permanently mounted.

Each vessel saddle leg incorporates a lifting point where the transporter is installed for moving the vessel. The four point lift will be load balanced by the common hydraulic system. A hydraulic cylinder driver system similar to the one used at Fermilab for both the D0 and CDF detectors will be employed.

Typical roller profile

A recirculating roller device has been used for many years in heavy movement applications such as this one, and is very reliable. The rollers require a steel track and provide motion in only one direction at a time. Rollers are driven by hydraulic push cylinders mounted to the floor.

Safety Criteria

SSCL seismic design criteria have not yet been developed. Seismic design of the vacuum vessel follows the criteria specified in the Comanche Peak Steam Electric Station Final Safety Analysis Report. Peak ground accelerations are 0.12g horizontal, 0.08g vertical. A factor of safety of 1 is required on seismic stress based on yield strength, according to LLNL Design Safety Standards and ASME Boiler and Pressure Vessel Code..

The GEM vessel is not designed to be code stamped by ASME. However, it is designed and fabricated within applicable rules for allowable stresses in the ASME Pressure Vessel Code, Section VIII, Division 1. Other structural elements of the vacuum vessel are designed in accordance with the Unified Building Code, American Institute of Steel Construction, or American Welding Society codes, as applicable.

Manufacturing Criteria

A Fabrication Specification, in addition to drawing notes, has been generated to provide construction guidance to the vessel manufacturer. Some of the major requirements are listed here.

Cleanliness of the vacuum vessel will ultimately be determined by a rate of rise test after final assembly and leak checking. The rate of rise specification is 1×10^{-2} torr in 24 hours. Welders and weld procedures shall be certified per ASME Section IX. Weld filler rod for 304L shall be 308L. Filler rod for low carbon steel will be determined by the type of weld processes selected. Dye penetrant inspection is required in accordance with ASME Section V article 2 on root pass welds only. Vessel will be leak checked to 1×10^{-5} atm cc/sec helium at 10^{-4} torr. All cylindrical shapes shall be rolled, not brake formed.

Documentation

All calculations will be documented in the vacuum vessel design basis report, including ASME pressure vessel and AISC structural analysis. The complexity of the multiple load types on this vessel demands that a thorough analysis be performed. Magnetic, thermal, vacuum, and seismic loads are all superimposed simultaneously in the finite element analyses.

A Fabrication Specification will document the general fabrication and quality assurance requirements of the vessel. The content of the Fabrication Specification includes specific allowable and recommended practices for material and personnel certification, fabrication, leak checking, finishes, rigging, testing, and documenting the construction.

Calculations

Sufficient structural analysis has been carried out to verify the big features of the vacuum vessel design. Fatigue analysis has not been performed for this vessel, which is not expected to see more than a thousand pump

down cycles in its lifetime. ASME Boiler and Pressure Vessel Code, Section VIII, is used as a guide for allowable stresses, pressure testing, and some elements of weld design. However, strict adherence to the code is typically neither required nor practical for vacuum vessel construction.

The vacuum vessel sees a complex loading due to vacuum, dead load, thermal, magnetic, and seismic loadings. Detailed finite element modeling has determined stresses and deflections of the vessel and support structures (see Fig. 6-6). Vessel stress calculations fall into three categories. Analyses of the vessel containing the cold mass determine the forces the cold mass and supports exert on the vessel and the resulting vessel stresses and deflections. Second, detailed models of the vessel end rings and support structure, with applied loads reflecting the cold mass and other loadings, ensure that sufficient has been used, and verify that there is no local buckling or stress concentration. Third, a model of the entire vessel, cold mass, and possibly the support structure, gives the resonant frequencies of the magnet and vessel and estimates the deflections and stresses due to the expected earthquake ectrum. Analyses were done using the finite element programs NIKE3D[29] and GEMINI[30], and their associated pre- and post-processors INGRID[31], SLIC[32], and TAURUS[33].

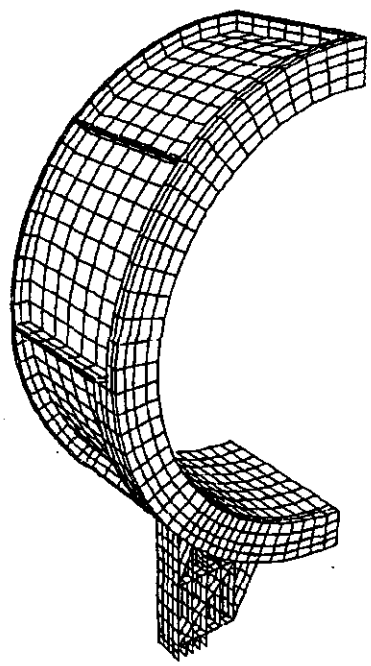

Figure 6-6 Finite element model of the vessel with end ring support structure

A model of the cold mass inside the vessel consists of the coil, radial and axial support rods, and the vacuum vessel. The vessel must withstand the weight of the coil (about 520 metric tons) as well as its own weight. During operation, the coil temperature is 4 K, the vessel is at 300 K, and the connecting rods' temperature varies from 4° at

[29] Maker, B.N., Ferencz, R.M., Halliquist, J.O., "NIKE3D A Nonlinear, Implicit, Three dimensional Finite Elem for Solid and Structural Mechanics User s Manual", University of California, Lawrence Livermore National Laboratory, Report UCRL-MA-105268 (January 1991).

[30] Murray, R.C., "GEMINI-A Computer Program for Two and Three Dimensional Linear Static, and Seismic Structural Analysis-CDC 7600 Version", University of California, Lawrence Livermore National Laboratory, Report UCID-20338 (October 1984).

[31] Stillman, D.W., Hallquist, J.O., "INGRID: A three-dimensional roesh generator for modeling nonlinear systems" ,Univer California, Lawrence Livermore National Laboratory, Report UCID-20506 (1981) Revision 1 (July 1985).

[32] Gerhard, M.A., "SLIC The Interactive, Graphic Mesh Generator for Finite-Element and Finite-difference Application Pms", University of Ca Lawrence Livermore National Laboratory, Report UCRL-MA-108429 (September 1991).

[33] Spelce, T., Hallquist, J.O., "TAURUS: An Interactive Post-Processor for the Analysis codes NIKE3D, DYNA3D, and TOPAZ3D", University of California, Lawrence Livermore National Laboratory, Report UCRL-MA-105401 (May 1991).

the bobbin, to 80 K at the thermal shields about half way along the rods, to 300 K where the rods attach to the vessel. Thermal shrinkage, then, tends to put radially tensile loads on the vessel. In addition, the force that the magnetic field exerts on the coil inside the vessel is about 50 along the beam line, toward the central membrane. The vessel also sees axial end loads of about 12 from magnet loading of the Forward Field Shaper and vertical gravity loads from muon sectors mounted on the vessel end rings. A finite element model of a magnet vessel alone was run using estimates of the loads the coil, FFS, muon sectors, and atmospheric pressure would exert on the vessel. The model had a smaller radius than the current baseline design, only 9.1 m innner radius, but was similar in other respects to the current design. Under these estimated loadings, the vessel had a 26 mm vertical sag, a 21 mm horizontal spread, and an axial tilt of 29 mm. The maximum Von Mises stress in the bulk of the vessel was about 40 MPa.

Three finite element models were created. Two global models, created on two independent software systems, included the vacuum vessel major structural components, such as the support saddles, end rings, longerons, shells, and cold mass. The results of these global models correlated well. A detailed local model of the end ring was created to more accurately assess the stresses and deflections at the cold mass support rod interaction areas.

Gravity, vacuum, cold mass cool down, and magnet activation load cases were independently run for the global model to determine the cold mass radial support rod loads. The dominating load condition which affected the support rods was the cool down of the cold mass, which produced rod loads an order of magnitude higher than the vacuum and gravity loads combined. The magnet load, simulated as a 50 psi internal pressure condition on the ID of the cold mass, tended to relieve part of the load on the radial rods by partially reversing the cool down contraction of the cold mass. All 8 axial support rods were assumed to carry the axial magnet load equally.

Table 6-1 Summary of Global Model Results

Sag of vessel end ring due to gravity:	
12 o'clock vertical sag	0.24"
3 & 9 o'clock horizontal expansion	0.24'
3 & 9 o'clock vertical sag	0.05'
3 & 9 o'clock Z rotation	4.8×10^{-4} radians
Sag of vessel end ring due to other loads combined:	
12 o'clock vertical sag	0.04"
3 & 9 o'clock horizontal contraction	0.02"
3 & 9 o'clock vertical sag	0.01"
3 & 9 o'clock Z rotation	7.4×10^{-5} radians
maximum radial rod load (all load cases combined)	600,000 lb
maximum axial rod load (magnetic load)	750,000 lb
Maximum Z rotation on ID of vessel end ring	8×10^{-4} radians

Table 6-2 Summary of local Results*

Maximum Y displacement	0.032"
Maximum X displacement	0.011"
Maximum Z rotation	2.3×10^{-3} radians

*Based on the global model, the local model was run using the maximum rod loads. The local model did not include gravity loads. The local model is considered to be more accurate for deflection analysis because of its finer detail.

6.2 Thermal Radiation Shields.

The primary function of the thermal radiation shields is to provide a thermal radiation barrier between room temperature surfaces and liquid helium (LHe) cooled surfaces such that the heat load to the LHe surfaces is minimized. To do this effectively, each half coil assembly is totally enclosed in a LN_2 cooled radiation shield. In addition, two areas of the shield assembly will be designed such that the potential high maintenance areas of the magnet, namely the superconducting joints and the cooling-tube-to-manifold weld joints in the LHe plumbing system can easily be accessed.

Thermal radiation shields are required in three locations. The shields must be inserted between the outer vacuum vessel wall and the half coil assembly (outer panels), between the half coil assembly and the inner vacuum vessel wall (inner panels), and at both ends of the half coil assembly (end caps). This will provide an enclosure which effectively stops all room temperature radiation from having a direct line of sight to a LHe surface (Figure 6-7). The panels are nominally 0.32cm (0.125") thick, 3.7m (145") wide and 14.6m (575") long and made from 6061-T651 aluminum sheet. Aluminum angle and plate stock is welded to the sheet (Figure 6-8) in a box type configuration so that the large panel will retain some structural rigidity. This box area will also be used as a framework and attachment points for the superinsulation. In addition, a 4.45cm (1.75") square extruded 1100-0 aluminum tube with a 3.5cm (1.38") hole serpentines back and forth across the length of the panel and is skip welded to the panel using the GMAW process. Tubes are spaced apart every 15 degrees which corresponds to a tube to tube spacing of approx. 2.5m (98") This allows for a 0.5K maximum change in temperature at the hottest point on the panel from the nominal LN_2 temperature (80 K) assuming a very conservative heat load of 1.0 watts per square meter. LN2 will circulate through this tube to provide the cooling medium at a mass flow rate of 100 grams/sec. The LN_2 flow will start at the bottom end of each half coil and via series flow, traverse up through each panel. The LN_2 panel flow circuits are divided into two halves about the vertical axis of the coil so that each cryogen circuit services half of the panels, thus reducing overall pressure drop (Figure 6-9). Calculated pressure drops are 0.18 psi for single phase flow and 4.0 psi for fully developed two phase flow. Panel to panel tube joints will be made utilizing an automatic tube welder. Joints made using this technique are extremely reliable at cryogenic temperatures and the use of 1100 aluminum for the tube material guards against crack propagation concerns at the weld joint. Weld tests are currently being conducted to validate this fabrication technique. Each half coil assembly requires 16 outer and 16 inner panels, making a total of 64 panels required for the entire magnet. Both panels are constructed identically with the exception that the inner panels are slightly smaller than the outer panels because of its smaller radius.

Superinsulation will also be used to minimize the heat load to the LHe cooled surfaces. It will consist of 1/4mil (0.00025") thick polyester film with one side having a high purity aluminum deposit of 250 angstroms. Approximately 10 to 20 layers of superinsulation will be applied separately to both sides of the thermal radiation shields. They will be installed in blankets with each blanket having 5 layers of superinsulation each. This will decrease the radiation heat load to both the LHe and LN_2 cooled surfaces since the emissivity of the assembly decreases by at least an order of magnitude.

The thermal radiation shields will be supported off the vacuum vessel utilizing a pin-in-slot arrangement. Low thermal conductivity fiberglass blocks with slotted holes will be bolted to steel blocks that are welded onto the inner and outer vacuum vessel. Epoxy-fiberglass pins will be attach to the LN_2 panels and ride in the slots provided. This will allow for the panel movement required due to thermal contraction of the long shields as it cools from room temperature (300K) to LN_2 temperature (80K). The fiberglass blocks supply adequate structural support yet provide enough thermal resistance so that the vacuum tank is not subject to cryogenic temperatures and potential embrittlement and fracture toughness concerns. The long panels will be attached to both the inner and outer vacuum vessels prior to the installation of the half coil assembly. This will allow ease of access for panel installation and also allow for cold testing and leak hunting of the LN2 system prior to final coil installation. During cooldown the panels will contract approx. 6 cm (2.4") in length and 1.5cm (0.6") in width. Two of the panels will have removable sections for access to the superconducting joints and LHe weld joint areas. The end cap shields will be made up of aluminum C-shaped segments and cover the end of the half coil assembly and overlap the inner and outer panels. They will be attached to the ends of the long LN2 panels which will provide structural integrity and

also conduction cooling since the end caps will not be actively cooled. This will provide a complete LN2 shielded enclosure to ensure minimum heat load to all LHe cooled surfaces on the half coil assembly. All LN2 tubing joints will be made at the end of the half coil assembly away from the central detector support. Ports will be located on the end flange of the vacuum vessel so that access to all weld areas is possible for tube repair and leak hunting.

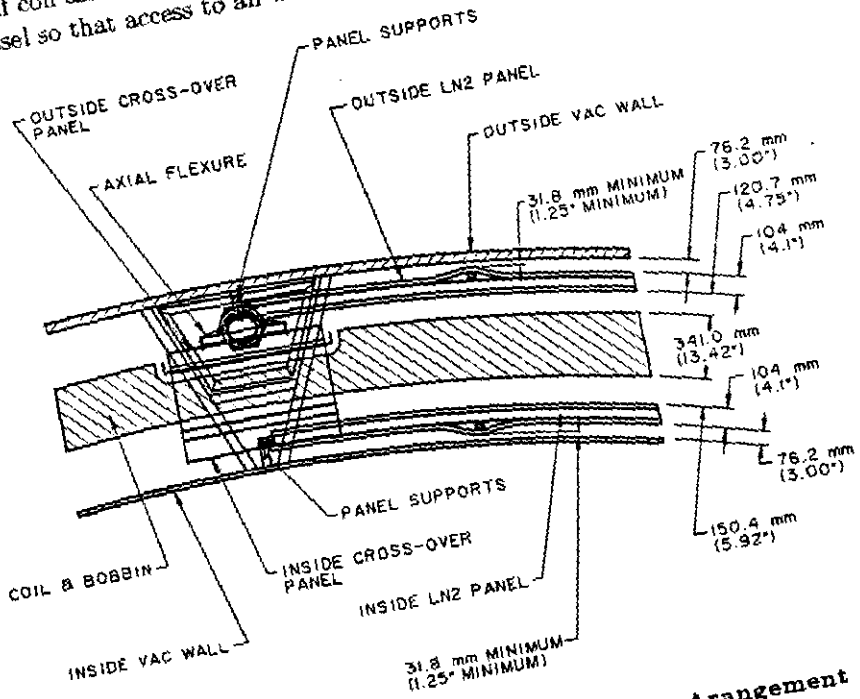

Figure 6-7 Thermal Radiation Shield Arangement

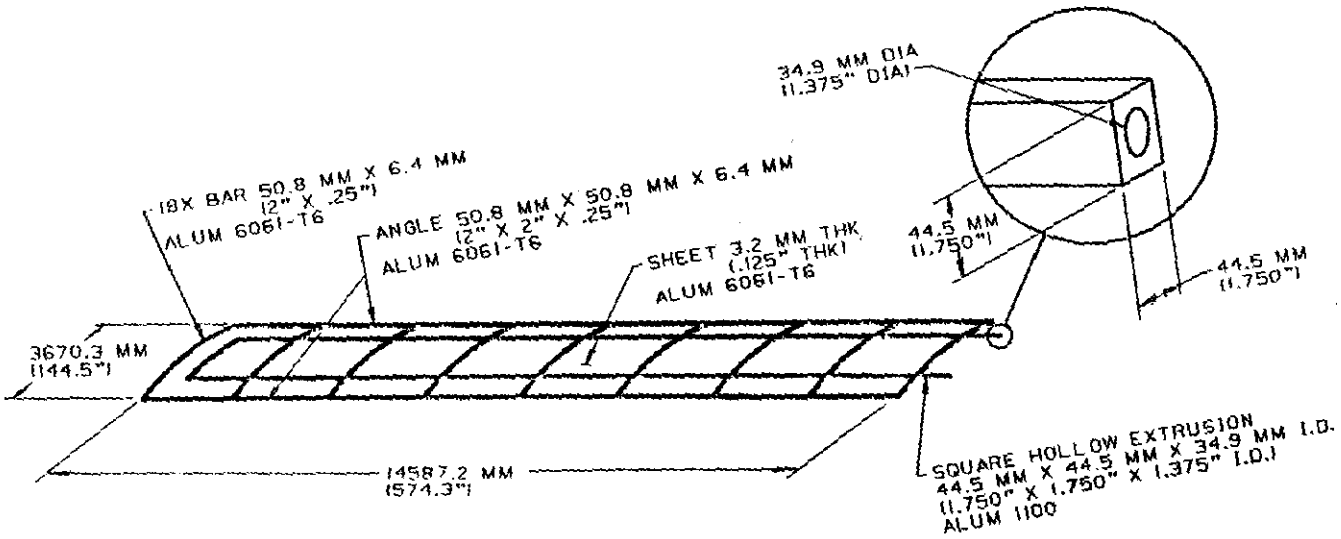

Figure 6-8 Thermal Radiation Shield, Detail

12/1/92

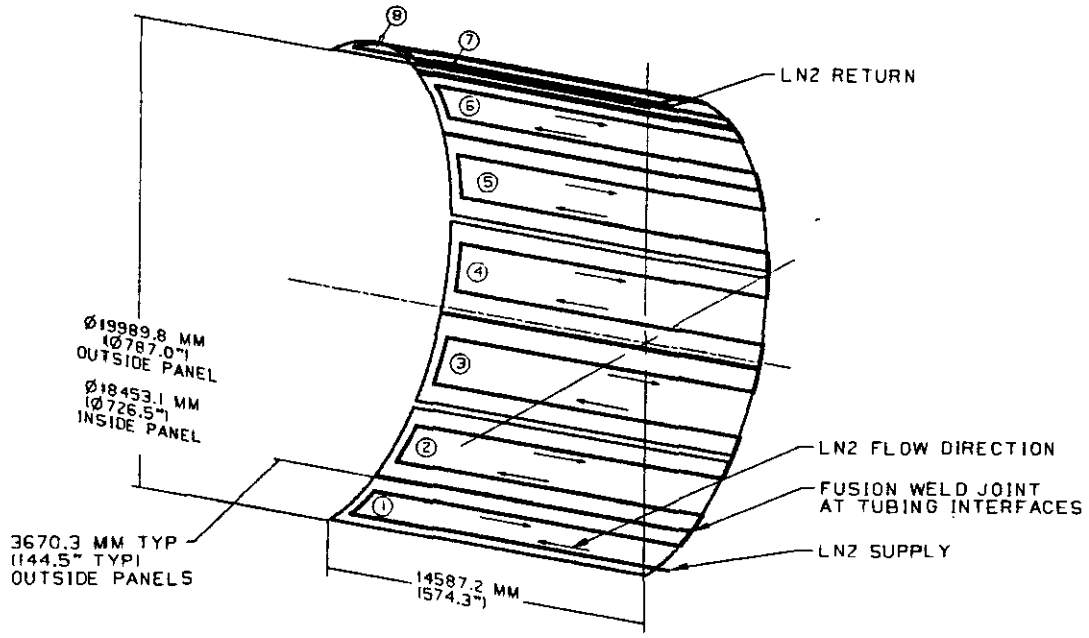

Figure 6-9 Liquid Nitrogen Flow Assembly

6.3 Cold Mass Supports.

The function of the cold mass supports is three fold: to support the static weight of a half coil assembly (520 metric tonnes per half coil), to maintain the magnetic alignment of the coil to the beam axis and to counteract the axial magnetic force exerted by the coil when energized (52 mega-newtons per coil half). In performing these functions the supports must also minimize the heat load to any LHe cooled surfaces and also allow for thermal contraction of the half coil without inducing any additional stresses and consequent distortion to the assembly. The half coil assembly will contract approx. 8.1 cm (3.2") on the diameter and 6.1 cm (2.4") axially as it cools from room temperature to LHe temperature.

The cold mass support rods are divided into two types: radial rods and axial rods. The radial rods support the static weight of the half coil assembly and allow the coil to contract symmetrically about the beam axis so that the magnetic centerline of the coil remains constant. The radial supports are nominally 7.6 cm (3.0") diameter 6A1-4V titanium rods approx. 3.4 m (132") in length (see Figure 6-10). One end of each rod has a spherical bearing which attaches to the outside flanges of the LHe cooled (4K) half coil assembly. The other end of the support rod is threaded and attaches to the room temperature vacuum vessel via a spherical washer/nut assembly. The use of these spherical bearing surfaces eliminates any bending moment the rods may be subject to during cooldown from room temperature (300K) to LHe temperature (4K). A tension preload is exerted on each rod in paired assemblies so that the rods are always in tension during all cooldown and steady state operating scenarios. This preload is maintained by a series of Belleville spring washers that are at the warm end of the support rod. The magnitude of the preload is determined by equalizing the pressure in the hydraulic cylinders that tension the rods so that a uniform preload can be applied to all of the rods. The radial rods are oriented in pairs about the circumference of the coil, spaced at 45 degree increments and aligned tangent to the circumference. Eight pairs of rods are required for each coil end, making a total of 32 pairs or 64 individual rods required for the entire magnet. As the coil assembly cools down from 300K to 4K, it contracts both radially and axially. The radial support rods rotate toward the beam centerline during this transient time using the spherical bearing surfaces provided, and allowing the half coil to contract uniformly about its horizontal axis. This design preserves the position of the magnetic centerline of the coil relative to the beam centerline of the system. The rods also continue to support the static weight of the coil.

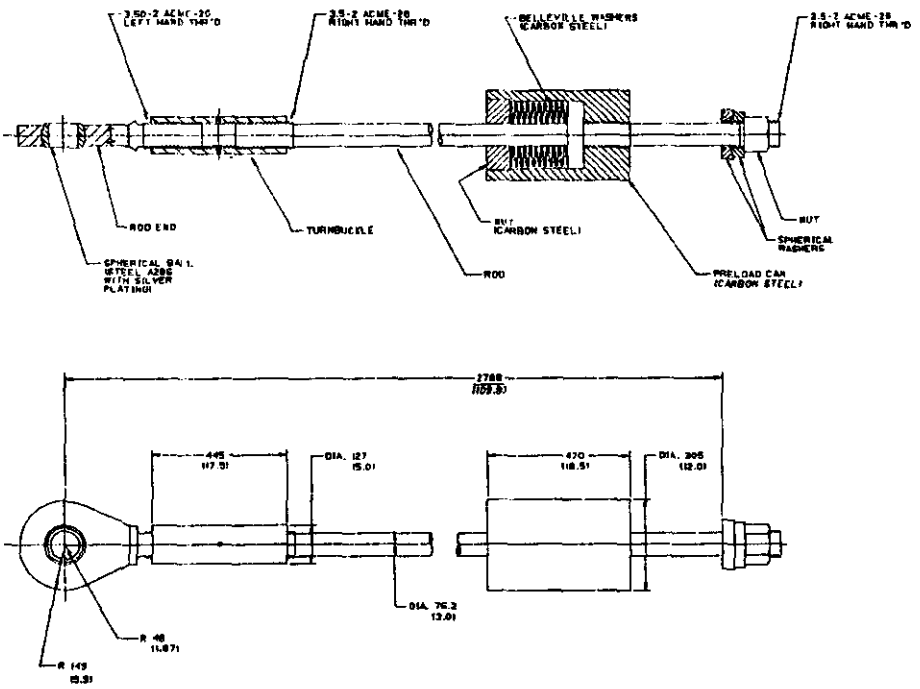

Figure 6-10 Radial Supports Rods

The axial support rods' sole function is to counteract the load on the coil due to the magnetic forces generated when energized. They resemble a large oar being normally 45.7 cm (18.0") wide, 5.1 cm (2.0") thick and 7.5 m (295") in length. One end of the rod is threaded allowing for length adjustment during final assembly and utilizes a spherical washer/nut assembly (see Fig. 6-11). The axial rods do not need pretensioning as they do not see any load until the magnet is energized. Once energized, the rods are under tension and are sized such that the stress in the rods is 1/3 the allowable yield stress for the material. The cold end of the rod are secured in wedge-shaped depressions which are machined into the outer surface of the coil bobbin about its centerline. The warm end of the flexure is attached to a stiffening member welded to the vacuum vessel which also is the attachment point for the radial rods (Figure 6-4). Eight axial rods are spaced at 45 degree intervals about the circumference of the coil and are used to counteract this magnetic load (Figure 6-12). The rods are placed so that they transfer their load to the eight large longitudinal support members that are welded to the outside of the vacuum vessel. The two half coils tend to be attracted to one another when energized so that the net force at the centerline of the detector is zero. Therefore, the axial support rods are placed on the outside half of each half coil assembly so that the rods are always under tension. The axial rods also secure the half coil assembly in the z-direction.

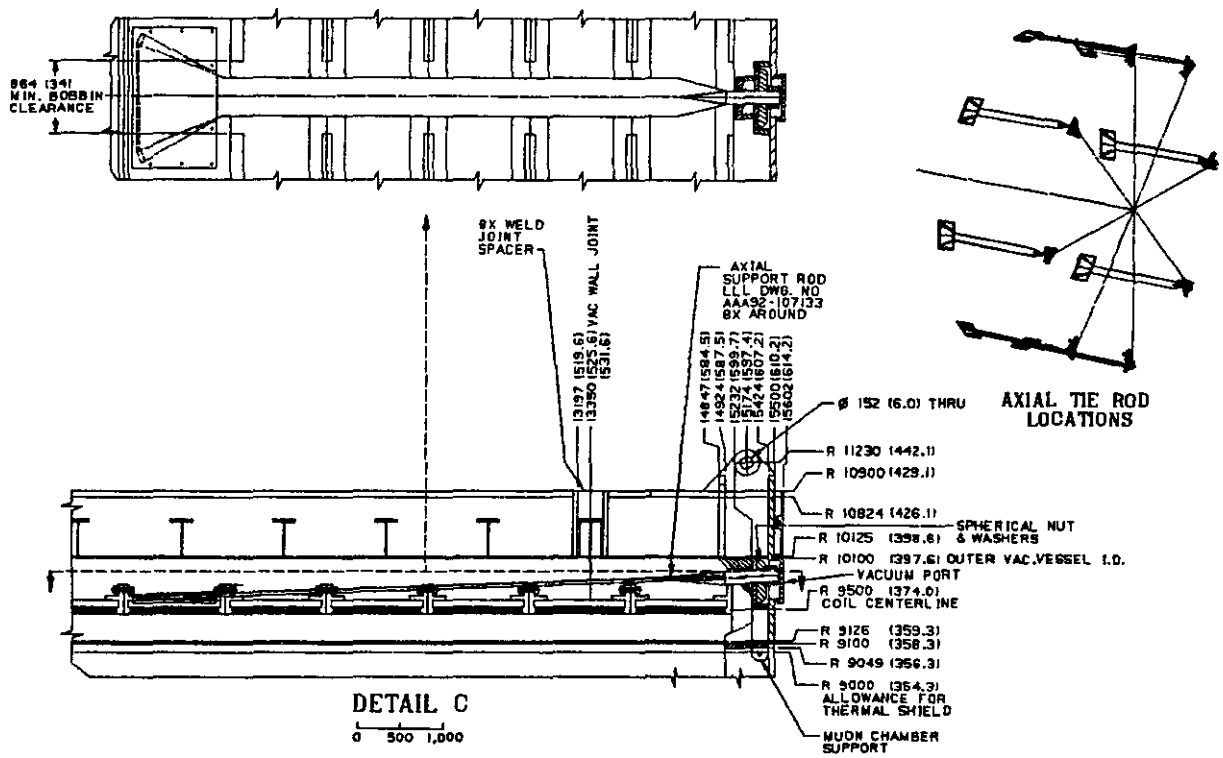

Figure 6-11 Radial Support Rod, Detail

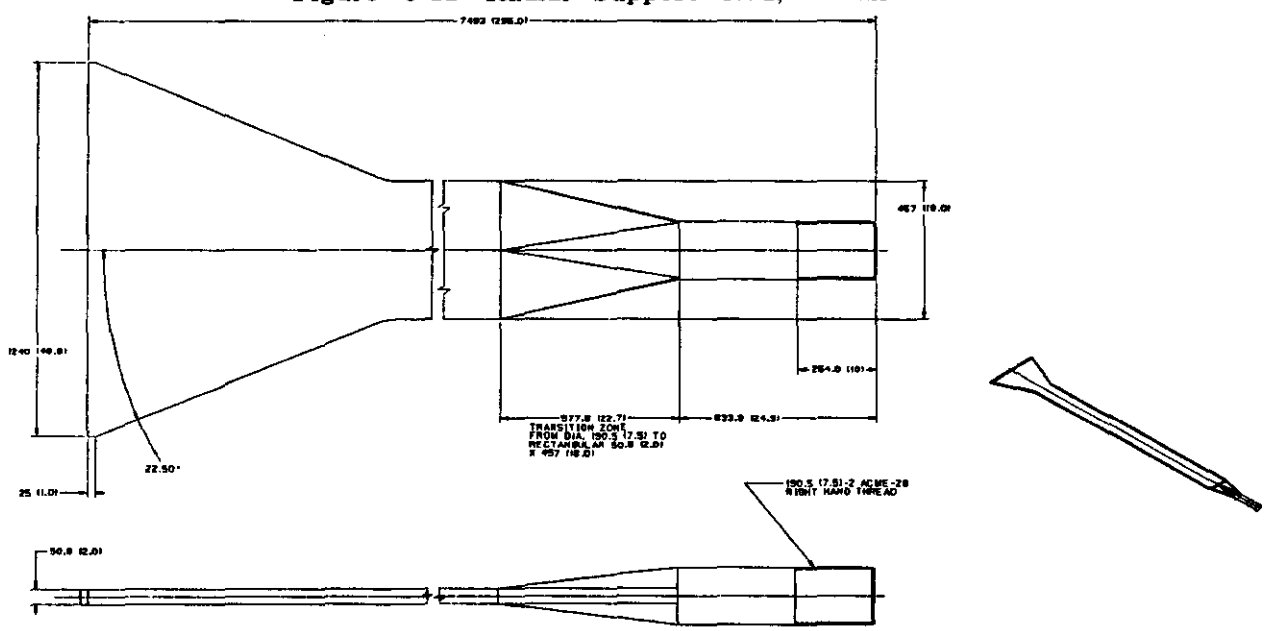

Figure 6-12 Axial Rods

The size, quantity and material of the supports are governed by the following considerations: space available inside the vacuum vessel which governs both the size of the support and their position, minimization of LHe consumption (thermal conductivity material issues), yield strength of material, minimization of distortion to the half coil assembly at the support attachment points and access to the supports for both initial installation and

tensioning under all anticipated work configurations. Based upon the above requirements, titanium 6Al-4V material was chosen. It has a slightly lower thermal conductivity than 300 series stainless steel, which helps minimize LHe consumption but more importantly, has a yield strength of approximately 130ksi at room temperature, about a factor of 4 better than stainless steel. This helps reduce the overall size of the supports and also the number required. Eight areas (hard spots) on each coil assembly end and at the center of the coil form were chosen to take the weight and magnetic loads. This allows for the stresses to be distributed about the entire circumference of the coil assembly so as to not induce significant stress concentrations and consequently large distortions to either the coil assembly or the vacuum vessel. In addition, it reduces the number of components, considering cost, ease of assembly and installation, size, etc. These areas also correspond to hard spots on the vacuum vessel so that there is a direct one to one correspondence between the load carrying area on the vacuum vessel and the coil assembly.

Both the radial and axial supports have LN2 intercepts attached to them to reduce the overall LHe heat load. These intercepts are placed approximately halfway along the length of each type of support and provides a thermal short to LN2 temperatures. Using this concept, the LHe heat load imposed by the radial rods is about 60 watts and the axial rods about 35 watts. These values are well with the estimated heat load budget contemplated for the cryogenic system. This concept uses LN2 as the "sacrificial" cryogen since its cost is significantly less expensive than that of LHe and assumes an average intercept temperature of approximately 100K.

Structural Analysis of Cold Mass and Supports

The magnet coil and supports see a complex combination of loads from gravity, thermal changes, and magnetic forces. Although hand calculations are sufficient for initial sizing of the cold mass bobbin and support rods, detailed finite element analysis has been required to characterize the load distributions and resulting deflections and stresses. The initial load case is gravity alone, which occurs after final assembly up to operation. A second case models the shrinkage of the cold mass and its effect on connections and supports. Finally, the magnet loads are simulated, which are represented as distributed body forces in the cold mass both in the radial and axial directions.

The aluminum bobbin was assumed to act as the only structurally viable element in the model of the cold mass. Although the coil windings did not contribute to the strength of the cold mass, they were included in the weight. The resulting 526 tonne structural model of the cold mass was a bobbin with a density increased to include the weight of the windings.

Gravity Loads

Figure 6-13 shows the configuration of the radial rods about the coil. Most of the coil weight is carried by four of the radial rods in tension at each end of the cold mass. The maximum rod load is 0.6 MN (135,000 lbf), corresponding to a nominal axial stress of 74 MPa (10 ksi). The bobbin displaces downward at about 3 mm (0.12 in.) and is out of round by about 4.5 mm (0.18 in.). bobbin stresses due to gravity loading are about 4 MPa (0.6 ksi). The conclusion is that with gravity considered alone, the design is very conservative.

Although the axial rods' primary function is to carry axial magnetic loads during operation, they also are required to hold the entire dead weight of the cold mass during the vertical assembly sequence of the magnet. This cold mass weight is transferred to the radial rods as the magnet assembly is rotated from axis vertical to axis horizontal orientation. An analysis has been performed to prove that during this rotation operation, loads in the axial rods do not exceed those when the magnet assembly is in the vertical position. Similarly, radial rod loads are maximum when the magnet assembly is in the horizontal position. Because the axial rod loads in the vertical assembly scenario are an order of magnitude less than the operating magnetic loads, they are addressed in the following section.

Thermal Loads

When the coil is cooled from 300 to 4K, it contracts both radially and axially. If unconstrained, it would shrink 80 mm (3.1 in.) in diameter and 60 mm (2.4 in.) in length. However, the radial support rods tend to resist this shrinkage and pull the coil our of round. The finite element model produces conservative results for both the out of roundness and rod loads during coil shrinkage, because the radial rods were modeled as beam elements, which assumed a solid member for its entire length. In reality, the design of the radial rods also includes a compliant section at the warm end to absorb the rod strain induced by the radial shrinkage of the cold mass. This compliant end consists of a compressive stack of Belleville washers which have a spring rate much less than that of the rod. Therefore, axial forces produced by the finite element analysis are very conservative. In addition, due to the dame modeling assumption of fixed rod ends, it is possible to see a compressive load on the rods in the gravity analysis. Column loading cannot occur in the real system due to the design of the compliant end of the rod. Despite these differences, the finite element model bounds the problem and the resulting stresses, allowing a sound design to be generated. The model of a shrinking coil with no rod shrinkage results in radial rod loads of 0.3 MN (67,440 lbf) tension, corresponding to a stress of 63 MPa (9.5 ksi). Coil stresses from reacting these loads are 4 MPa (0.6 ksi). Maximum coil shrinkage in the constrained condition is the same as in the unconstrained condition.

The axial rods do not significantly resist the radial shrinkage of the cold mass since they are nearly parallel to the coil axis and are designed to flex in the radial direction with low strain. During axial shrinkage, both ends of the cold mass move toward the center plane where the axial rods are connected. No load is generated in the axial rods from axial shrinkage of the cold mass.

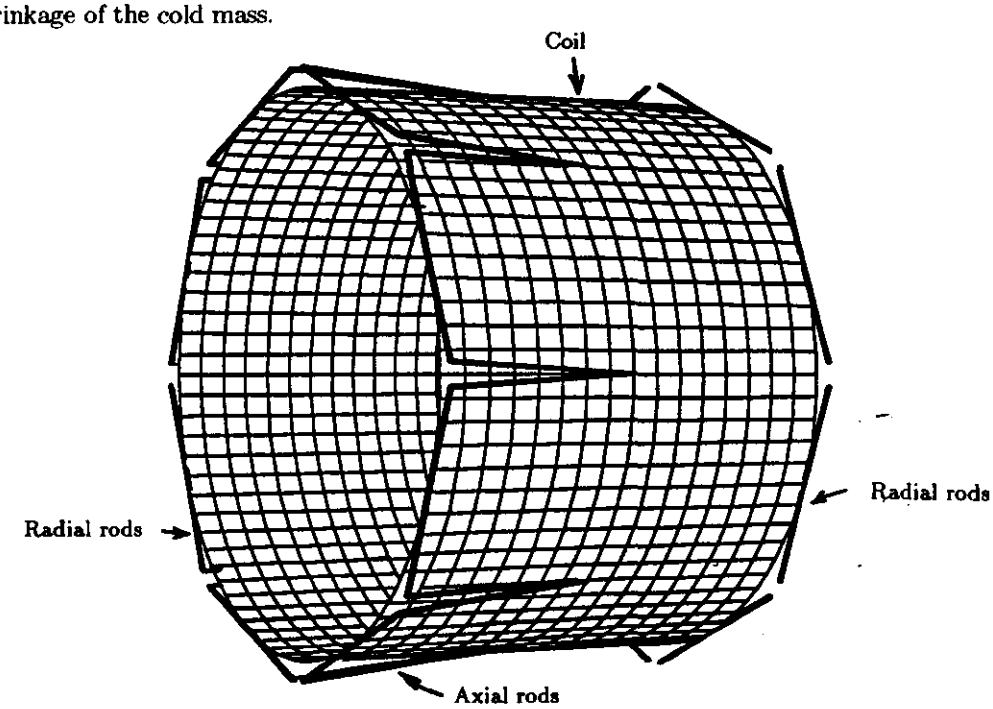

Figure 6-13: Finite element mesh (NIKE3D) used with gravity, thermal, and magnetic loadings, consisting of the magnet coil and its radial and axial support rods.

Magnetic Loads

Magnetic loading has radial and axial components. The coil windings inside the bobbin exert an equivalent outward radial pressure of 0.32 MPa (0.05 ksi), estimated from the values of the operating magnetic field. An axial force of 52 MN (11.2 million lbf) is exerted on the bobbin in the direction of the central membrane. These loads were applied to the finite element model of the bobbin with the axial and radial support rods. Fig. 6-14 shows von Mises stress contours for combined magnetic loads. The radial pressure induces a hoop stress in the coil of 40 MPa (6 ksi), expanding it 10 mm (0.4 in.) in diameter. Note that this tends to reduce the rod loads created by the shrinking coil

in the thermal analysis. The axial force makes the cold mass displace 25 mm (1 in.) axially due to strain in the axial rods. Nominal tensile stress in the axial rods is 280 MPa (42 ksi), assuming 8 rods having a 2" × 18" cross section.

Combined Loadings

Gravity, thermal, and magnetic loading were applied to a model of the cold mass with support rods. The magnet loading was the dominant effect on the axial rods, while the thermal and gravity loads mainly affected the radial rods. The resulting global bobbin von Mises stress was at an acceptable value of 40 MPa (6 ksi), mostly due to the radial magnetic pressure. The maximum load von Mises stress was at the rod attachment points, reaching 72 MPa (10.4 ksi). The middle of the cold mass translated 25 mm (1 in.) axially, while it shrank 60 mm (2.4 in.) in length. Radial thermal contraction overcame expansion due to radial magnet loading, resulting in a net shrinkage of 80 mm (3.1 in.) in diameter. The cold mass was out of round by 6 mm (0.2 in.) at its ends. It is concluded that the current baseline design will exceed safety requirements and is consistent with meeting all functional and engineering requirements.

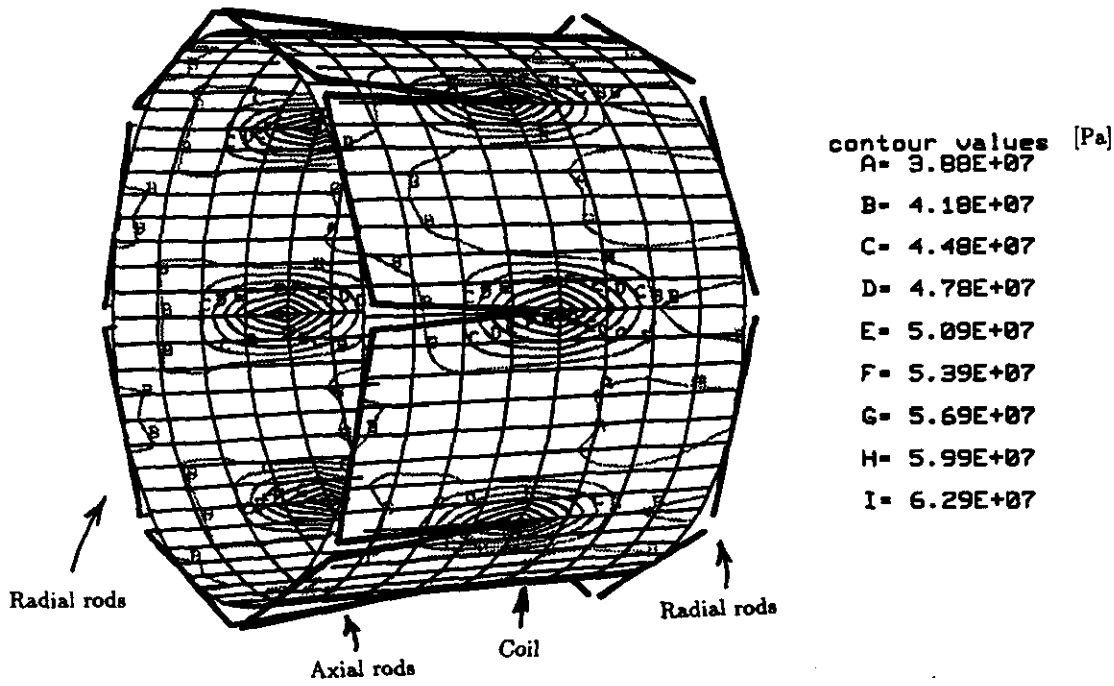

Figure 6-14: Magnet loading: contours of Mises equivalent stress in coil, from finite element analysis (NIKE3D). Loads on Axial support rods are 3.2 MN.

6.4 Magnet System Assembly.

The magnets will be assembled as two independent halves. The function of magnet assembly is to place components within the vacuum vessel into an integrated magnet that is ready for final installation and acceptance testing. The assembly of components will be engineered so that the performance of the magnet is assured. The sequence is designed to meet the overall program schedule and accommodates the beneficial occupancy dates of assembly areas and the detector hall. Parallel activities are planned whenever possible to assure timely delivery. A detailed Manufacturing Plan has been prepared that describes in detail the assembly steps and the equipment,

procedures and facilities required to assemble and test the magnet at the IR5 site. The description below summarizes that plan.[34]

Several assembly options have been identified. They can be classified into two main categories; assembly of components with the axes vertical or assembly with the axes horizontal. While each assembly method has strengths, we believe that the baseline presented here is the minimum cost approach consistent with acceptable handling risk. The baseline assembly approach presented here was developed in conversations with vessel and magnet fabricators, qualified rigging specialists and engineers experienced with large special equipment handling. The baseline approach requires assembly of all heavy components with axes vertical followed by the uprighting of each magnet assembly prior to its preparation for movement into the detector hall. It allows the vessel fabrication and the coil winding and assembly to be carried out in the most favorable orientations, with the axes vertical. It allows the liquid nitrogen thermal shields between the warm vessel skin and the cold coil mass to be assembled and leak-checked in the most accessible orientation. It reduces the number of special handling fixtures to a minimum. The biggest risk is rotating the assembly. Rotating a single 1500 Ton magnet assembly rather than rotating numerous 200 T to 800 T subassemblies requires additional lift capacity. But a number of qualified riggers with experience in rotating large pieces of equipment claim 1500 T is well within their capacity. Whether one rotating of 1500 T section or three or more smaller subassemblies, each lift must be carefully engineered applying appropriate practices, procedures assurances and reviews conforming to DOE rigging and handling standards[35].

Assembly of large super conducting systems can be hindered or aided by the methods chosen to carryout leak detection of components destined for the vacuum chamber. The investment in rigorous leak-hunting first of components and then of sub-assemblies as they are assembled, will pay off later with a shorter and more predictable assembly schedule. The objective is to assure each potential leak has been eliminated prior to combination with large numbers of other potential leaks. Prior to completing preliminary design a preliminary leak-hunting plan will be generated, that will assure that leak-detection issues are considered as part of the component design requirements. Leak detection should occur on systems that approximate the final condition of the assembly (e.g. cold, strained, etc.) as closely as possible. This discipline assures the minimum confusion as larger and larger systems are integrated. It is the strong recommendation of leak detection experts for assembling complex systems[36]. Table 6-1 identifies measures of insuring quick and successful leak detection.

Table 6-3 Measures to mitigate failures of systems not readily accessible after assembly

Components	Potential reason to need access	Mitigation measure to eliminate need for ready access
		Most vacuum vessel systems are readily accessible after assembly
Vacuum vessel	unacceptable vessel vacuum leaks	Use good vacuum practice and assurances in design and fabrication Design vacuum welds for external repair Leak hunt and repair prior to installing other components Verify leak-tightness after major lifts Engineer lifts and uprighting to minimize unwanted strains in the vessel Design the external vacuum for extra capacity if needed Provide extra high-conductance vacuum ports on the outer vessel

[34] GEM Detector Magnet On-Site Fabrication, Assembly and Installation Plan LLNL-GEM-92-049.
[35] DOE RDT Standard F8-6T Hoisting and Rigging of Critical Components and related Equipment 1980.
[36] Wilson and Beavis, Handbook of Vacuum Leak Detection, AVS Monograph Series, 1976

Table 6-3 Measures to mitigate failures of systems not readily accessible after assembly (cont.)

cold mass supports and axial rods	structural failure	Conservative design, proper materials choice and detailed analysis for • Magnetic Fault cases • Lifts and upsetting Proof test all load bearing members at temperature to 125% maximum load
support rod LN intercepts	LN shunt leak	Use good welding practice for design, qualify welders and procedures Evacuate and carefully leak-hunt during assembly Provide redundant LN supply lines to allow valving off one leaky system Provide an external method to evacuate the leaking system
	LN shunt	Redundant LN shunts on the cold mass support
	thermal detachment	Provide temperature sensors on the strut to estimate the He heat load Extra capacity in the LHe system If these fail significantly, provide extra refrigeration
LN panel	supply line vacuum leak	Use good welding practice for design, qualify welders and procedures Evacuate and carefully leak-hunt during assembly Cold leak hunt in the vacuum vessel prior to installing coil assembly Redundant LN supply lines on each panel to allow valving off one leaky conduit Provide an external method to evacuate the leaking system
Multilayer thermal insulation	Thermal short	Use proper procedures at assembly Thermal shorts are not likely to fail catastrophically Extra LN and LHe refrigeration capacity provided Assembly in clean, dry, dust-free environment
Temperature sensors	fail to give believable temperature	Verify sensor reliability prior to specification Provide secure mounting points with adequate strain relief Position near access ports where possible Provide redundant sensors where access is not possible
All LHe supply line	cold vacuum leak	Design external pumping system tolerate a large He leak; 0.1-1.0 atm-cc/s Use good welding practice for design, qualify welders and procedures Leak-hunt components at LN temperatures prior to installation Make all vacuum joints accessible through ports Provide seamless tubing between access ports Provide external isolation methods to allow easier leak-detection
	plugged	Purifiers and filters on all cryogenic inlets Warm if necessary
Electrical wiring	electrical system failure	Proper selection of wiring and protection Minimum wiring in the vessel, provide access ports Redundant systems

Table 6-3 Measures to mitigate failures of systems not readily accessible after assembly (cont.)

Oil diffusion pump	Oil migration	Provide reliable backing pumps Provide LN or water-cooled traps
	Oil blown into tank	Provide fast-acting isolation valves Provide extra refrigeration in the event that the oil degrades vacuum Seal the conductor pack to assure oil doesn't degrade insulation Use a benign grade of diffusion pump oil
Coil assembly	Unlikely super conducting, electrical or structural failures	Provide a R&D Program to assure all components in this application Use only adequately certified materials and components Prove all systems by analysis and analogy Provide the highest level workforce proper training and assurances Formal certification prior to installation Engineered supports during lifts and uprighting Diagnose and fix by cutting through vacuum vessel wall
	vacuum leak	Design external pumping system tolerate a large He leak; 10 atm-cc/s Use reliable, good welding practice for design, qualify welders and procedures Leak-hunt at LN temperature and high pressure prior to installation Make all vacuum joints accessible through ports
Conductor splices splice He supplies Voltage taps	Unlikely	Provide a R&D Program to assure all components in this application Provide access ports to all coil splices
Coil leads	unlikely	Provide for external disassembly and refurbishment of all components

Assembly Sequence

Magnet Assembly

Magnet assembly begins with the stacking of the 43 metric Ton coil segments. Twelve 1.2 m-long coil segments are required to make up a half coil assembly. (Fig 6-15) Each half coil assembly weighs approx. 520 metric tons and is 14.4 m long. Each coil segment will be wound in the South Assembly Building. As the coil segments are completed, they will be transported to the North Assembly Building (NAB) where they will be assembled together. In the NAB the overhead crane will be used to transport the coil above the in-process assembly, where the flanges can be bolted together and the conductor joints made.

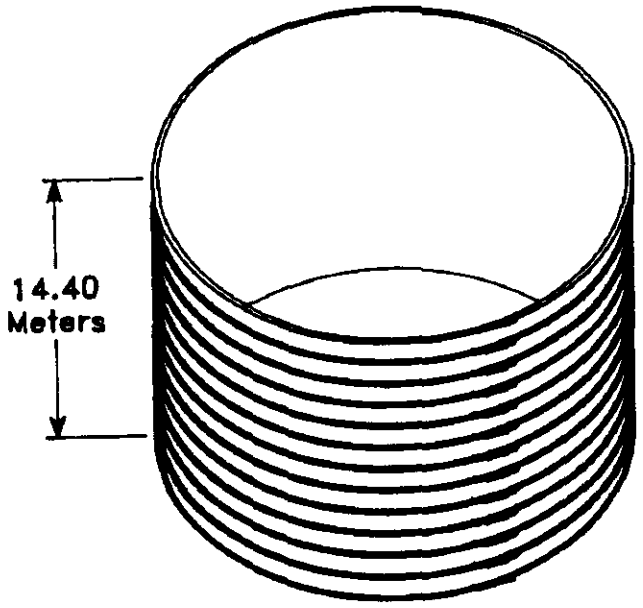

Half Coil Assembly
520 Metric Tonnes

Fig 6-15 **Twelve 43-ton coil segments are assembled with the axes horizon tall to forma half coil assembly.**

Another assembly option under consideration is assembly for underneath. In this scheme, a special lifting fixture will be available to lift the completed coil segments so that the next segment can be inserted underneath the assembly. In this way, the overall height of the coil assembly building can be reduced since the segments do not have to lifted over one another. They are inserted from the bottom up rather than from the top down. Eleven splices are required to link the twelve coil segments together. The final product will be a completely assembled half coil.

Each half coil assembly will have provisions for movement to the assembly and staging area outside of the magnet assembly building, where the heavy lifts will take place. The half coil will be certified as ready prior to further assembly into the vacuum vessel. All He manifolds and lines to the conductor, the bobbin, the joints and to the leads will be verified as leak-tight and free of blockage. These lines will be temporarily capped to prevent inadvertent contamination during handling. The conductor insulation and splices will be enclosed and protected from dust and weather conditions whenever the assembly is in weatherproof enclosures. A ground-fault indicator with a loud alarm will be attached to immediately alert technicians or handlers in the unlikely event that the ground plane insulation has been shorted. The bobbin flange bolts that join each coil segment and provide a primary structural support for the coil weight and magnetic forces will be certified as properly installed, torqued and locked. The lifting and support hardware attached to the half coil assembly will have been load-tested and certified for use. The attachment points will be inspected and approved. All diagnostic systems and sensors such as voltage taps, liquid level indicators, temperature sensors and strain gauges will be verified as operational and protected from inadvertent mishandling. When the cold-mass has been inspected as ready for assembly it will be covered with removable weatherproofing and moved to the assembly area.

Several other key components are fabricated and sub-assembled in parallel activities to the half coil assembly. The thermal radiation shields, the cold mass support rods, the current leads, and a large fraction of the cryogenic piping internal to the vacuum vessel will be fabricated and tested off-site at the vendor's place of business and then shipped to SSCL.

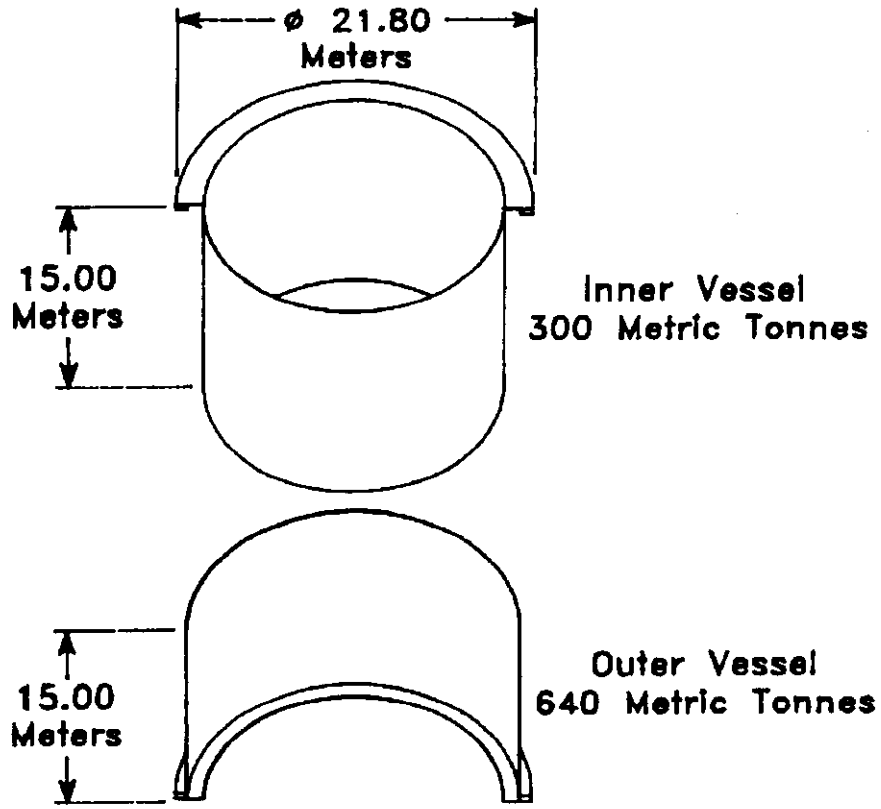

Fig 6-16: **The inner and outer vacuum vessel shells will be erected in the most favorable position, with each axis vertical.**

Vacuum Vessel Preparation

Because of its large size, the vacuum vessel must be erected on site. The vendor will fabricate the largest possible vessel components at fabrication facilities but the erection of these components into the final vessel configuration will be carried out in the staging and erection area next to the magnet assembly hall. All experienced vendors contacted stated that conventional practice leads to erection with axes vertical for the inner and outer vessels, followed by a vacuum-leak hunt and acceptance testing (Fig 6-16). The joints between the inner and outer vessel flanges will be temporary and demountable allowing successful, rapid leak detection and repair prior to restricting access to the joints during subsequent assembly. Acceptance testing of the vessel will assure it is ready for further assembly. Following vacuum certification for base pressure, leak-rate and rate-of-rise; the vessel will be inspected for key form and function dimensions and features, including inspection of assembly tolerances and certification of critical lift points. After certification, the vessel will be disassembled into the two primary parts by grinding the temporary seal welds. The vessels are still oriented with axes vertical to provide optimum access for the next step.

LN Panel Assembly on the vacuum vessel shells

The next step is the installation, plumbing and leak-hunting of the LN panels and multilayer thermal insulation simultaneously on the inner and outer vacuum vessel shells. (Fig 6-17) The LN panels will be cold leak-hunted as subassemblies prior to delivery to the SSCL. The LN subassemblies are mounted on the inside of the shell. The aluminum LN tubing is then formed and cut to the proper length and butt welded together using an automatic tube welder. Mounting the panels on the vacuum vessel shells saves a significant amount of time from the

assembly schedule since the completion of the vacuum vessel is likely to precede the completion of the half coil assembly by many months. This operation will take place at assembly stations in the North Assembly Building after each vessel segment has been cleaned and moved indoors. After the tube welds have been leak-checked and repaired, the two vessels segments will be cleaned and protected from the weather. The LN panels will be certified as leak-tight and the multilayer insulation will be inspected to assure that it is properly supported and has no apparent thermal shorts. The assembly of the LN panels and supporting manifold and sensors can be carried out within the magnet assembly building if space allows.

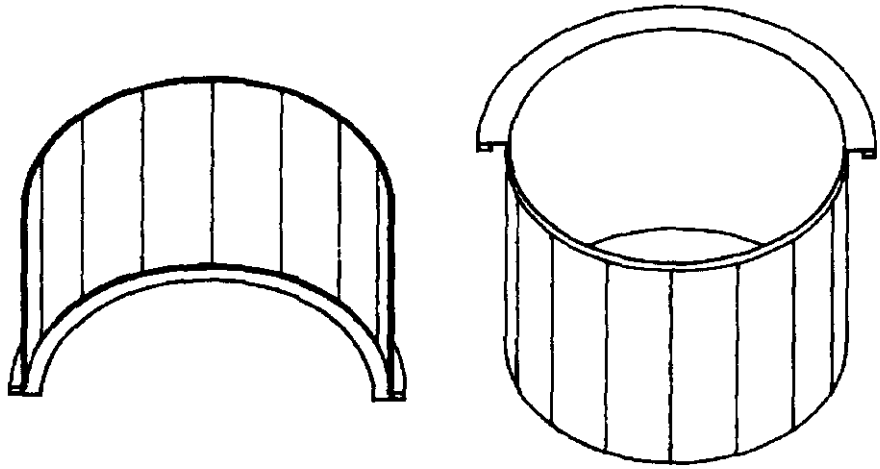

Liquid Nitrogen Thermal Shield Assemblies

Fig 6-17: The Liquid Nitrogen Panels and multilayer thermal insulation are assembled inside of both vacuum vessel shell simultaneously.

Install the inner vacuum vessel assembly in the half coil assembly

When both the inner vacuum vessel assembly and the half coil assembly are ready for mating, both will be moved to the assembly area and prepared for lifting. The half coil assembly will be protected from the weather with temporary weather-proofing as necessary. The lift and insertion of the 300T, 20-m-dia., 15-m-long inner vessel into the bore of the half coil assembly will be the first of many engineered critical lifts. (Fig. 6-18)

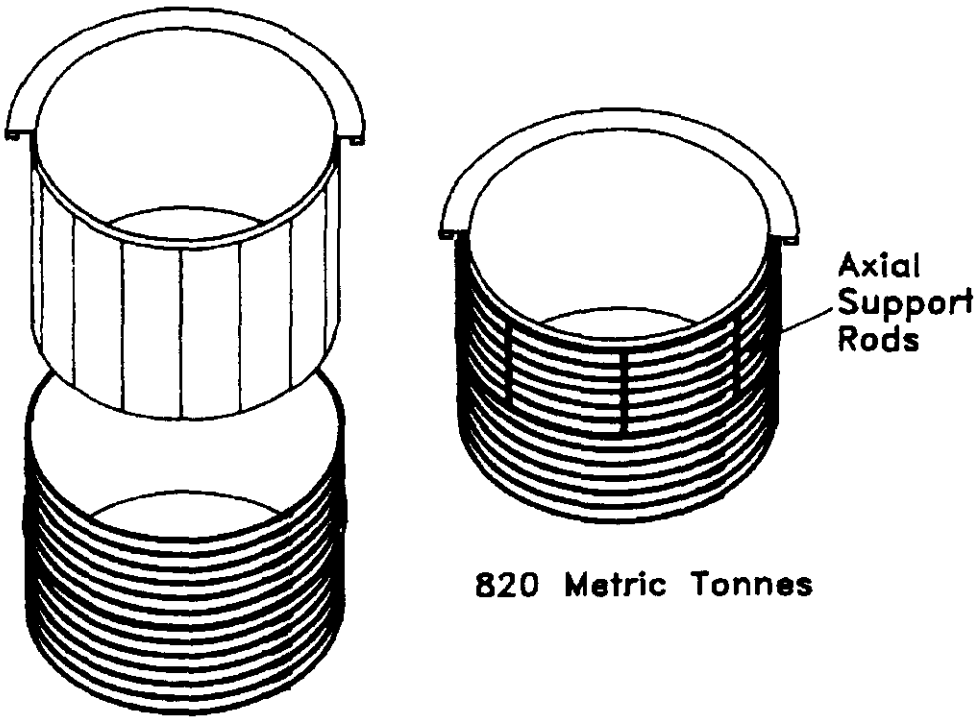

Fig 6-18: The inner vacuum vessel is lifted over the half coil assembly and lowered into position. The upper radial and axial rods are then installed and tensioned

Qualified rigging specialists will provide specially designed fixtures and proof-tested equipment that has been qualified for this lift. Prior to the lift a rigging readiness review will be held to ensue all components meet specifications and that the subassemblies as well as the rigging equipment are ready for the lift. The radial clearance between the two cylindrical surfaces will be approximately 5cm.

The inner vacuum will be supported on a devices that can place it at the proper height relative to the half coil assembly to allow the attachment of sixteen outer radial rods and eight-pairs of axial rods to the support points on the top vacuum vessel support flange. The thermal intercept, MLI and appropriate sensors will be added to the radial and axial support rods, leak-tested and certified. The coil will be roughly oriented within the vacuum vessel opening to allow preliminary tensioning of the upper radial and axial rods using hydraulic tensioning rams. Temporary supports will be attached between the bottom of the coil and the inside of the vacuum vessel to assure the rigidity of the structure during future lifts. During this phase plumbing for the liquid He supply that cannot be installed later will be installed, evacuated and leak-tested. As this assembly phase nears completion a complete set of external interface dimensions will be taken and recorded for both the inner vessel/coil assembly and the outer vessel assembly to assure proper fit-up for the next step.

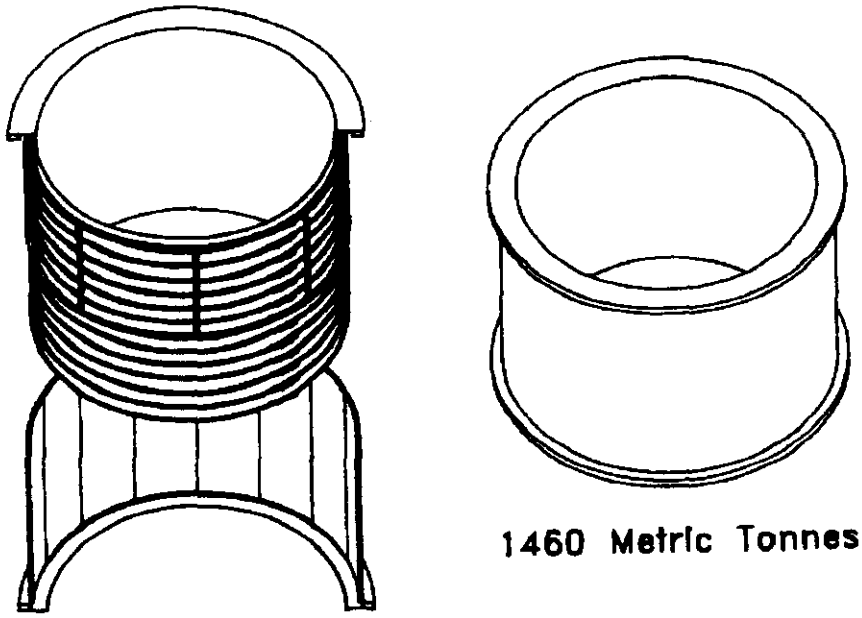

Fig 6-19: The half coil/vacuum vessel assembly is lifted into the bore of the outer vacuum vessel.

Insert the Inner Vessel/ Coil assembly into the Outer Vessel

When both units are ready for mating, they will again be moved on heavy hauler type trailers to the assembly area and prepared for lifting. The lift and insertion of the 820 T, 20-m-dia., 15-m-long component into the bore of the outer vacuum vessel will also be carried out along a vertical assembly axis. (Fig 6-19) It is another in the series of engineered lifts. Prior to this lift another rigging readiness review will be conducted to assure all components meet specifications and that the subassemblies as well as the rigging equipment are ready for the lift. The radial clearance between these two cylindrical surfaces will be approximately 5 cm.

The inner vessel/coil assembly will be supported on a device that can place it at the proper height relative to the outer vessel assembly to allow the attachment of the sixteen lower radial support rods to their attachment points through openings in the vessel provided for this purpose. The thermal intercept, MLI and appropriate sensors will be added to the lower radial support rods and leak-hunted and certified as required. The inner assembly will be positioned within the outer vacuum vessel opening to allow welding of the closure weld on the top and bottom of the vacuum vessel assembly. Temporary supports will be attached between the bottom of the coil and vacuum vessel to assure the rigidity of the structure during the next handling step, the uprighting of the 1500T magnet assembly. During this phase, plumbing for the remaining liquid He supply will be installed, evacuated and leak-hunted. When all internal vacuum systems have been leak-hunted and repaired, the vessel will be cleaned, and buttoned-up so that the system vacuum performance can be certified with all cryogenic joints at low temperature. The coil will be chilled to 80K using He gas circulating through a LN chiller (Fig 6-20). The LN panels will be chilled to operational temperature. Most of the newly made joints including He piping and the high-current conductor lead assemblies will be accessible through openings provided in the vessel. However, kilometers of piping and a large number of joints will be exposed to cryogenic temperature for the first time. The investment in procedures to assure leak-tightness of the major components will pay-off at this point because elimination of significant hidden leaks will save expensive re-entry or disassembly.

After the desired 10^{-5} Torr vacuum is achieved, the vessel ports are opened and additional temporary supports are installed as required in preparation for the uprighting of the magnet assembly into its final axis-horizontal orientation.

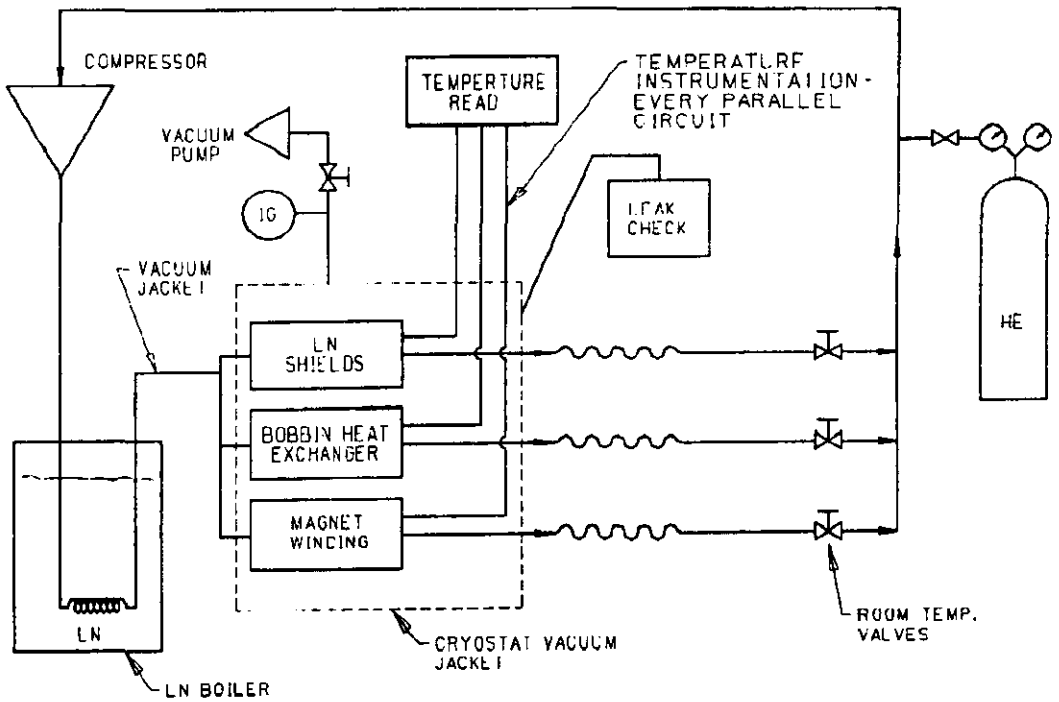

Fig 6-20. Schematic of a chiller system to provide cold He gas to chill the magnet assembly to allow cold leak detection prior to commissioning in the detector hall.

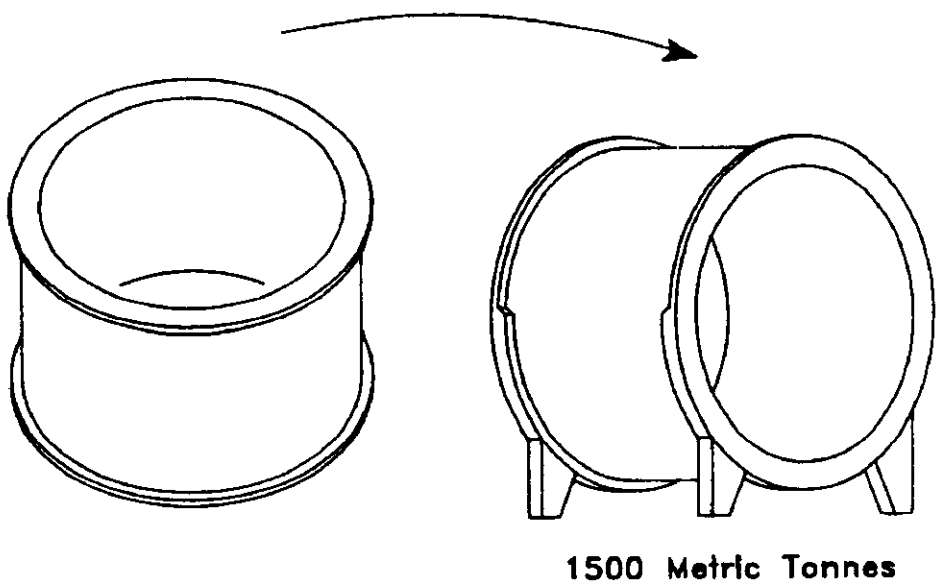

Fig 6-21: The uprighting of the 1500 T assembly is within the capacity of a number of U.S. rigging specialists.

Uprighting the magnet assembly

This, like the other lifts, requires adequate preparation culminating in a readiness review of all systems prior to the commencement of the lift. All internal systems will be secured. The uprighting will take place in the assembly area and will culminate with the placement of the 1500T, 23-m-tall, 15-m-long solenoid on the four permanent support structures (Fig 6-21). This type of rotation has been presented to qualified rigging specialists and is within their capacity. After the uprighting all key systems will be inspected to verify that they came through the change of orientation properly. Although no repairs are expected, unexpected fixes can be carried out while the coil cold mass supports are tensioned for the new orientation. When the assembly of the solenoid magnet is complete, it can be moved to the detector hall. Final acceptance testing will be conducted in the detector hall after the magnet is lowered into the hall, and installation is complete.

The assembly approach presented is the strongest of many considered. It is thought to be the least cost approach because it eliminates many rigging and support fixtures required by other procedures. Other advantages of this method include:

- It allows for simultaneous erection of the vacuum vessel shells
- Winding and erection use the preferred fabricator orientation
- It allows early LN shield assembly and cold tests
- It eliminates coil exposure to longitudinal close-out welds and overhead welds.

The main risk is that heavy components are handled and a large mass must be rotated. But the high lifts of bulky, heavy components and the rotation of the entire magnet can be safely completed by proper engineering by qualified experts. In short, this method will successfully assemble the largest solenoid ever built in a timely manner. For more details refer to the On-Site Fabrication and Assembly Plan.

7.0 FORWARD FIELD SHAPERS

The Forward Field Shapers (FFS) are large conical steel masses used to shape the magnetic field inside the GEM detector. Field calculations determine the size and form of the field shaper, as well as its location relative to the vacuum vessel.

The GEM detector has two identical forward field shapers. Each field shaper is held in space by a support structure which butts to the end of the vacuum vessel and is supported at four places by the floor of the experimental hall.

Each FFS weighs approximately 1000 metric tons. Each support structure weighs an additional 1000 metric tons. The FFS is an approximately 8 meters long truncated solid cone varying in diameter from 3.1 to 5 meters (see Figure 7-1).

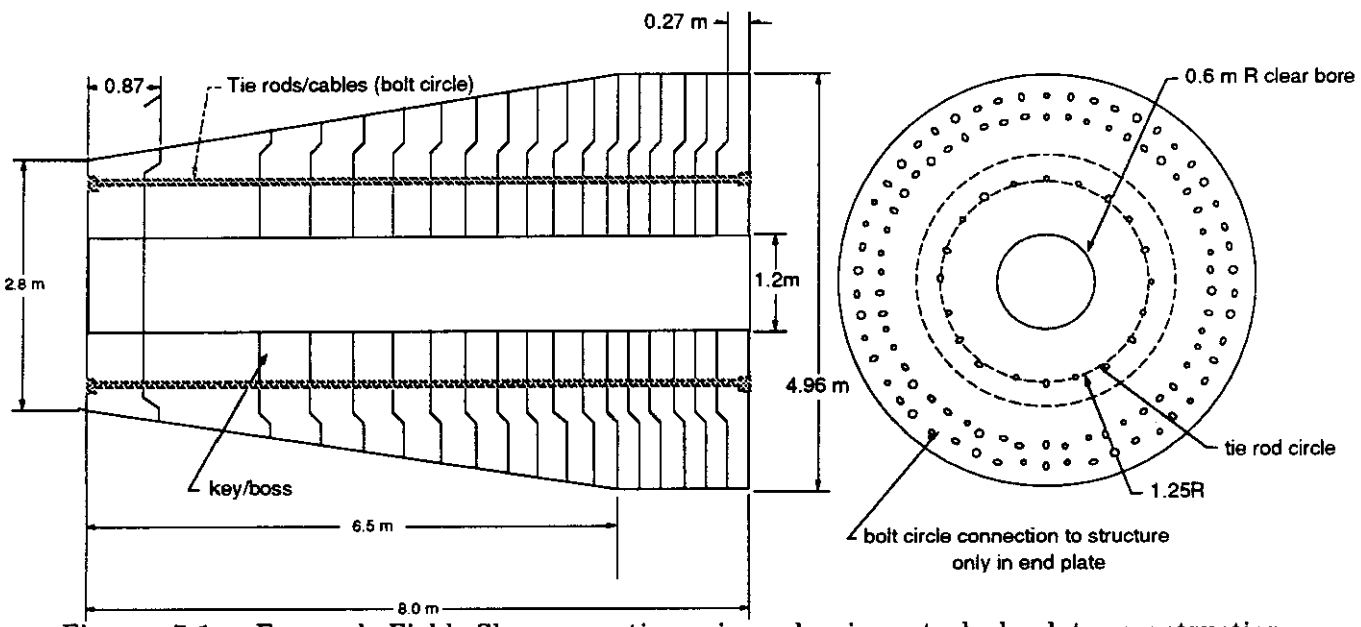

Figure 7-1 Forward Field Shaper section view showing stacked plate construction

Each FFS assembly, including the support structure, is independently mounted on the experiment hall floor at specially reinforced mounting locations. For initial installation and ongoing maintenance and repair, each assembly can be lifted and moved along the beamline to the end of the experimental hall.

The Forward Field Shapers is a static structure with no moving parts. Three load cases are possible during normal use of the field shaper.

case 1: Free standing structure: When retracted from the vessel for detector access, the field shaper assembly is free standing. In this case, the structure must support the moment from the cantilevered field shaper any additional seismic loads.

case 2: Assembled with magnet off: When assembled with the vacuum vessel, the support structure bears on the vessel end ring. Part of the cantilevered load from the field shaper is borne by the vessel.

case 3: Assembled with magnet on: With the FFS support structure bearing on the vessel end-ring, the magnet load imposes a 3 million pound force on the FFS in the -Z direction. This load is transferred through the FFS support structure to the vessel, and represents an addition to the static load.

7.1 Vacuum Vessel Interface

During magnetic loading the force exerted on the FFS is transferred to the vacuum vessel through the FFS support structure. Conceptually, the structure consists of eight deep-section I-beams extending radially out from the FFS to the vacuum vessel. The flanges of these eight I-beams are tied together to form continuous, axisymmetric plates. At the intersection of the eight I-beams and the vessel end ring, there are eight points of load transfer from the support structure to the vacuum vessel. These interfaces at the vessel are landing pads located at each of the eight vessel longeron stiffeners described in chapter 6 (see Figure 7-2).

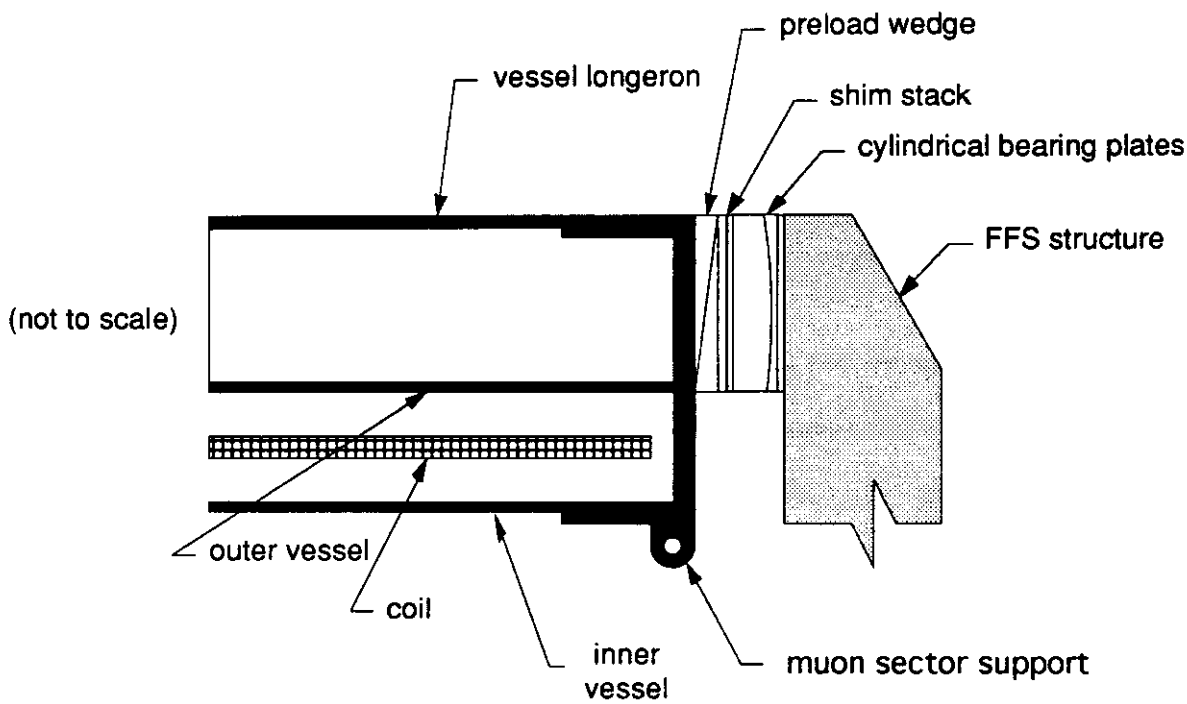

Figure 7-2 Vacuum Vessel. Forward Field Shapers Interface

Each landing pad consists of shims and a cylindrical bearing pad. This bearing pad allows the forward field shaper to deflect under magnetic load without imposing moments or stress concentrations into the end of the vacuum vessel. This gives that field shaper structure a hinged end condition which limits end moment loading on the vessel that can misalign the muon sectors mounted to its end rings. The shim stacks consist of two types of shim elements. Simple flat plates are stacked to provide nominal space filling, while wedge plates are jacked in to provide preload between the vessel and the FFS support structure. The small amount of preload is necessary to insure that all eight bearing points are loaded equally when the magnet is turned on.

Other than the bearing pads, there is no restraint between the vessel and the forward field shaper; each is independently mounted to the floor.

7.2 Temperature changes during cold mass activation

Temperature changes will occur in the vessel due to heat leaks to the cryostat. This may cause some amount of radial shrinkage in the vessel, and cause a change in the interface at the forward field shaper support structure.

The cylindrical surface bearing plate assemblies will be connected to either the FFS support structure or the vessel end ring, so that radial movement of the vessel will have no effect on the face-to-face contact areas.

7.3 Forward Field Shaper Support Structure

The FFS support structure is a large steel plate girder weldment, which supports static, magnetic, and seismic loads. The 1000 ton FFS is cantilevered into the vacuum vessel, putting large moments into the support structure. When retracted from the vessel during maintenance or repair, the field shaper structure is free standing, with no support from the vacuum vessel. The moment from the cantilevered field shaper is reacted by structural beams which extend under the vacuum vessel and straddle the vacuum vessel saddles.

Since the FFS support structure and the vacuum vessel support saddles compete for floor space, there is a trade-off on size, shape, and location of the support areas. The moment reacting support beams near the bottom the FFS support structure must fit outside the vessel support legs, with enough clearance for jacking, shimming, and transport.

Each FFS support structure is supported by four support blocks. The function of the block, a steel weldment, is to provide a disposable structure which can be easily replaced if the floor heaves or settles excessively. This block is described in a chapter on coil assembly design.

Each FFS support structure can be lifted and transported to allow access for maintenance and repair of the muon sectors and central detector areas inside the vessel. The actual amount of lift will be limited to the clearance between the sixteen muon sectors supported by the vessel end rings and the sixteen muon sectors supported by the forward field shaper support structure. Once lifted off the mounting blocks, the structure can be moved on tracks embedded in the experimental hall floor.

The transporter is described in a chapter on coil assembly design.

7.4 Operational Requirements

Two FFS assemblies are required. Each must provide the required mass and form needed to shape the magnetic field in accordance with calculations. Each must be mobile, and will move axially away from the central membrane to mounting points at the ends of the experimental hall. Each must support the dead load of 16 muon sectors weighing approximately 10 tons each.

The stiffness of the FFS support structure must be sufficient to prevent the FFS from spacially interfering with the muon sectors due to transient motion when the magnet is energized. In addition, any deflections due to amplification of ambient ground motion need to be less than the interference envelope described.

Materials shall be chosen to meet the above criteria in the most cost effective manner. Subject by further analysis, the baseline material for any non-axisymmetric structures will be 304L stainless steel to prevent local perturbations in the magnetic field. All axisymmetric structures will be constructed from A36 low carbon steel.

7.5 Design Criteria

The FFS support structure is mounted to footings in the GEM experiment hall. Although earthquake criteria for the SSC have yet to be established, it is known that earthquakes occur in this area of the country. DOE facilities are typically covered under UCRL-15910, "Design and Evaluation of Department of Energy Facilities Subjected to Natural Phenomena Hazards". SSCL is not yet covered in UCRL-15910. The baseline design for the FFS structure will follow the criteria specified in the Comanche Peak Steam Electric Station Final Safety Analysis Report. Comanche Peak is a nuclear power plant located in the Fort Worth area. This design criteria is considered to be conservative.

Ground accelerations:

Horizontal : 0.12g
Vertical: 0.08g

Amplification factors will be determined using the Comanche Peak's design response spectra as described in its Final Safety Analysis Report.

A factor of safety of 1 is required on seismic stress based on yield strength, according to LLNL Design Safety Standards. Structural elements are designed in accordance with the Unified Building Code or American Institute of Steel Construction, as applicable.

A thorough Fabrication Specification, in addition to drawing notes, will provide construction guidance to the vessel manufacturer. Some of the major requirements are listed here. Welders and weld procedures will certified per ASME Section IX, or AWS D1.1, as applicable. Filler rod for 304L shall be 308L. Filler rod for low carbon steel will be determined by the type of weld processes selected. All stainless steel surfaces, except vacuum sealing surfaces are sand blasted and bead blasted for cleanliness and better appearance.

7.6 Description of Possible Failures

The FFS support structure or mounting system can fail if seismic ground movement causes stresses greater than the yield stress of the materials.

Such failure can destroy equipment and injure personnel. All load bearing fasteners and structural elements will be designed with acceptable factors of safety, as described in the Engineering Note, so that the risk of failure is minimized. All fasteners will be torque-tested to their maximum allowable preload to verify their integrity. All fasteners will be certified as to material content and load rating. All structural shapes are analyzed using finite element techniques to verify their design limits.

7.7 Documentation

An Engineering Note will document calculations supporting the baseline design of the Forward Field Shapers and support structure which includes structural calculations.

A Fabrication Specification will document the general fabrication and quality assurance requirements of the vessel. The content of the Fabrication Specification includes specific allowable and recommended practices for material and personnel certification, fabrication, leak checking, finishes, rigging, testing, and documenting the construction.

7.8 Summary of Design Calculations

A combination of hand calculations and finite element analysis was used to design the Forward Field Shaper (FFS) and its support structure (see Figure 7-3). This includes the conical FFS itself, the disk-like structure it attaches to, and the supports under this disk which rest on the floor of the hall. Finite element analyses were done using the LLNL codes NIKE and GEMINI and their associated pre- and post-processors INGRID, SLIC, and TAURUS. Structural elements are designed in accordance with the Unified Building Code or American Institute of Steel Construction, as applicable. A factor of safety of 1 is required on seismic stress based on yield strength, according to LLNL Design Safety Standards.

The conical FFS, composed of cast segments, is assumed to be a rigid body. In such a case, the tip of the FFS would sag 0.2 mm (8 mils) with respect to its wide end under gravity. When the magnet is turned on, a load of 12 MN (2.7 million lbf) is applied to the FFS in the direction of its tip. If this force is treated as a distributed body

force, the tip will not rise significantly and will stretch less than 0.1 mm (4 mils) axially. Note that these deflections are small, but do not include the deflections of the support structure, which are much larger. The maximum stress in the FFS cone from these gravity and magnetic loads is only 3 MPa (0.4 ksi), which is small compared to a design stress of 70 MPa (10 ksi).

Finite element analyses were done on several configurations for the disk shaped structure that supports the FFS. They show that several designs are feasible: an open-backed, radially-gusseted disk, an enclosed gusseted disk, or an enclosed gusseted disk that is concave towards the central detector (MIT analysis). The three configurations of FFS support disk have been designed to a maximum stress of 70 MPa (10 ksi).

The conical FFS, composed of cast segments, is assumed to be a rigid body. Analysis shows this to be a reasonable assumption. Finite element analyses were done on several cases for the FFS and support structure. For static and magnetic load case (see Figure 7-4) symmetry allowed the model to be cut in half about a vertical plane to improve run time. A full model was required for simultaneous X, Y, and Z seismic excitation.

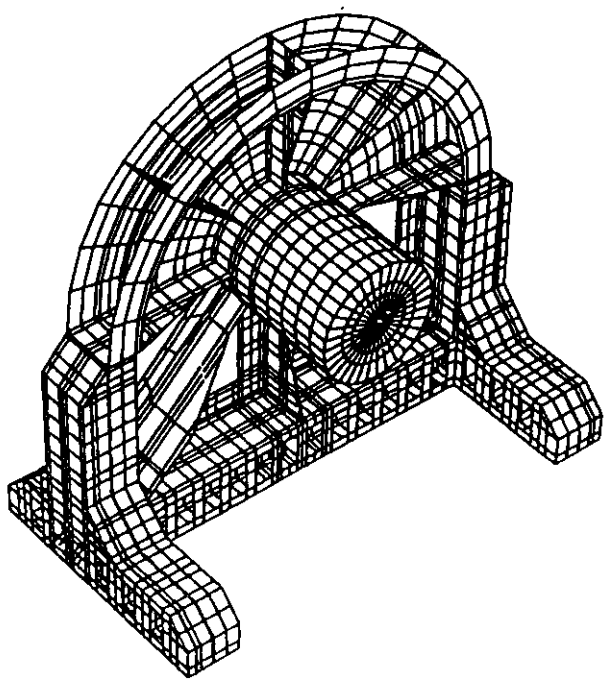

Figure 7-3 Forward Field Shaper final element model

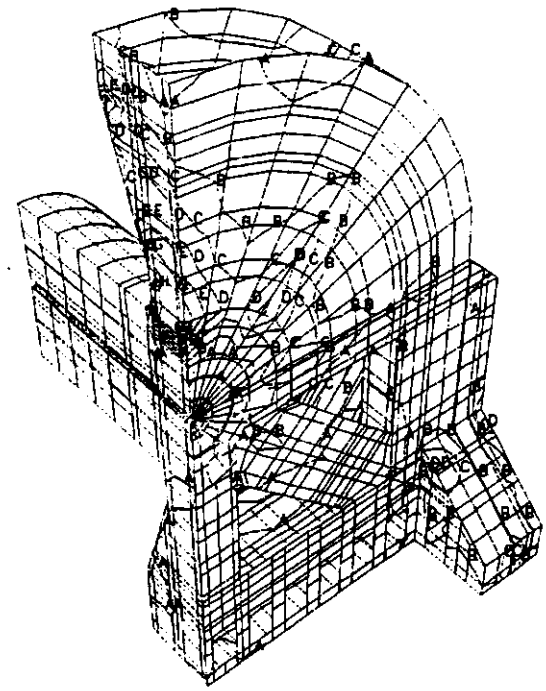

Figure 7-4 Forward Field Shaper: Stress contour plot on a symmetry model for gravity and magnetic loads.

Case 1: Free standing structure (static)

When retracted from the vessel for detector access, the field shaper assembly is free standing. In this case, the structure must support the moment from the cantilevered field shaper.

Y (vertical) displacement at end of FFS	-0.66" (down)
Z (axial) displacement at end of FFS	-0.3" (toward interaction zone)
Z (axial) displacement at top of FFS structure	-1.1" (toward interaction zone)

Case 2: Free standing structure (seismic)

Structure is retracted from the vessel for detector access, and supports the moment from the cantilevered field shaper plus its own weight under seismic conditions. These maximum displacements are in addition to static displacements. Structure is fixed at four support points. Input spectral peaks = 0.12g horizontal, 0.08g vertical.

X (transverse) displacement at end of FFS	+/- 0.1"
Y (vertical) displacement at end of FFS	+/- 0.3"
Z (axial) displacement at end of FFS	+/- 0.46"
Z (axial) displacement at top of FFS structure	+/- 0.92"

Case 3: Assembled with vessel (static)

When assembled with the vacuum vessel, the support structure bears on the vessel end ring. Part of the cantilevered load from the field shaper is borne by the vessel.

Y (vertical) displacement at end of FFS	-0.15" (down)
Z (axial) displacement at end of FFS	-0.05" (toward interaction zone)

Case 4: Assembled with vessel (magnet on)

The magnet load imposes a 3 million pound force on the FFS in the -Z direction. These maximum displacements are in addition to the static displacements in case 3.

Y (vertical) displacement at end of FFS	0.001" (down)
Z (axial) displacement at end of FFS	-0.13" (toward interaction zone)

Case 5: Assembled with vessel (seismic)

Seismic load is imposed on the FFS and support structure. Vessel support at eight places is modeled as fixed in Z direction. These maximum displacement are in addition to the static displacements in case 3.

Input spectral peaks	0.12g horizontal, 0.08g vertical
X (transverse) displacement at end of FFS	+/- 0.1"
Y (vertical) displacement at end of FFS	+/- 0.03"
Z (axial) displacement at end of FFS	+/- 0.05"

8.0 CENTRAL SUPPORT

The central support is comprised of two large low carbon steel diaphragms separated by one-half meter and connected with radial stainless steel plates. The diaphragms are approximately twenty-three meters in diameter with a seven meter diameter hole in the center for mounting the barrel calorimeter. The central support will provide structural support and coarse alignment for the calorimeters and central tracker independent of the rest of the detector. The central support will provide a load path for axial magnetic forces during normal operating. The entire weight of the central support, calorimeters and central tracker will be approximately 2800 tonnes

All utilities for the calorimeters and central tracker will be routed through the one-half meter space of the central support. The calorimeter utilities will include 172 power and electronic conduits, 24 cryogenic return lines, 3 cryogenic support lines, and 3 vacuum lines. The central tracker utility requirements are much less stringent requiring only 80 cm^2 of area for routing electronics, power, and cooling. Along with numerous utilities to support the calorimeters other requirements exist such as slope for cryogen supply and return lines, and the vacuum and cryogen lines must remain intact during endcap maintenance periods.

The central support will be designed and constructed as per all standard engineering design codes and DOE guidelines, specifically UCRL 15910 "Design and Evaluation for the Department of Energy Facilities Subjected to Natural Phenomena Hazards". Currently no site specific guidelines exist but guidelines from similar sites are being applied using the UCRL15910 philosophy. Performance goals are being applied as if the facility has been officially classified as an "Important or Low Hazard Facility". For the specific case of earthquake design this classification will provide minimal design guidelines for the central detector. Due to the expense that would be experienced from structural failure more stringent design practices will be employed. For instance along with the current static analyses with symmetric and asymmetric loads the Safe Shutdown Earthquake Design Response Spectra for the Comanche Peak Steam Electric Station in Fort Worth will be applied. This is a very extreme case but the central support could be made to survive such a self imposed criteria.

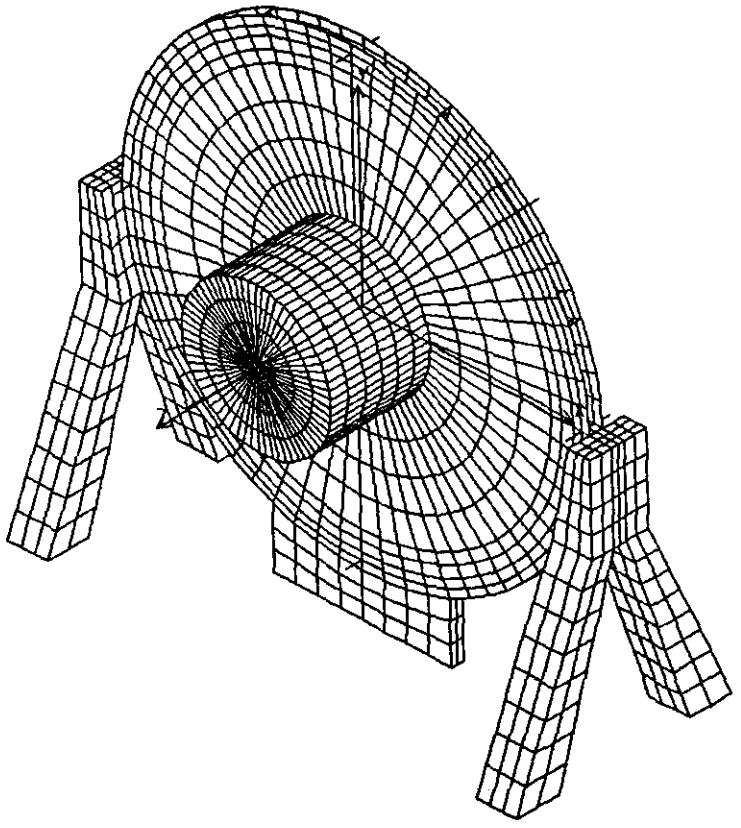

Figure 8-1 Finite Element Mesh of the Central Support and Calorimeters

The central support has been analyzed (See Figure 8-1) for stress levels with symmetric and asymmetric loads which simulate endcap calorimeter installation and unequal filling of the endcaps. Along with stress levels the structure has been analyzed for its resistance to structural failure due to buckling, especially when loaded asymmetrically. No unsolvable scenarios have been discovered.

Future work will include attempts to reduce the size of the complete membrane to a pedestal design. This would have obvious cost and schedule implications.

9.0 CRYOGENIC SYSTEM

9.1 System Description

The GEM magnet is cooled by liquid helium which flows by natural convection in a thermosyphon loop coupled to a large storage dewar located at the ground level with the magnet some 50 m below. A second flow circuit supplies a small flow of supercritical helium, cooled to the temperature of the thermosyphon loop, to the conductor conduit. This flow enhances the conductor stability, cools the conductor splices, and supplies lead cooling. A flow schematic is shown in Figure 9-1.

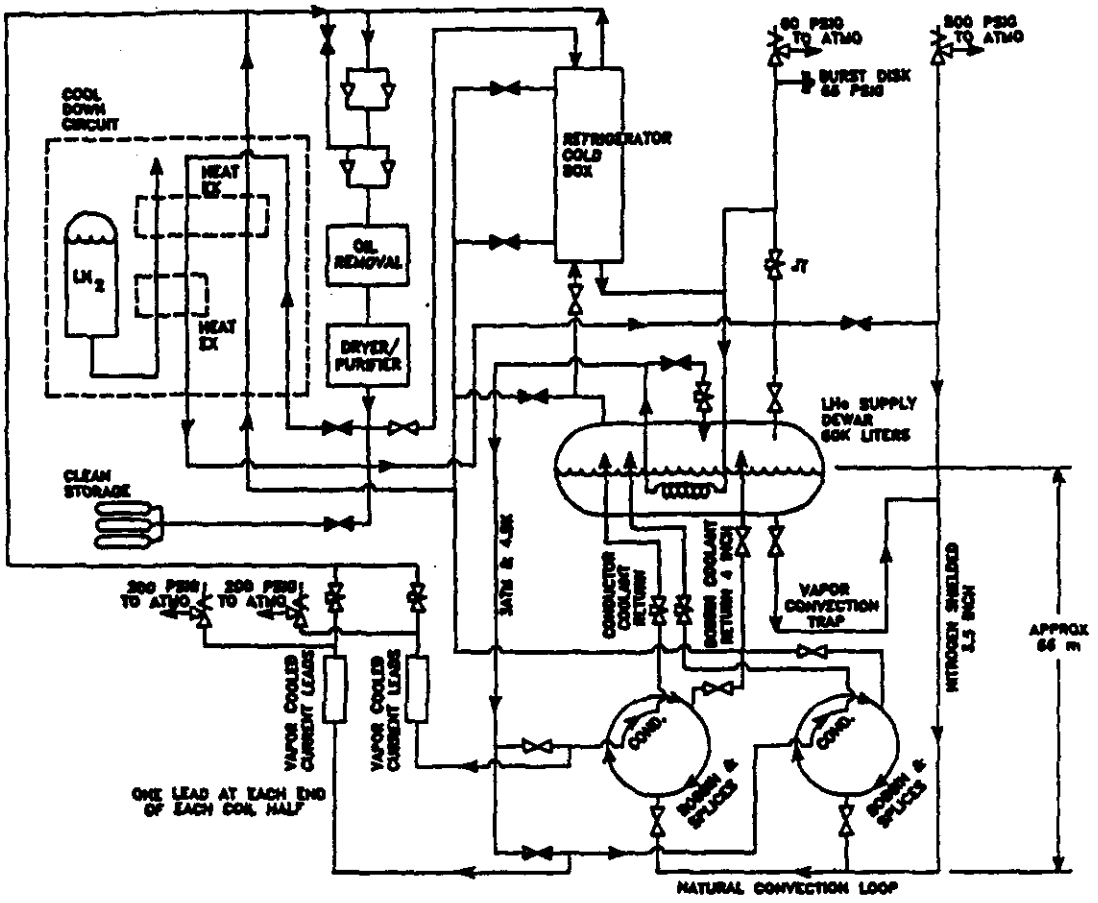

Figure 9-1 GEM Magnet, Helium Flow Schematic

Refrigerator

The steady state refrigeration loads to be encountered here could be satisfied by the helium refrigerators specified for the SSC Accelerator String System Test which are rated at 2 kW plus 20 g/s liquefaction. The cool down loads are another matter, however, and a separate cool down circuit is needed to bring the magnet down to the vicinity of liquid nitrogen temperature. The cool down circuit which can be see within the dotted outline on Fig 9-1 will also be used for the above ground cold testing of the magnet assembly prior to lowering into the experimental hall, Two of the helium refrigerators may be ultimately used in the circuit. The second refrigerator, aside from providing additional refrigeration capacity which could be useful on cool down, would also greatly enhance the system reliability by providing redundancy.

Storage Dewar

The refrigerator supplies cold two phase helium to a ground level helium storage dewar of approximately 60,000 liquid liter capacity.

Thermosyphon

Liquid helium flows from the bottom of the storage dewar down through a 3.5 inch (3 inch pipe) vacuum insulated and liquid nitrogen shielded line to the bottom of the magnet approximately 66 m below. The flow branches and flows upward through heat exchangers located on the various bobbin segments, is manifolded together and returns via a 4 inch (3.5 inch pipe) vacuum insulated line to the storage dewar. The vertical head insures that the liquid remains sub-cooled while in the magnet heat exchangers. A shut-off valve with downstream convection trap in the thermosyphon feed line allows magnet warm up with the maintenance of a cold and perhaps partially filled supply dewar.

Forced Flow Circuit

Supercritical helium branches upstream of the JT valve and flows through a subcooler in the liquid helium storage dewar and then down to the magnet where it splits into parallel paths through each of the conductor segments and splices. Because of voltage isolation requirements each of these paths must contain non-conductive segments. In order to minimize these non-conductive segments which are potential leak points, two alternatives to the baseline design where all of the splices are cooled in parallel are under consideration. In the first of these, the splice cooling is in series and downstream of the adjacent conductor segments. The disadvantage of this is that because of the large flow impedance through the conductor conduit, large increases needed to accommodate a deterioration of the joint resistance in the joint cooling would not be possible. The second alternative under consideration involves doing the cooling through an electrical insulator so that all of the splices may then be placed in series. The forced flow circuit also provides current lead coolant. Ideally, the current leads would be placed in series down stream of the adjacent conductor segment, but because of the large flow requirement for these and the high flow resistance of the conductor conduit it becomes necessary to place these in parallel with the conductor segments.

Liquid Nitrogen System

A liquid nitrogen dewar with a bottom outlet supplies coolant to the magnet shields. This dewar, which is located in the experimental hall at an elevation such that the free surface of the liquid is at the same height as the top of the magnet shields is supplied by 40,000 liter storage dewar located at the ground surface. The storage dewar at ground surface also supplies liquid nitrogen to the precooler in the helium refrigerator/liquefier, to the helium purifier and to the helium transfer line shields. A flow schematic is shown on Figure 9-2.

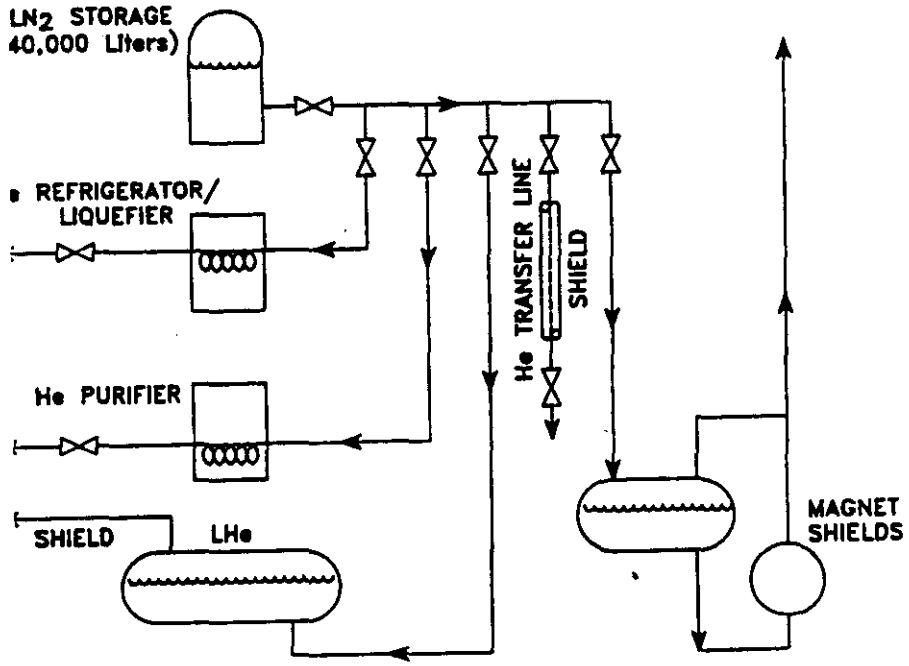

Figure 9-2 Nitrogen Flow Schematic

Facilities

The cryogenic helium refrigerator/liquefier is housed in three rooms of the surface level Utility Building. An acoustically insulated room contains the helium gas compression system. The system is composed of the compressors, oil removal and purification systems, coolers, air compressors, vacuum pump and other support equipment for the compressors. Another room contains the refrigerator/liquefier cold box module, expander modules, distribution box, dryer/purification station, cool down heat exchanger, vacuum pumps, and regeneration skids. The third room, adjacent to the cold room will serve as the control room housing all equipment necessary to maintain continuous control of the refrigerator/liquefier, heating, cooling water and H.V.A.C. High and low pressure gaseous helium storage tanks and a liquid helium storage dewar are located adjacent to the building.

The liquid helium supply transfer lines are routed from the output of the liquid storage dewar to the utility shaft, down the shaft to the utility tunnel, and into the underground hall to the detector. The return transfer lines follow the same path as the supply lines. The path length is approximately 200 m.

Cool Down

On cool down from temperatures in excess of about 85 K, the cool down circuit with it's large nitrogen heat exchanger is used to extract heat from the circulating helium gas. If the storage dewar is also warm the cool down flow may be routed through this dewar and it's temperature brought down along with that of the magnet. This is not necessarily optimum, however, since by doing so we limit the pressure for the cool down flow which otherwise could be at full compressor discharge. Once a magnet temperature approaching that of liquid nitrogen is achieved the cooling is switched to the refrigerator with flow initially through just the upper portion. If, for instance, the MTL refrigerator is the selected design, the flow would exit after expander 2 and heat exchanger 5. When a magnet temperature of about 20 K is achieved, the lower two expanders in the MTL design would be brought on line and the flow taken through the entire heat exchanger stack.

In another possible cool down scenario, portions of the system may be at operating temperature while others are warm. For example, after a magnet half has been moved for maintenance, it is possible that the cold mass will be

warm, while the refrigerator is cold and the supply dewar contains some liquid helium. In order to cool the magnet under this circumstance, we have provided the capability for the warm helium gas to bypass the cold storage dewar. Initially in this mode, warm helium from the magnet is returned to the compressor suction inlet of the refrigerator. As the cold mass temperature is reduced, the cooler gas is routed to the cold side of successively lower temperature heat exchangers in the cold box. In this way, system elements which are already cold can remain cold as the rest of the system is cooled.

Quench

On quench detection, the supply side of the thermosyphon loop is closed at the storage dewar and the liquid helium down stream from the shutoff valve is vaporized and returned to the storage dewar. There are approximately 700 liquid liters of helium in the supply side and 800 liters on the return side of the thermosyphon loop. Within the bobbin heat exchanger and headers, there is about 400 to 1400 liquid liters depending on the number of bobbin heat exchanger tubes used. In addition to the helium contained in the thermosyphon system, the helium within the forced flow system is returned to the storage dewar on quench. With good mixing in the storage dewar an appreciable fraction of this helium can be contained there without exceeding the working pressure of this vessel. Because of cost constraints a helium recovery system has not been included in the design and on quench, helium in excess of that which can be contained in the storage vessel is vented to to the atmosphere.

9.2 Analysis

Heat Loads

The steady state heat load is estimated at 1600 W plus 13 g/s liquefaction of the current lead coolant flow. The above heat load total is the sum of the following contributions.

Magnet side wall heating at 0.18 W/m^2 (inside and outside)	580 W
Cold mass supports	120 W
Current leads (self sufficient[37], 0.125 g/s kA pair)	250 W
Piping	300 W
Bayonets	200 W
Supply Dewar (0.3%/day loss)	20 W
Valves and misc.	150 W

Eddy current heating during magnet charging can be significant for short ramp up times. Ramp up times must be specified consistent with refrigerator capacity.

Thermosyphon

The thermosyphon loop is shown schematically in Figure 9-3. Because of a density difference between the two legs of the flow loop, a circulating flow of liquid helium is established with a flow of liquid from the bottom of the reservoir, descending through the height H1, then up through the load (magnet heat exchanger) and returning to the top of the reservoir at point 2.

[37] The heat flow at the cold end has been assumed just sufficient to vaporize the required coolant flow of 0.125 g/s kA pair when the leads are used in the usual arrangement where the heat flow at the cold end is to a saturated liquid bath.

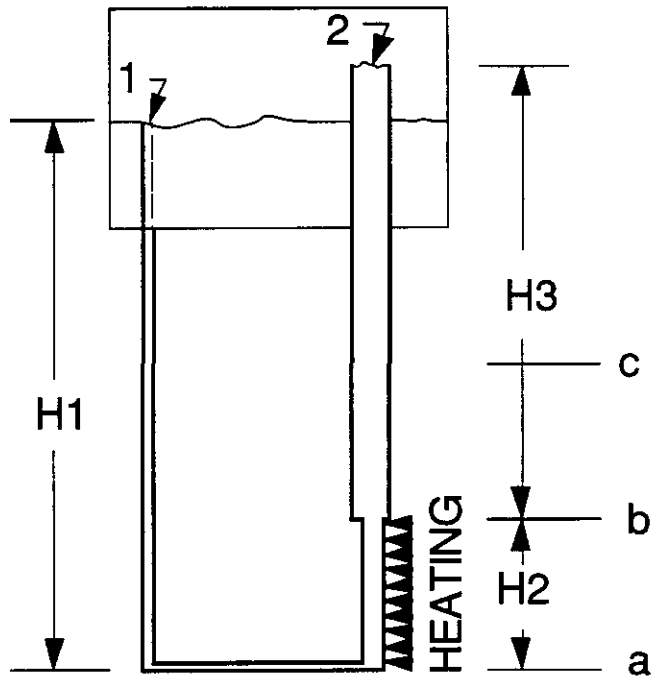

Figure 9-3 Gem Thermosyphon

We proceed to calculate the magnitude of the flow in the thermosyphon. We write the Euler equation.

$$\frac{dP}{\rho} + udu + gdz + \frac{\tau}{\rho(\frac{D}{4})} d\ell = 0$$

then multiply through by ρ and integrate from 1 to 2

$$\int_1^2 dP + \int_1^2 \rho u\, du + g\int_1^2 \rho\, dz + \frac{4}{D}\int_1^2 \tau\, d\ell = 0.$$

The pressure in the vapor region is everywhere the same, so that

$$\int_1^2 dP = P_2 - P_1 = 0.$$

The acceleration term,

$$\int_1^2 \rho u\, du = \dot{m}\int_1^2 \frac{du}{A}$$

could be integrated term by term but is in fact quite small. (This will be demonstrated later). Consequently, it will be ignored for the present.

The head term may be written

$$g\int_1^2 \rho\, dz = g\int_1^a \rho\, dz + g\int_a^b \rho\, dz + g\int_b^2 \rho\, dz .$$

In order to perform the indicated integrations we assume that density is constant and equal to $\overline{\rho_1}$ in the interval 1, a and equal to ρ_b in the interval b, 2.[38] In the interval a,b we assume that $\frac{\delta\rho}{\delta z} = const.$ This then leads to

$$g\int_1^2 \rho\, dz = g\left[\rho_b\left(\frac{H_2}{2} + H_3\right) - \overline{\rho_1}\left(H_1 - \frac{H_2}{2}\right)\right].$$

The shear stress in the fluid at the wall can be written in terms of the head loss as follows:

$$\tau\pi D\ell = \Delta P_f \frac{\pi}{4} D^2$$

or

$$\tau = \frac{D}{4\ell}\Delta P_f$$

and, therefore,

$$\frac{4}{D}\int_1^2 \tau\, d\ell = \Sigma\Delta P_f ,$$

where $\Sigma\Delta P_f$ is simply the sum of all the frictional pressure loss for all of the flow elements. Substituting the hydrostatic and head loss terms into the integrated Euler equation results in

$$g\left[\rho_b\left(\frac{H_2}{2} + H_3\right) - \overline{\rho_1}\left(H_1 - \frac{H_2}{2}\right)\right] + \Sigma\Delta P_f = 0 .$$

If we assume some temperatures at a and b that will provide us with the densities for the hydrostatic term. Then if we assume a refrigeration load, it, together with the temperature rise will allow the computation of the required flow rate. With that flow rate, we determine pipe sizes for which the frictional head loss will match the hydrostatic term as required.

State points

Supply Dewar, point 1:

We would like to keep the pressure in the supply reservoir at approximately one atmosphere. For the present calculation we will assume that it is 1.3 atm. We expect that we can keep it lower than this. The saturation temperature at 1.3 atm. is 4.52 K and the liquid density is 0.1185 g/cm^3.

[38] The density in the interval b,2 is in fact not constant but is reduced as vaporization occurs as the liquid approaches the surface. The effect of this is that we will be underestimating the head term and the thermosyphon will actually work a little better than we compute here.

Bottom of Magnet, point a:

For the location chosen for the experimental hall, the height, H_1, is about 66 m. The height, H_2, is 20 m and H_3 is then about 47 m. For a liquid density corresponding to that at point a, the hydrostatic head for 66 m is 0.76 atm. which brings the pressure at point a to 2.06 atm which is just a little below the critical pressure. If we assume a temperature rise in the liquid as it descends from the reservoir to point a of 0.05 K, the enthalpy there is 11.64 J/g and the density is 0.1227g/cm^3.

Top of Magnet, point b:

We now pick a temperature at b, say, 4.7K. Subtracting off 20 m of hydrostatic head, the pressure there is 1.8 atm. The enthalpy and density are 12.76 J/g and 0.115 g/cm^3.

Return Flow, point 2:

Assuming no further heating above point b, we can compute a quality of 7.6% corresponding to 1.3 atm. and enthalpy of 12.76 J/g. An average density for this quality is 0.111 g/cm^3 which is not significantly different than the density at b.

Mass Flow

The enthalpy rise from a to b is 1.12 J/g. We can now specify a heat input and compute the mass flow. For the heat load we use 760 W which is just a little greater than the sum of the heat loads that come in via the structural supports and through the insulation. The mass flow is

$$m = \frac{760\,J/s}{1.12\,J/g} = 680\,g/s$$

Driving Force

For $\overline{\rho_1}$ we take the average of ρ_1 and ρ_a which is 0.121 g/cm^3. The head term then becomes

$$g\left[\rho_b\left(\frac{H_2}{2}+H_3\right)-\overline{\rho_1}\left(H_1-\frac{H_2}{2}\right)\right]=-4434\,N/m^2$$

which is approximately 0.044 atm.

Frictional Pressure Loss

The thermosphon line layout is shown on Fig 9-4.

Supply Above Branch

We assume a 3 inch schedule 10 pipe (diameter is 8.28 cm). The area is 53.8 cm^2, and for 680 g/s and density of 0.1185 g/cm^2, the velocity is 107 cm/s. The Reynolds number is 3.5x10^6, so the friction factor is about 0.01. The velocity head is 67.8 N/m^2 and $f\ell/d$ is 7.5, so that the pressure loss in this segment is 506 N/m^2.

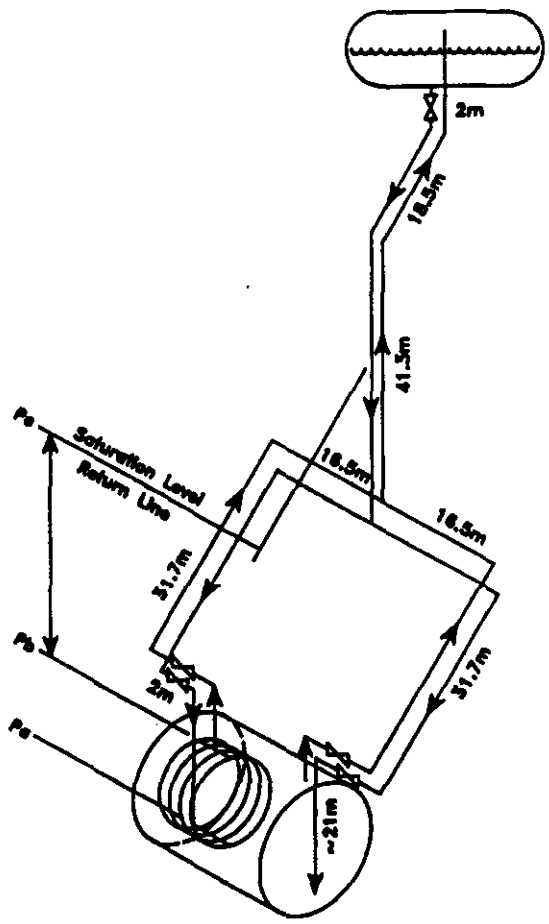

Fig 9-4 Thermosyphon line layout

Supply Below Branch

We assume 2.5 inch schedule 10 pipe here (diameter is 6.69 cm). The area for both branches is 70.4 cm^2, and for 680 g/s and density of 0.1185 g/cm^2, the velocity is 81.7 cm/s. The Reynolds number is 2.1×10^6, so the friction factor is about 0.015. The velocity head is 39.5 N/m^2 and $f\ell/d$ is 16, so that the pressure loss in this segment is 631 N/m^2.

Bobbin Heat Exchanger

We assume that the bobbin heat exchanger consists of one 3/4 inch O.D. tube with 0.06 wall on each bobbin segment. The diameter is 1.6 cm. The total flow area for 48 flow passages is 96.5 cm^2. The velocity is 60.8 cm/s. The Reynolds number is 3.8×10^5 so that the friction factor is about 0.014. The velocity head is 21.6 N/m^2 and $f\ell/d$ is 24.7 so that the pressure loss is 535 N/m^2.

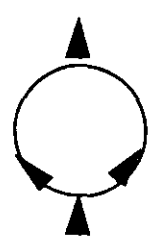

Return below Tee

We use the density at 2 and assume the same piping as on the supply below the tee. The velocity is 84.2 cm/s. The Reynolds number is 2.2×10^6, so that the friction factor is about 0.01. The velocity head is 40.7 N/m^2 and the $f\ell/d$ is 7.5 but we increase this to 10 to account for bends, so the pressure loss is 407 N/m^2.

Return above Tee

We compute for single phase flow of density 0.113. We set the line size at 3.5 inch pipe which has an internal diameter of 9.55 cm. The velocity is 84.1 cm/s. The Reynolds number is 3.1×10^6, so that the friction factor is about 0.01. The velocity head is 40 N/m^2 and the $f\ell/d$ is 6.9 but we increase this to 9 to account for bends, so the pressure loss is 360 N/m^2. This may be somewhat low due to two phase flow effects.

Total Pressure Drop

The total drop is then the sum of those listed above, plus one velocity head loss at the exit for a total of 2439 N/m^2. This is substantially less than the available head of 4434 N/m^2 which means that for the line sizes chosen, the flow will be higher than assumed and the temperature rise across the magnet less.

Conclusion

For the 760W heat load, the thermosyphon system with piping sizes as assumed will supply a flow in excess of 700 g/s with a temperature rise of less than 0.2 K.

Refrigerator Backup

A flow schematic is shown on Figure 9-5. Helium gas at a pressure in the range of three to four atmospheres, taken either from the first stage compressor discharge or from storage, is cooled first in the cold box LN precooler (upper heat exchanger in flow schematic), and then cooled further, to temperature T_2, in subsequent exchangers by the vent flow from the storage dewar which returns through the cold box. This vent flow is generated in most part by the heat load on the thermosyphon and can be relatively large compared to the flow in the forced flow circuit. The high pressure flow is further cooled to near the storage temperature in the immersed heat exchanger within the storage dewar and exits the storage dewar at T_3. This flow splits into parallel circuits through the current leads, through the conductor and through the conductor splice heat exchangers. The current leads flow exits the leads at room temperature and returns to compressor suction. The conductor and conductor splice flow is heated at most to about 0.3 K above the storage temperature after which it is throttled to storage conditions and returned to the storage dewar with a relatively high liquid fraction.

The heat load on the storage dewar consists of the thermosyphon heat load plus the forced flow enthalpy difference between points two and three. This latter term is sensitive to the effectiveness of the counter flow heat exchanger. Assuming an effectiveness, e, of 0.98 leads to

$$\varepsilon = 0.98 = \frac{80 - T_2}{80 - T_5}$$

We assume a storage pressure of 1.3 atmospheres so that

$$T_5 = T_{storage} = 4.52 \text{ K, and}$$

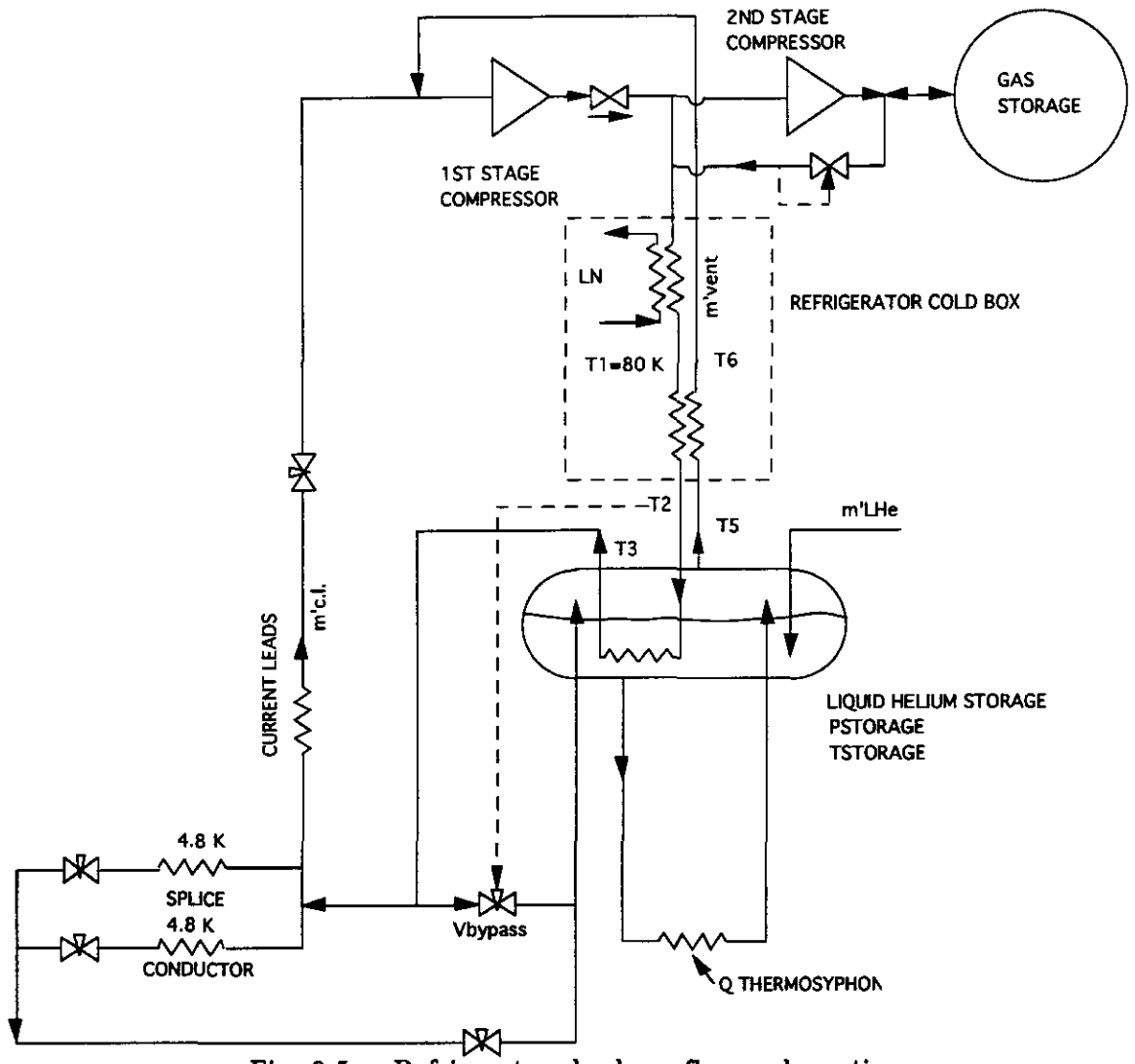

Fig 9-5 Refrigerator backup flow schematic

$T_2 = 6.03$ K

Now assume $T_3 = 4.55$ K. At 4 atm, the enthalpy difference between points 2 and 3 is 12.1 J/g K.

The mass flows through the current leads is about 13 g/s. There are 24 coil segmentsand each end of each segment requires 1/2 g/s for splice cooling. At the four places where the current leads connect, however, we choose to cool the conductor end with the current lead coolant before this coolant is used in the current lead. So that the splice flow is 22 g/s. The conductor flow is not well defined at this time but is thought to be small. The total flow in the forced flow circuit is then about 35 g/s and the total enthalpy difference from 2 to 3 is 35x12.1=424 W. The heat load on the thermosyphon is nominally about 1000 W, so that the total load on the storage dewar is about 1400 W. The latent heat at 1.3 atmospheres is 18.4 J/g so this heat load will vaporize 76 g/s.

Assuming that the splice flow coolant is heated to 4.8 K in the splice heat exchanger and then throttled to 1.3 atmospheres, the return to the storage dewar will be 90 % liquid, or 22 g/s liquid. The net loss rate from the storage dewar is 76-22=54 g/s. or 1560 l/hr. In other words if liquid helium were to be supplied at a rate of 1560 l/hr, steady conditions would be maintained in the storage dewar. Or if we begin the depletion with a one half full storage dewar of 30,000 liters we can operate in this mode for almost 19 hours which is perhaps enough time to change a turbine or replace a bearing or seal on a screw compressor.

It is worth noting the sensitivity of this calculation to the effectiveness of the heat exchanger. If the effectiveness were to drop to 96%, the temperature at 2 goes from 6.03 K to 7.53 K and the total enthalpy difference from 2 to 3 goes from 424 W to 1069 W. The 19 hour lifetime drops to 12 hours.

One way to increase the heat exchanger effectiveness would be to decrease the flow in the forced flow circuit by switching the splice cooling to the thermosyphon. If the heat exchanger effectiveness was in fact low, a decrease in the flow rate in the forced flow circuit would result in a decrease in the heat exchanger capacity ratio while at the same time increasing the NTU of the heat exchanger, both of which would have the effect of increasing the heat exchanger effectiveness. On the other hand, as long as the heat exchanger effectiveness is high, it is advantageous to keep the flow in the forced flow circuit high so as to extract as much refrigeration as possible from the vent flow. Hence the bypass valve, V_{bypass}, which is modulated in response to T_2.

10.0 MAGNET POWER SUPPLY AND PROTECTION SYSTEMS

The functions of the Magnet Power Supply and Protection Systems are to supply a controlled DC current to the magnet, to detect magnet quenches and dissipate the energy stored in the magnet during normal discharge and emergency dump situations. The Power Supply System consists of a 20 VDC, 50.2 KA power supply, high current buswork, magnet discharge resistor, charge/discharge switch, quench resistor, DC current interrupters and local controls. The Protection System consists of magnet sensor cabling, instrumentation modules and a local control station. A simplified schematic of the power supply system is shown in Figure 10-1.

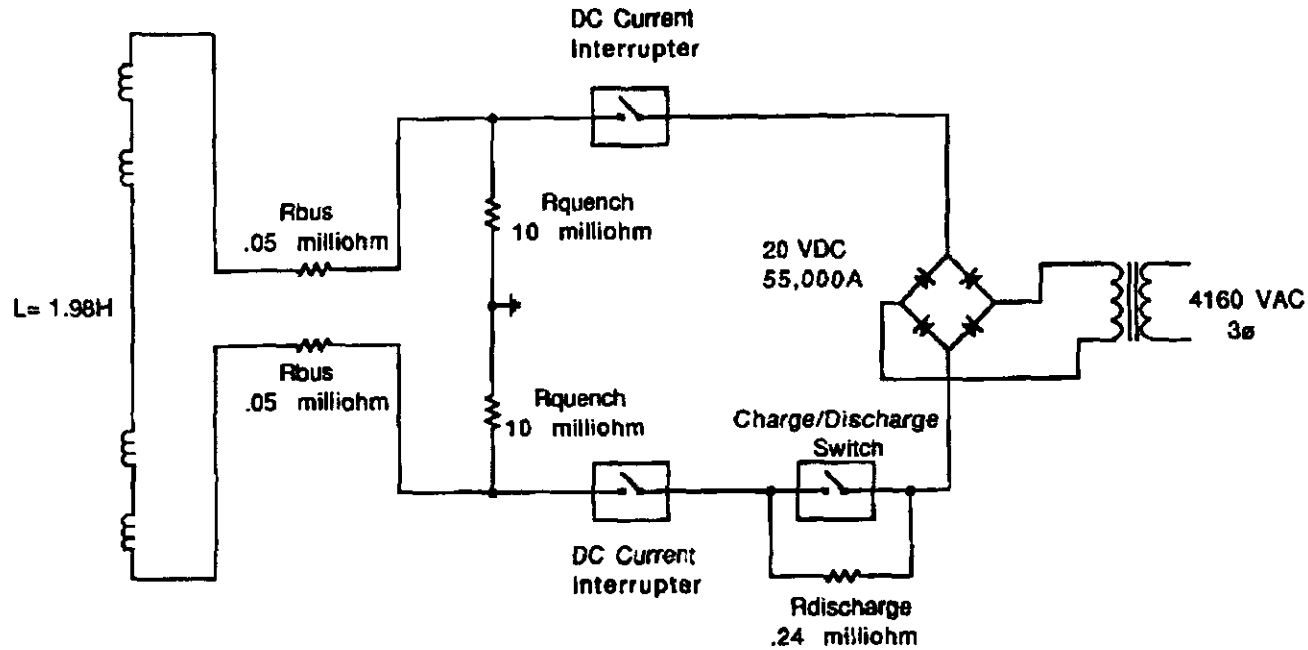

Figure 10-1 Power Supply Schematic

10.1 Magnet Power Supply System

The design requirements of the Magnet Power Supply System are dictated by magnet design and operating parameters. A list of the parameters which affect the power supply design is shown in Table 10-1.

Table 10-1 Magnet design and operating parameters

Inductance	1.98 henries
Operating current	50,200 amps
Stored energy	2.5 G joules
Ground isolation	500 V
Charge/discharge time(5t)	8 hours
Emergency dump time (3t)	300 seconds
The magnet assembly is designed to separate at the vertical centerline	
Magnet coil to power supply connections are at the outer ends of the assembly	

The power supply system components will be located inside the Utility Building at the surface of the experiment site. These components, along with portions of the high current buswork, will be contained within an interlocked restricted access area for personnel safety.

Magnet Power Supply

The power supply must be capable of providing a DC current of 50.2 KA to the magnet, during normal operation, with an output current regulation of .5%. The final design of the power supply will be left to the vendor of the unit. However, for units of this size it is common practice to use a multiple pulse (12 or 24) thyrister rectifier design. The input line voltage to the power supply will be 4160 V, 3 ø, 60 hertz. Primary filtering or phase shifting will be required to limit harmonic distortion on the input voltage lines to acceptable levels.

Under normal operating conditions, the principle load on the power supply will be the high current buswork. The voltage drop on the buswork will be slightly over 5 VDC. During a magnet charging cycle, however, the load voltage will increase to about 10 volts due to the drop across the magnet coil. In addition, the resistance parameters of the installed magnet and power supply system hardware may be slightly different from design levels. Consequently, the specified output voltage for the power supply must include a contingency which will accommodate these variations. A design value of 20 VDC at the power supply output terminals has been selected.

The magnet coil charging time has been specified at 8 hours. It has been determined that the heat load to the magnet cooling system is minimized if charging occurs at a linear rate. The power supply must therefore be capable of ramping up the output current at a linear rate of 6,725 amps/hour from zero to 50.2 KA.

The voltage between the power supply output terminals is expected to rise to about 960 V during an emergency dump of the magnet. The voltage isolation between the terminals must therefore be at least 1 KV. A ground reference connection in the dump resistor will keep the voltage differential between either output terminal and ground at less than 500 V. Therefore, the voltage isolation between the output terminals and ground must be at least 500V.

Low conductivity water (LCW) is available for cooling the output stages of the power supply. The maximum temperature of the water will be 40 C.

A summary of the power supply design requirements is provided in Table 10.2.

Table 10-2 Power Supply Design Requirements:

Input voltage	4160 VAC, 3 ø
Output voltage	20 VDC
Coil charging rate	6,275 A/hr
Output current	50,200 A
Current regulation	.5%
Output terminal ground isolation	500 V
+ & - terminal isolation	1KV
Output stage cooling	LCW @ 40° C (maximum)
Location	surface facility
Local and remote control capability	

Buswork

Air cooled aluminum bus bars is the preferred design for the high current buswork because of lower cost and lighter weight. The supply and return legs of the buswork will consist of six parallel bars, measuring 4 cm x 24 cm each, which provides a cross sectional area of 576 square centimeters per leg. A minimum of 509 square centimeters per leg is required to meet the NEC current density guidelines of 1.08E+06 amps per square meter for bare aluminum bus inside a duct.

The buswork will be routed between the power supply and the magnet assembly through the utility shaft. The one-way length of the buswork is approximately 125 meters (250 meters both ways). Buswork sections which are

outside of the power supply system protective enclosure will be housed in a non-magnetic duct for safety and cooling considerations.

Bracing between bars of the same polarity will be required in each leg of the buswork to offset an attracting force of 350 nt/meter. In those areas where the two legs of the buswork are adjacent to each other, bracing will be required to offset a repelling force of 2000 nt/meter.

Under normal operating conditions, the power dissipation in the buswork will be less than 260 KW. Cooling for the bus will be provided by 20° C air drawn from the experiment hall through the buswork ducting and returned to the hall air conditioning system located on the surface of the experiment site. A buswork temperature rise of approximately 40° C has been calculated using an air flow of 12.5 m/sec through the 1.5 meter square duct.

The buswork must also contain removable sections near the buswork to magnet coil connections and the connections between the two magnet sections to allow for disconnection of the bus when the two halves of the magnet assembly must be separated.

Bus to bus and bus to ground voltage isolation is the same as for the power supply output terminals, 1 KV and 500 V respectively.

A summary of the buswork design requirements is provided in table 10-3.

Table 10-3 Buswork Design Requirements:

Overall length	250 meters
Power dissipation	<260KW
Cooling	forced air
Current capacity	50,200 amps
Ground isolation	500 V
+ & - bus isolation	1KV

Magnet Discharge Resistor

The function of the magnet discharge resistor is to absorb the stored energy of the magnet during a normal discharge cycle. Its resistance (241 E-06 ohms) was selected such that, when combined with the buswork resistance, the stored energy would be dissipated within the required 8 hours.

The resistor must accommodate a large transition in current flow during the magnet discharge cycle. Consequently, it must be designed for low inductance. Also, the power dissipation to surface area ratio must be less than 1.26 MW/m^2 to prevent the formation of steam on the resistor surface. Stainless steel alloy strips arranged in a parallel configuration can be used produce the required resistance, low inductance and sufficient surface area to dissipate the absorbed energy. The resistor will be cooled by water immersion.

Bus connections to resistor must have the same bus-to-bus and bus to ground isolation voltage capabilities as that stated above for the buswork, i.e., 1 KV and 500 V, respectively.

A summary of the discharge resistor design requirements is provided in Table 10-4.

Table 10-4 Magnet Discharge Resistor Design Requirements:

Energy dissipation	2.5 G joules (8 hrs)
Resistance	241 E-6 ohms
Construction	parallel plate alloy resistors
Cooling	water immersion
Bus to bus isolation	1 KV
Bus to ground isolation	500 V
Location	surface facility

Magnet Charge/Discharge Switch

While the added resistance of the discharge resistor in the high current circuit is necessary during a magnet discharge cycle, it is not desirable to have it in the circuit during magnet charging or normal operation. Consequently, the charge/discharge switch is used to bypass the resistor during these operations to reduce the load on the power supply. The switch must be capable of interrupting the power supply output current of 50.2 KA DC.

The magnet charge discharge switch may be either a mechanical type circuit breaker or a solid state switch device. The selection will be left to the power supply system vendor. The switch unit will be provided with manual controls so that it may be operated in a stand-alone mode for maintenance and test purposes. A remote control interface will also be provided so that the unit may be operated from the magnet system control workstation via a LAN type cable.

The switch terminals must have the same bus to bus and bus to ground isolation as specified for the other high current components (See Table 10-5).

Table 10-5 Magnet Charge/Discharge Switch Design Requirements:

Current interrupt capability	50,200 ADC
Bus to bus isolation	1 KV
Bus to ground isolation	500 V
Number of interrupt cycles	200 before rebuild (breaker type device)
Location	surface facility
Local and remote operation capability	

DC Current Interrupters

Removal of supply current to the magnet in the event of a quench is of critical importance. Consequently, the power supply system will contain redundant DC current interrupters, one in each bus leg, to insure that the magnet coil current flow is diverted to the quench resistor. Each unit must be capable of interrupting the current flow from the power supply, 50.2 KA DC.

The current interrupters may be either a mechanical type circuit breaker or a solid state switch device. The selection will be left to the power supply system vendor. The interrupters will be provided with manual controls so that they may be operated in a stand-alone mode for maintenance and test purposes. A remote control interface will also be provided so that the units may be operated from the magnet system control station via a LAN type cable. Voltage isolation for the high current terminals on the devices is the same as that specified for the power supply output terminals.

A summary of the DC current interrupter design requirements is provided in Table 10-7.

Table 10-7 DC Current Interrupter Design Requirements:

Current interrupt capability	50,200 ADC
Ground isolation	500 V
Open contact isolation	1 KV
Location	surface facility
Redundant current interrupt capability	
Local and remote operation capability	

Quench Resistor

The quench resistor must be capable of absorbing the 2.5 GJ of energy stored in the magnet in the event that a quench occurs. The 500 second dump time ($\tau = 100$ seconds) and 1 KV maximum bus to bus voltage isolation dictate that the resistance of the dump resistor be 20 mΩ.

During the quench cycle, the change in current flow through the resistor will be very high. Consequently, the resistor must have little or no inductance. The resistor must also have a power dissipation to surface area ratio less than 1.26 MW/m^2 to prevent steam formation on the surface of the resistor. A common design used for this application is a parallel plate stainless steel resistor of the type shown in Figure 10-2. These plates can be arranged in a series-parallel configuration to produce the desired resistance, low inductance and surface area power density. The advantages of this type of resistor over other types are that they are easy to manufacture and assemble.

The requirement for a voltage isolation from bus to ground of 500 V dictates that the quench resistor design include a center tap which can be grounded. Since this connection is not in the high current loop, it only needs to be capable of carrying a few hundred amps for a short period of time in the event of a fault situation.

A summary of the dump resistor design requirements is provided in Table 10-8.

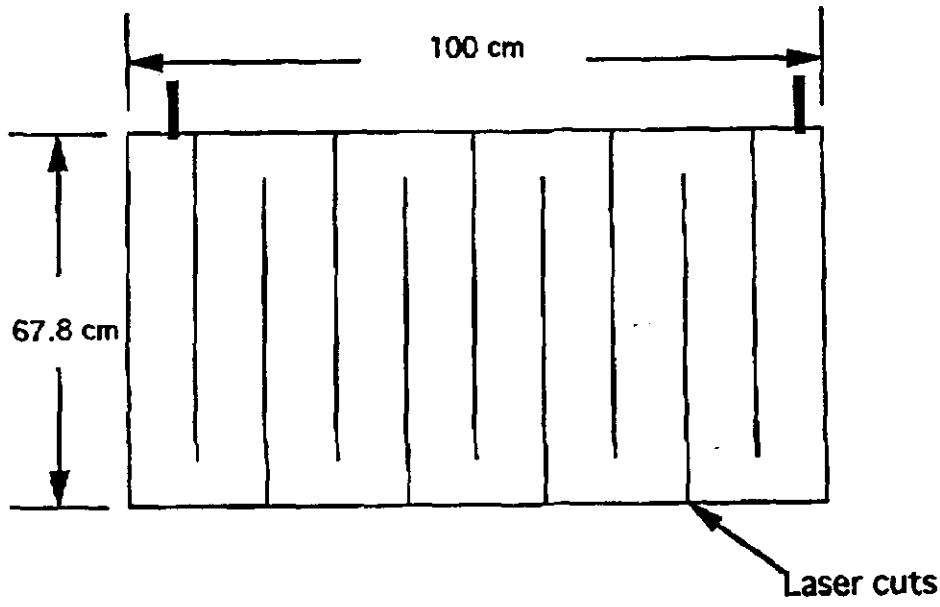

Figure 10-2 Quench Resistor Configuration

Table 10-8 Quench Resistor Design Requirements:

Current capacity	50,200 amps DC
Energy dissipation	2.5 G joules
Resistance	.02 ohms total
Power dissipation/surface area	< 1.26 MW/m^2
Cooling	water immersion (3155 gal = 50°C ΔT)
Bus to ground isolation	500 V
+ & - bus isolation	1 KV
Location	surface facility
Manual and remote operation	

Local Controls

The power supply will be equipped with a local control station to allow complete operation of the supply as a stand-alone unit. A summary of the control and monitor functions to be provided at the local station is shown in Table 10-6. The local control station will also provide an interface for remote operation by a programmable controller via a LAN type cable.

Table 10-6 Power Supply Local Control and Monitor Functions

Controls:	Monitors:
Control power on/off	Output voltage
Power supply output on/off	Output current
Output current setpoint	Interlocks status
Output overcurrent setpoint	Control power on/off
Current rampup setpoint	Current rampup setpoint
Interrupter #1 open/closed	Interrupter #1 open/closed
Interrupter #2 open closed	Interrupter #2 open/closed
Charge/Discharge sw open/closed	Charge/discharge sw open/closed
Local/remote operation	
Internal/external interlock inhibit	Power supply output on/off
	Local/remote operation
	Quench resistor water level
	Interlock inhibit on/off
	Output current setpoint
	Overcurrent setpoint
	Ground tap current

10.2 Magnet Protection System

Magnet Sensor Monitors

The magnet assembly will contain a variety of sensor elements to monitor the operating parameters of the system, detect off-normal operating conditions and initiate actions to protect the magnet. The sensors will include voltage taps, strain gauges and cryogenic lead temperature sensors (CLTS). Although the exact number of sensor channels is still being considered, it is expected that there will be 34 voltage taps, 240 strain gauges and 400 CLTSs; 200 for coil monitoring and 200 for LN2 panel monitoring. Commercial instrumentation modules will be used, where possible, to monitor the sensors and provide readout capability.

It is likely that the voltage on some or all of the sensor signal leads will jump to 1 KV between lead sets and 500 V from leads to ground during a emergency dump of the magnet. Therefore, the instrumentation modules must have comparable voltage isolation while continuing to provide readout capability.

The instrumentation modules will be housed in a rack mounted system located in the Utility Building. Sensor signal cables will be routed between the magnet assembly and the Utility Building through the Utility Shaft.

Local Controls

The Magnet Protection System will include a local control station which will provide the capability of monitoring magnet system sensors and initiating an emergency dump of the magnet coil. A summary of the control and monitor functions to be provided at the local station is shown in Table 10-9.

Table 10-9: Protection System Local Control and Monitor Functions

Controls:	Monitors:
CLTS readout channel selector(s)	Coil temperatures
Voltage tap readout selector(s)	LN2 shield temperatures
Emergency shutdown	Voltage tap readout
Local/remote operation	Quench detected alarm
Strain gauge readout	
Emergency shutdown	
Local/remote operation	

The local control station will contain the magnet quench detection circuitry, or other off normal operation, and for initiating a dump sequence. Since this is a critical function, all quench detection circuitry will be redundant. The local control station will also provide an interface for remote operation by a programmable controller via a LAN type cable.

11.0 MAGNET CONTROL SYSTEM

The function of the Magnet Control System is to provide the capability for complete operation of the magnet from a single workstation. The present plan calls for the system to be housed in the Utility Building.

The architecture of the system is a simple hierarchical structure which allows control and monitor functions to be passed from one level to the next without interrupting system operation. A simple block diagram of the system is shown in Figure 11-1.

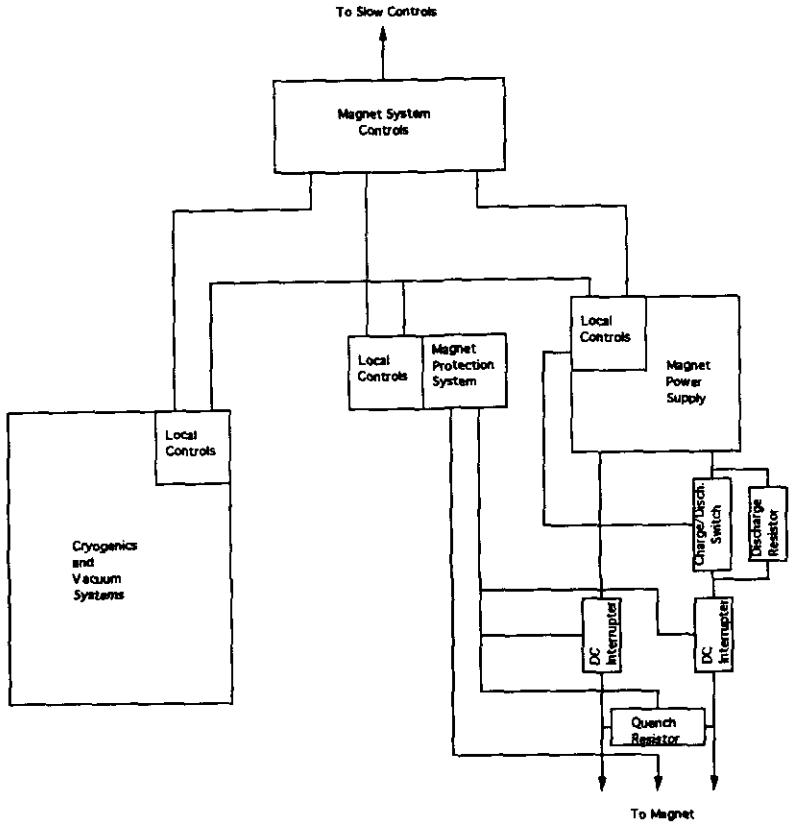

Figure 11-1 Control System Block Diagram

The system will consist of a workstation with one or more programmable controllers, an operators console and some local storage media. These are commercial items which are readily available. Final selection of the hardware will be coordinated with other GEM control related systems to help keep the costs down and to promote commonality throughout the project.

One of the commercially available software packages designed for interactive systems control, such as TACL or EPICS, will be used to form the core of the system software. Specialized control algorithms will be added as necessary. Selection of the particular core software package and the language to be used for specialized software development will also be coordinated with other GEM control related systems.

The system will consolidate and duplicate the control and monitor functions of the power supply, protection and cryogenics and vacuum local control stations. Control sequences for individual systems will be simplified for easier control of the overall system. Display of system monitors will be arranged in a logical manner consistent with the expanded level of controls at this station.

12.0 INSTALLATION SCHEME FOR MAGNET COMPONENTS IN THE EXPERIMENTAL HALL

The five major components of the magnet system, as detailed in the prior chapters, are: the two Forward Field Shaper (FFS) assemblies; the two Coil Assemblies (CA); and the Central Detector Support (CDS). The FFS and CA pairs are labeled North and South corresponding to their locations in the Experimental Hall. All five assemblies are independent, free standing units with provision for moving on rail type systems in the Hall and being supported on the floor of the Hall with shimmed stacks. The details of the moving systems and jacking necessary to accommodate the shims are provided elsewhere in this document. The alignment references described are surveyed into the Hall and documented prior to the Magnet installation sequence. The installation scheme envisioned at present is as follows:

- The South FFS will be transported, in the vertical orientation, to the North assembly shaft. It will be oriented in the North-South direction as it will be after installation. The FFS will be lowered into the Hall and placed on the rail system. It will then be moved South to its approximate final location. (Figure 12-1)

- The South CA will be transported, oriented, lowered, and moved South in the same manner. It will be near, but not connected to the South FFS. (Figure 12-2)

- The CDS, North CA and North FFS will follow in the same manner. (Figure 12-3, -4, -5) The CDS will be positioned with respect to the Hall alignment system, aligned, oriented correctly in all directions and placed on it's shimmed supports. The CAs will be moved to join the CDS and similarly aligned and oriented. The FFSs will follow.

- When the five major assemblies are in place, the magnet coils will be connected to all of their services for full system testing. All systems will be tested, in sequence, and the magnet will be taken to full power. (Figure 12-6).

- After the magnet systems have been certified and the magnet has demonstrated full power operation, the magnetic field will be mapped through out the magnet.

- After field mapping, the FFS's and CA's will be withdrawn to the ends of the Hall and supported on their shims. The calorimeter system will be lowered and installed in the CDS. (Figure 12-7) When the calorimeter installation has progressed far enough to free up the cranes, the barrel muon chambers will begin being lowered and installed into the CA's.

After the calorimeter system and barrel muon chambers have been installed, the CAs will be reconnected to the CDS and aligned and oriented. The endcap muon chambers will be lowered and assembled around the FFS's. When this is complete, the FFSs will be transported to the CAs, carrying the endcap muon chambers. The muon chamber assemblies will be joined and the FFSs will be joined to the CAs. All systems will be connected and the magnet system will be ready for final testing and operation.

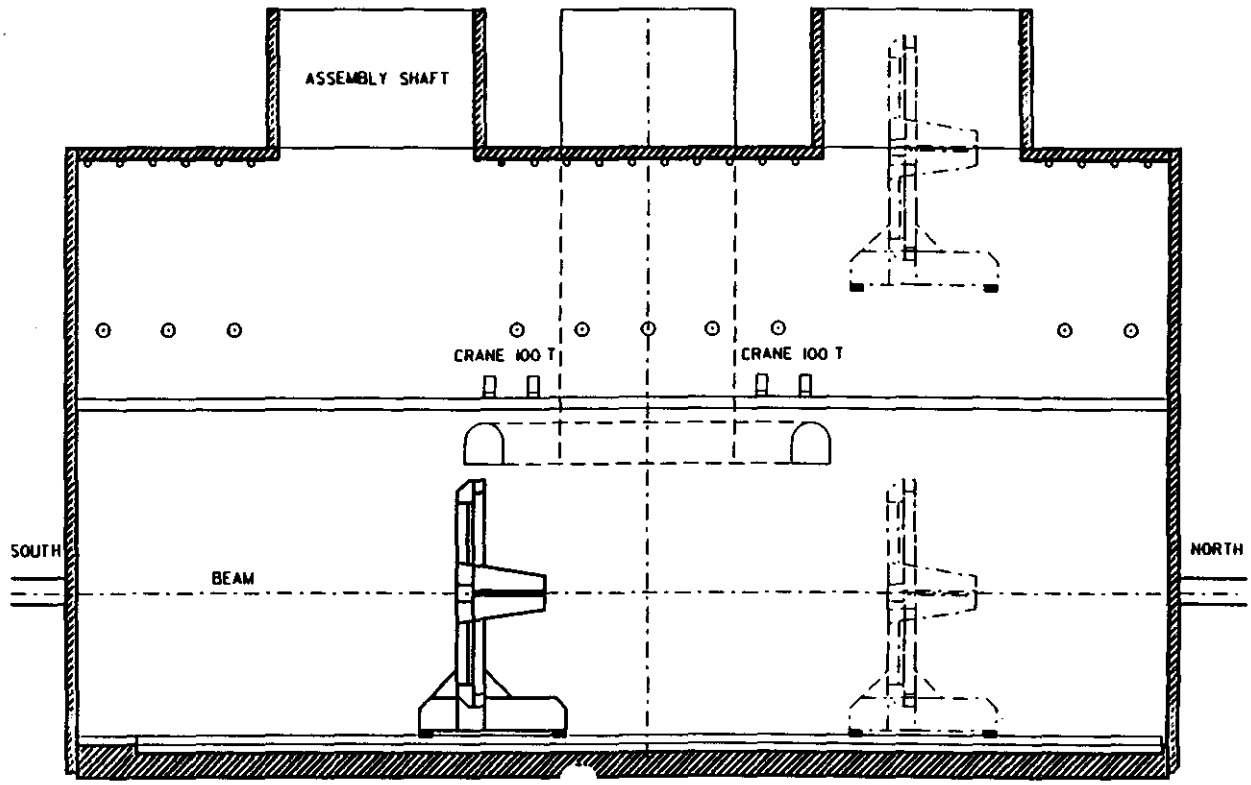

Figure 12-1: Phase 2, Install Magnet Flux Concentrator - South

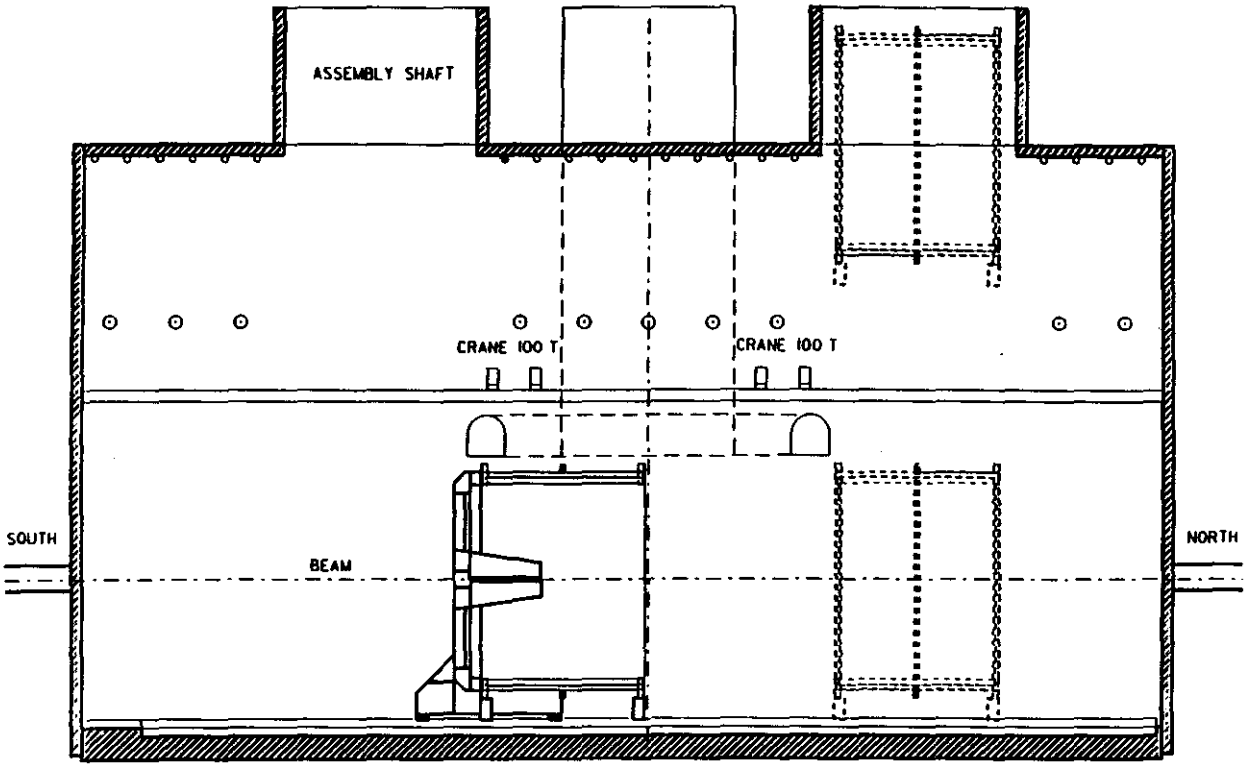

Figure 12-2: Phase 3, Install Magnet Half Coil - South

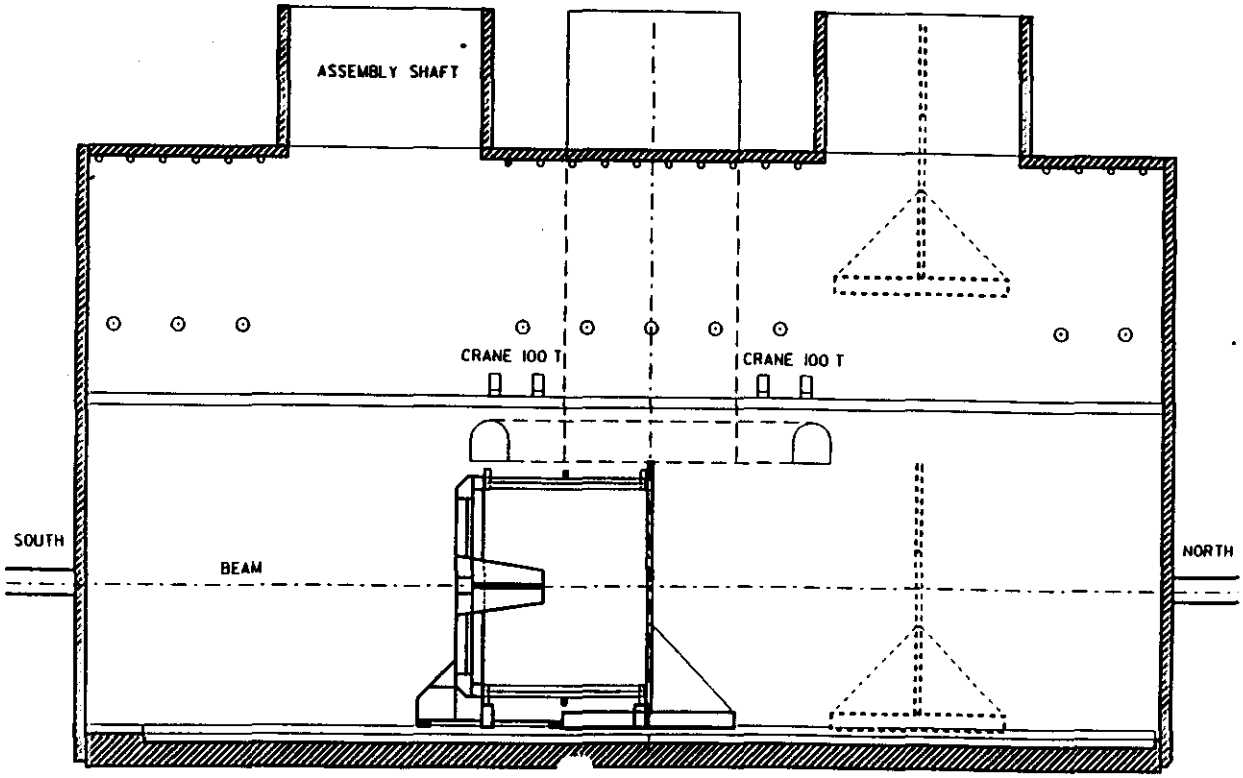

Figure 12-3: Phase 4, Install Central Membrane

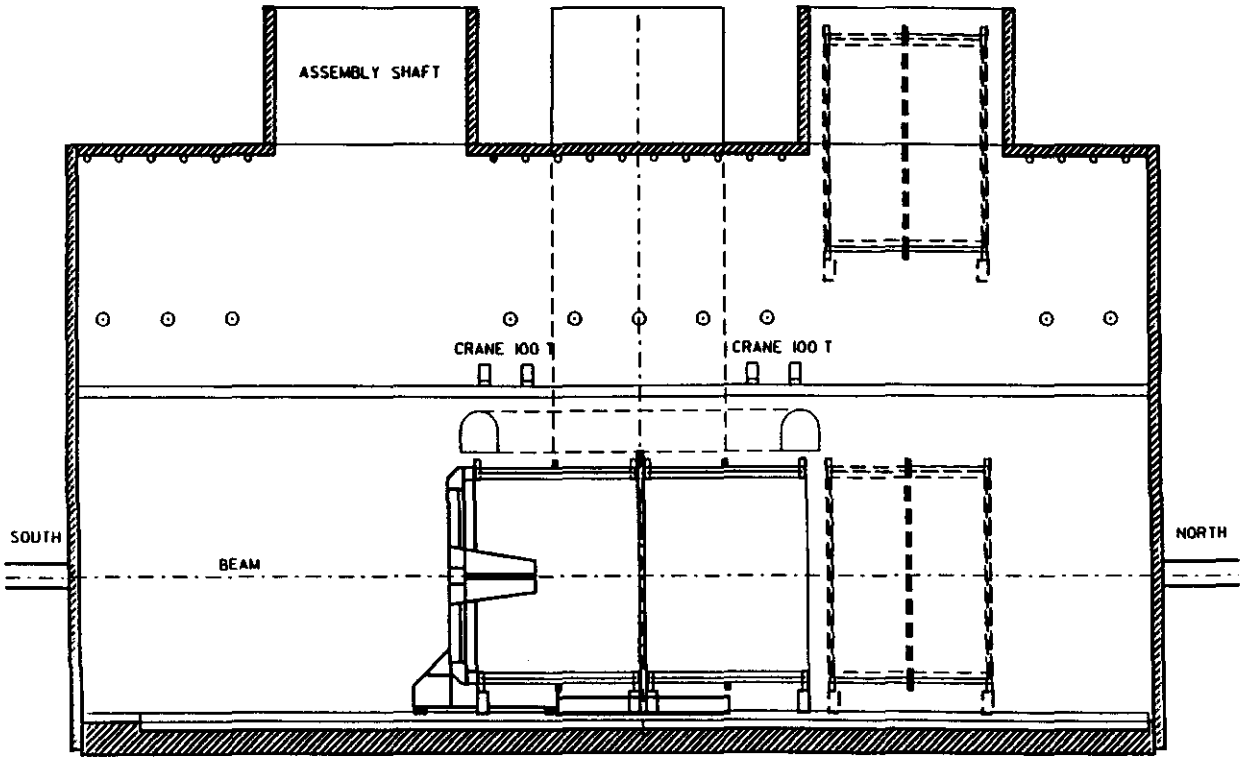

Figure 12-4: Phase 5, Install Magnet Half Coil - North

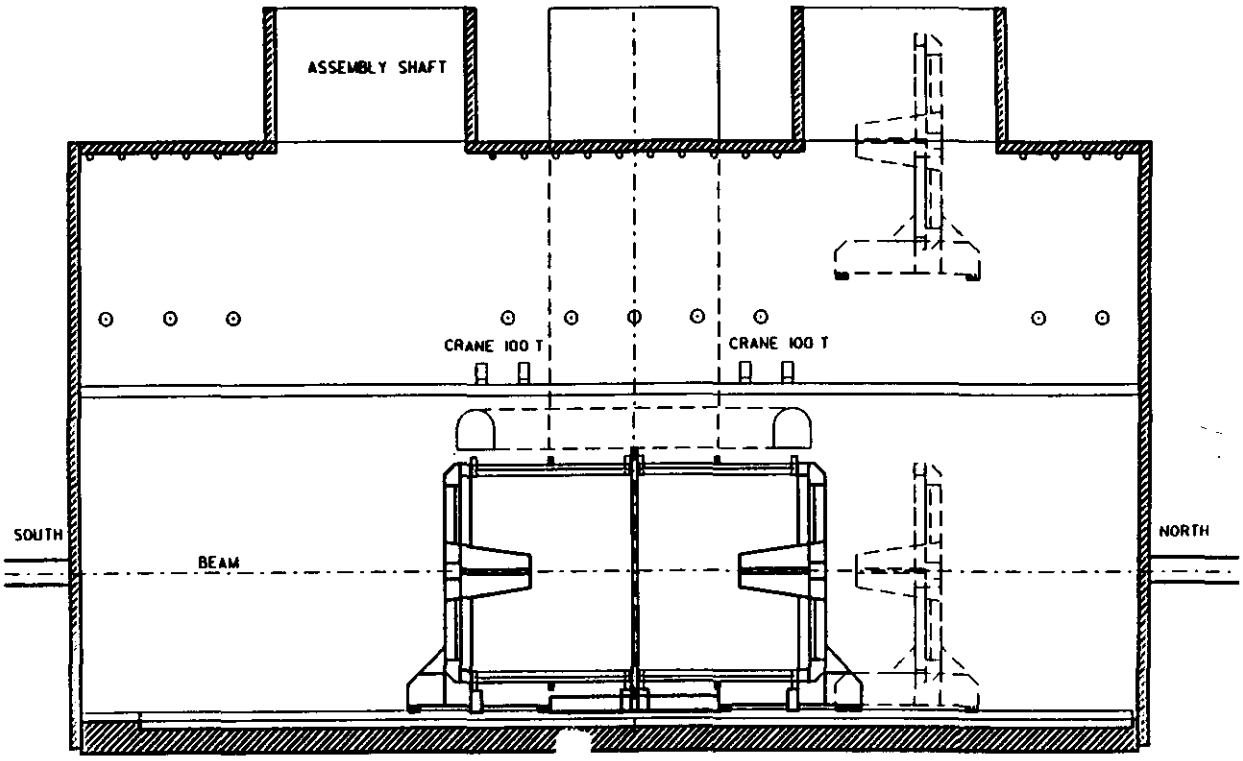

Figure 12-5: Phase 6, Install Forward Field Shaper - North

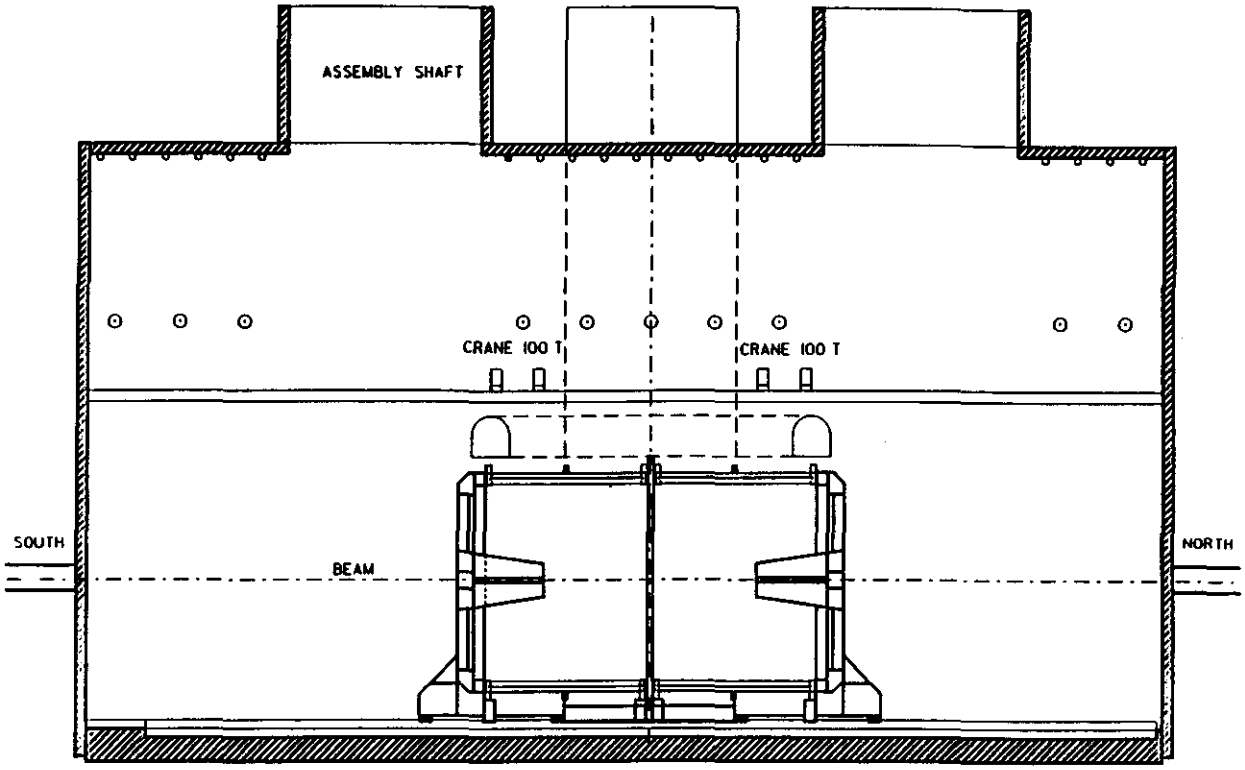

Figure 12-6: Phase 7-8, Test Magnet Systems / Map Magnetic Field

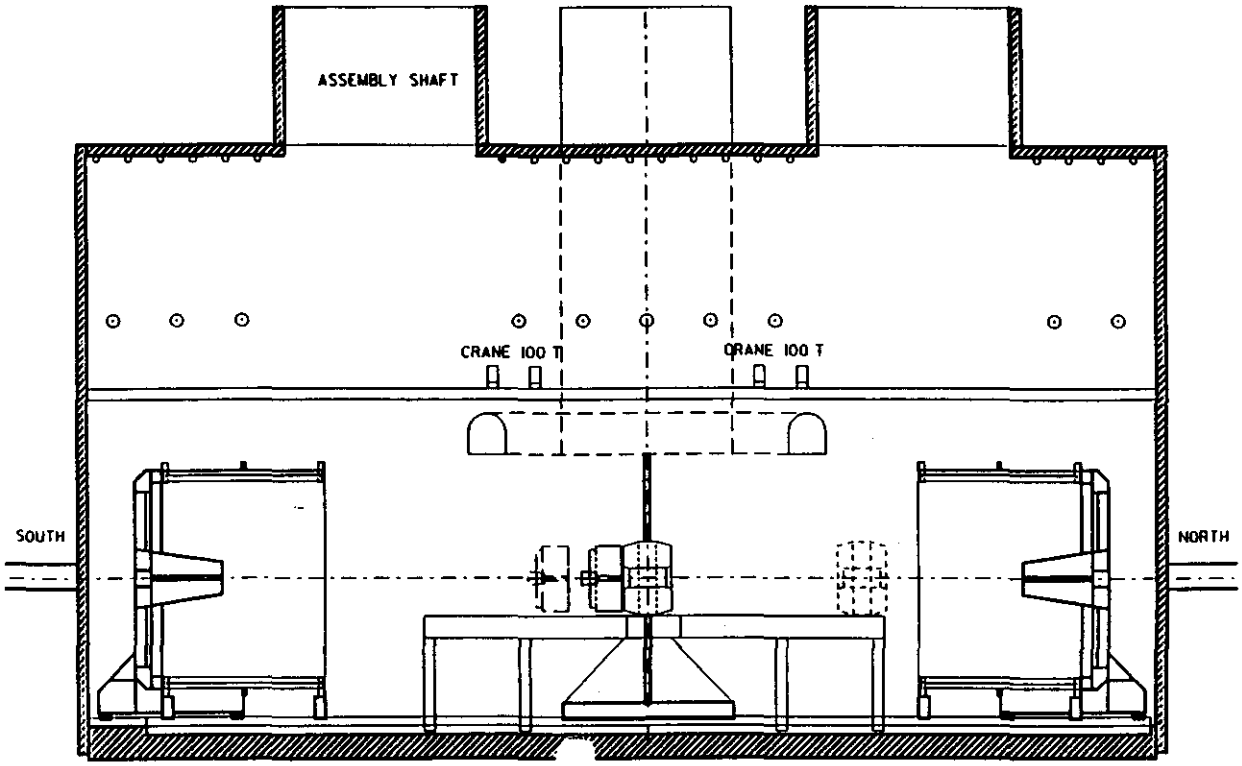

Figure 12-7 Phase 9, Open Magnet - Install Support and Calorimeter

13.0 MAGNET FACILITIES AT THE SSCL

There are two facilities at the SSCL for the manufacture and assembly of the magnets for GEM. They are the South Assembly Building (SAB) and the North Assembly Building (NAB) with its surrounding open welding pads. The SAB must be the first facility available for the on site manufacture and assembly of the various subsystems of the GEM detector. In this building, the 1.2m long bobbin sections are prepared, the conductor is formed inside it, and this winding is compacted. The coil segments will be assembled into the Coil Assemblies at the NAB. There is a continuing effort to consolidate the two buildings at the IR-5 site; it is expected to succeed but is not funded at this time.

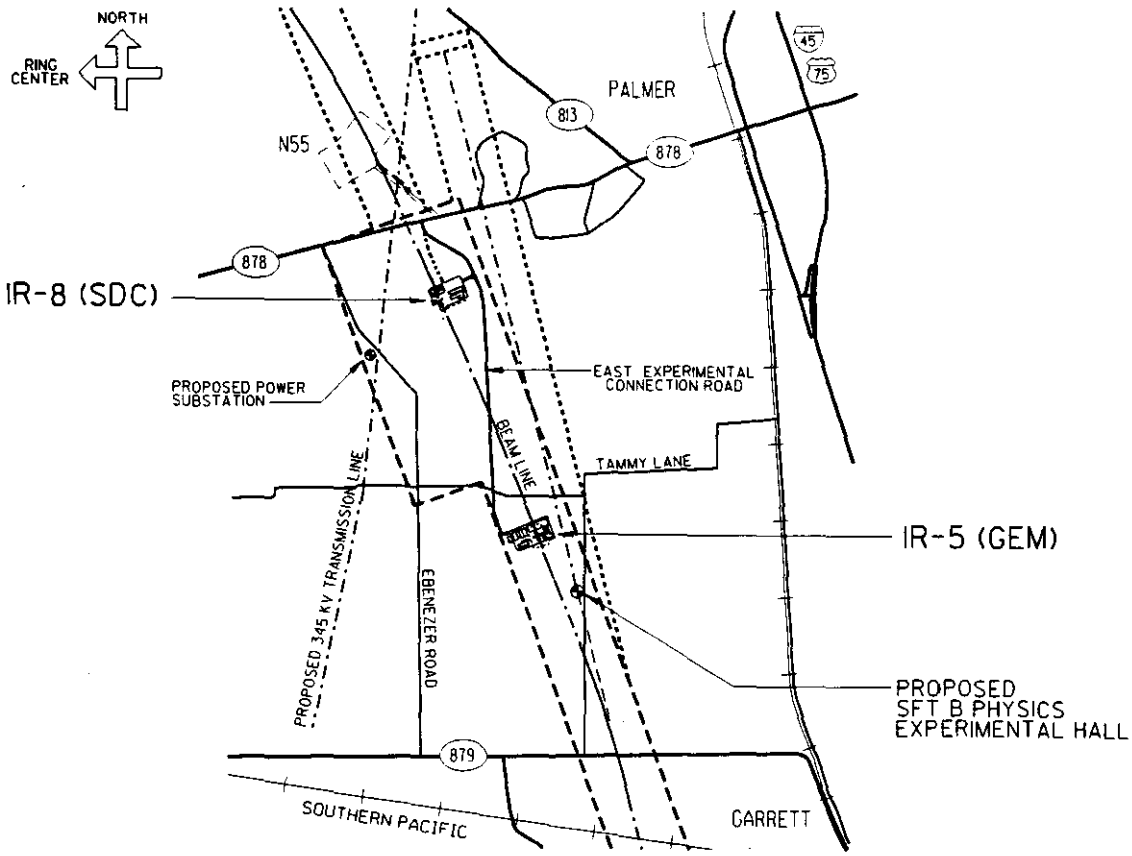

Figure 13-1 East Campus Access Roads

The SAB is a rectangular building approximately 30 meters wide by 110 meters long (Figure 13-2). It will have three manufacturing stations of approximately 25 meters square. The stations will be serviced by a single gantry crane with two hooks rated at 20 tonnes each and a hook height of 6.5 meters. The building will have large doors at each end that open to 28 meters wide and 10 meters high. The gantry crane will have tracks that allows it to travel out either end of the building for 2 meters. There will be an adjacent area of approximately 70 meters by 8.5 meters to include offices, rest rooms, lunch room and shop facilities.

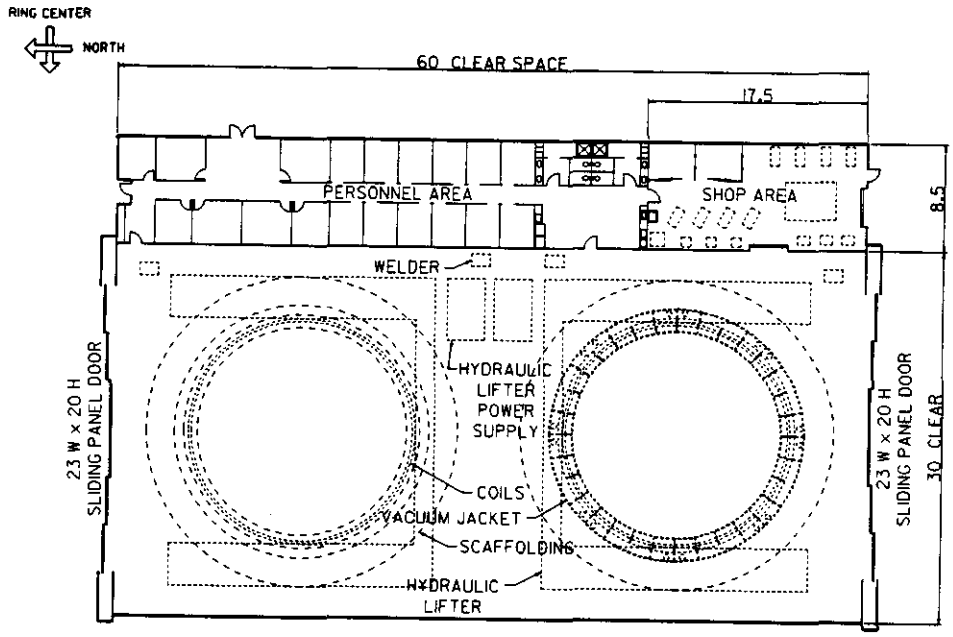

Figure 13-2: Coil Winding Building Floor Plan

The NAB will be constructed at the IR 5 site, where the GEM detector will be installed. The building will be approximately 30 meters wide by 110 meters long. (Figure 13-3) It will be an open high bay with 26 meters clear height for the entire bay. There will be two doors that open to 28 meters wide by 26 meters high, one at each end of the building. The high bay is expected to be equipped with two assembly stations of about 25 meters square. There will be an adjacent area of approximately 60 meters by 8.5 meters to include offices, rest rooms, lunch room and shop facilities. The NAB will be surrounded by open pads available for the construction of the large steel items needed for the manufacture of the coil assemblies, the central detector support and the FFS assemblies. One pad will accommodate the pair of inner and outer cryostat vessels. The other will accommodate the FFS assemblies and the CDS assembly.

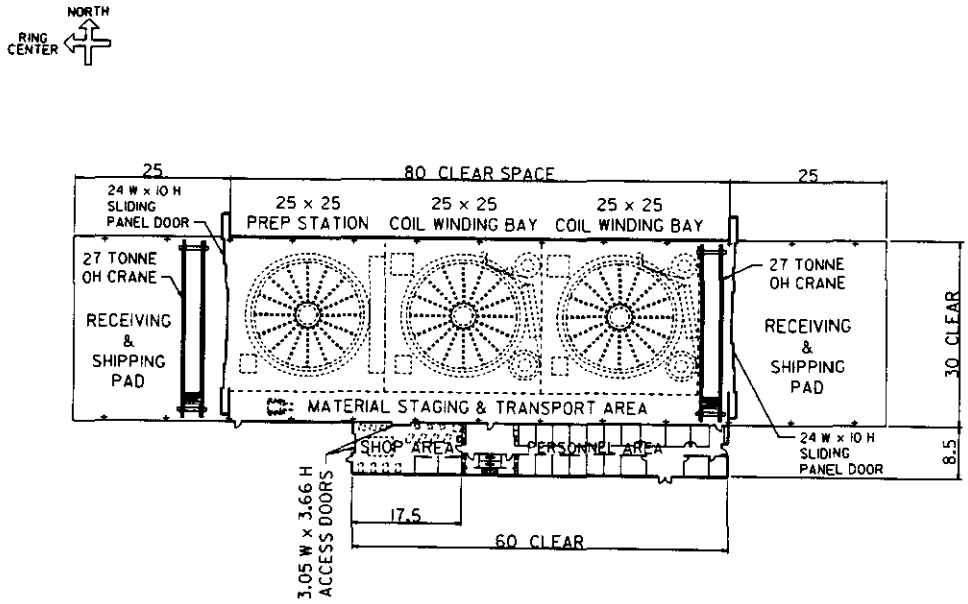

Figure 13-3: Magnet Assembly Building Floor Plan

The NAB and the adjacent pads will be connected to a heavy load path that leads to the installation shafts to the Experimental Hall. There will be ample access for the large lift system required for the installation of the coils into the cryostat vessels and their rotation to the horizontal position and attachment to their legs.

14.0 ES&H CONSIDERATIONS

The safety of the GEM magnet design comes under the auspices of the Associate Director of PRD, while the ES&H Oversight Office is primarily responsible for assuring compliance with the applicable DOE Orders, such as 5480.1B Environment, Safety and Health Program for DOE Operations. The overall safety analysis and review efforts are coordinated by GEM ES&H through the ES&H System Safety Group. The Gem Magnet subsystem will be constructed and operated in compliance with all applicable ES&H regulations.

The GEM Magnet Group has adopted a single-coil solenoid configuration, without iron flux return. The proposed safety-design methodology, will maintain compliance with DOE Orders 5481.1B and 5480.ACC, the SSC Final and Supplemental SSC Environmental Impact Statements (FEIS, SEIS), and applicable regulatory codes and standards. DOE Order 5480.5 Safety of Nuclear Facilities, does not apply. This proposed design action is described in GEM Magnet Safety Evaluation, GEM TN-92-222, Considerations Leading to the Choice of Open Field Magnet, GEM TN-91-30, and SSC GEM Magnetic Field Safety & Health Effects, GEM TN-91-19.

Among the safety hazards which will be considered and analyzed within the Magnet PSAR are:

1) Quench protection (from sources such as: 'Hot Spot' occurrence, Vacuum Loss, etc.)
2) Practical testing of the magnet performance
3) Helium cooling
4) High pressure within the conductor, from Quench (340 bar)
5) Magnetic Field Effects characterization (including Health impacts)
6) Open Circuit within the Dump Resistor
7) Magnet shutdown process-Detector access in 'B' Field
8) Stress Effects
9) Helium & Nitrogen Overpressurization protection and venting
10) Use of the vessel vacuum line as overpressure vent line, with rupture disc (no PRV)
11) Vacuum pump 'small-leak' handling capacity
12) Gross cryogenic liquid leak effects - embrittlement, electronics, personnel exposure
13) Radioactive hazardous waste handling

The use of Magnet structural materials having very similar coefficients-of-expansion/contraction prevents coil static instability from axial and radial thermal expansions/contractions during warming/cooling between ambient and cold mass (4.5 K) temperatures, from being a safety issue. Static instability of the internal vessel of the cryostat may result in case of overpressure due to helium leaks inside the cryostat. Liquid helium leaks could give cryogenic burns to workers and an eventual ODH problem. Compared to other thin superconducting magnets, the E/M value of 3.6 kJ/kg for the GEM magnet provides a margin of safety, in case of quench (note: SDC's E/M is ~7).

Quench can be expected to be a rare but potentially catastrophic event when the superconducting coil transitions to a normal state. This energy will be discharged in a 0.02 ohm Dump Resistor (DR) where GEM's quench detection system 'triggers' the fast dump switches, discharging in a time constant of ~100 seconds. This energy will actually be dissipated within the coil and the DR, in ratio to their resistance. The voltage across the DR will be 1kV or buss-to-ground voltage will be 0.5 kV, therefore stringent safety protection must employed. Quench results in heat generation and rapidly increases the pressure inside the magnet conductor channel to ~6,300 psig at a $T=100^{o}$ K. The helium system will be designed to safely handle this event. 'Hot spots' can occur inside the conductor where the (relatively) low quench velocity does not allow the heat generated to dissipate uniformly throughout the entire coil. If the quench detection system does not properly 'trigger' the DR switches, the hot spot(s) can heat-damage the conductor. The GEM magnet hot spots will mainly be within the aluminum conductor.

The most probable system disturbance is that of a quench. An opening of the electrical circuit between the coil and the DR, in which an overvoltage would be generated between the coil and the mass, is very unlikely to occur from development of resistance points inside the buss bar system, loose connections, etc.

The construction of the GEM Magnet superconductor is different in comparison to other existing superconductors. An advantage for the GEM conductor is that the conductor is directly cooled by the supercritical helium, an important factor for stability against quench. Superconducting wires are designed to be stable against all credible disturbances. A practical test should be performed upon several loops of the conductor to verify it's integrity.

Buckling and Load stress analyses have been performed upon the CDS. Refer to GEM TN-92-224 "Structural Analysis of the GEM Central Detector Support." Embrittlement and resulting fatigue cracking, from prolonged contact with accidentally spilled cryogenic liquid (from within the detector), do not present a collapse hazard.

The FFS may be designed to allow for access to the Tracker with resulting personnel access requirements. Minimum personnel entry dimensions and safeguards against accidental beampipe contact will be applied.

Safety Analyses

Safety analyses will be performed to systematically identify all inherent hazards, analyze their consequences, provide methods to eliminate, control, or mitigate them, and assess the system risk. This process began in the conceptual and preliminary design phases of the magnet, and allowed early hazard identification and elimination or control. Mitigation of the remaining hazards will provide reasonable assurance that operation of the magnet will limit risks to the public and employees health and safety, while adequately protecting the environment.

Interactions at all levels between the magnet and other detector subsystems will be analyzed to identify and resolve the effects of one subsystem's hazards/failures upon another. When common-cause failures of redundant equipment or subsystems occur, they can produce catastrophic, cascading results, due to the speed of sequential failure occurrence and lack of remedial response time.

Safety reporting and hazard tracking documentation will include all pertinent details of the analysis to assure traceability throughout the hazard's life cycle.

The hazard risks will be derived as quantitative or qualitative expressions of loss potential, which considers the hazard's probability of occurrence and the event's outcome severity. In analyzing the system safety, reliability, and risk involved, the following techniques may be employed:

1) Hazard Analysis and Risk Assessment
2) Failure Modes and Effects Analysis
3) Fault Tree Analysis

The GEM Magnet life cycle requires a multi-stage safety analysis and review program. A draft Preliminary Safety analysis Report will be initiated in the conceptual design phase and completed by the end of the preliminary design phase. This is followed by the final Preliminary Safety Analysis which is completed prior to start of construction, and the Safety analysis Report that is developed during the late-construction phase, completed and approved six months prior to commissioning. The final SAR includes detailed analysis of all 'as-built' design features of the GEM Magnet, and must be updated as design modifications are made.

Environmental

The environmental impact associated with the GEM magnet's static magnetic field has been addressed in the Supplemental Environmental Analysis of the GEM Magnet, GEM TN-92-190, and DOE-approved in GEM TN-92-191. The intent is not to produce any measurable negative effects upon the public or the environment. The existence of a small static magnetic field produces no adverse environmental impact. The SEIS Record of Decision

(ROD) stated that the overall potential for adverse environmental impacts is small, while substantial potential exists to mitigate any impacts .

A magnetic field has virtually no effect upon the medium (soil, air, water) in which it would exist. There would be no translational or rotational forces exerted upon the surrounding soil components and thus no soil/rock movement. The field outside of the detector hall would not be of sufficient strength to produce transportation of any buried ferromagnetic objects. A magnetic field produces no permanent physical or chemical changes in the absorbing media. The proposed single-coil magnet design is not dependent upon the type of hall construction excavation, and therefore there is no change in spoil quantity due to the hall cut-and-cover type of construction.

The proposed single-coil GEM magnet will produce above-surface ellipsoidally-shaped contours of equal field strength, and incorporation of mitigative actions will fully comply with all conditions set forth in the FEIS & SEIS.

The operating magnet produces a static, non-time-varying magnetic field only, and thus produces no radiation.

15.0 MAGNET RESEARCH AND DEVELOPMENT

Although most of the GEM magnet technology is well based in proven concepts verification testing is required on the conductor and joints simply to ensure that the design margins are as calculated. In addition, what is different about the GEM magnet is it very large size, and coil winding techniques must be verified at the 19 m coil diameter. These three R&D activities are described in this section.

Conductor R&D

The GEM detector requires a magnet which is highly reliable and, at the same time, the largest superconducting magnet ever built. A verification test is therefore required on the conductor to demonstrate the design under realistic conditions of temperature, magnetic field and current. The planned test article is a hairpin sample which will utilize about 60 m of prototype GEM magnet conductor. Parallel lengths of superconducting strand will be cabled, pulled through a 60 m length of butt-welded stainless steel conduit, and then clamped inside the welded aluminum sheath. The entire conductor will then be formed into the hairpin shape and mounted in a cryostat. The conductor will be interfaced to a set of vapor cooled leads, a 50 kA power supply and a cryogenic supply system. The sample will be instrumented with heaters and voltage tape and then tested under various heating conditions at full current.

Joint R&D

The GEM magnet is fabricated in modules which must be connected electrically for proper operation. This electrical connect is provided by the coil joints which must carry the full 50 kA current with low joints heating.

At present, two alternative joint concepts are being pursued. One is based on joints which have been fabricated before in the fusion community under the U.S. Demonstration Poloidal Coil Program. In this concept, the superconducting subcables are fanned out and soldered inside of a tube which is rolled to match the subcable diameter. The flattened tube is then soldered inside a copper or aluminum stabilizer. This much of this joint can be manufactured and leak tested in the factory. This entire subassembly is then soldered to its mating half during magnet assembly on site. Preterminating the conductor lengths in the factory imposes an accurate length requirement on the conductor and accurate tolerances on the winding process as well to ensure that each module mates with its adjacent module in the prescribed location.

The second joint concept requires assembly onsite, but in doing so relaxes the accuracy requirements on conductor length and winding tolerances. It also dispenses with the rolled and solder filled tube which is viewed as a potential manufacturing complication. Instead, the subcables are lapped with and soldered to the subcables from the adjacent coil module directly. The soldered subcables are then clamped inside a set of welded aluminum plates.

The joint R&D plan calls for fabricating and testing a set of subscale, followed by full scale, joint test samples of both types. Manufacturing procedures will be evaluated and compared for both joint concepts. In addition, the sub- and full scale joint samples of both types will be tested for resistance at full current. Following the full scale tests, the two candidates will be compared and the better one will be selected as the design baseline.

In addition to the joint resistance tests, a pair of coil module sector mockups are planned which will include the joint details. These mockups will be used to simulate the joining of production coil modules to verify the adequacy of the three-dimensional spatial clearances in the joint region.

Winding R&D

A major challenge of the GEM magnet is learning to deal with its large size. With a mean coil diameter of 19 m, the coil modules must be wound on site. A winding tool design to accommodate the 50 Mg mass of each coil module and its 19 m diameter needs to be developed.

The present concept for winding is to roll form the conductor on the inside of the aluminum bobbin/flange structure of the cold mass as the structure rotates on a motor-driven turn table. Details such as to the correct number of roll forming machines, roll forming tolerances, driving force and speed, conductor spool diameter and drive, insulation station design and the synchronization of all drives are among the issues which are to be addressed through the winding R&D program. In addition, small programs are planned to evaluate the winding stack axial stability and support requirements.

A winding development activity has already begun. The plan for this activity calls for performing some initial bending experiments on 5 to 15 m lengths of full scale cross-section conductor. Residual keystoning of the conductor is being evaluated as the conductor is formed first to a 3 to 4 m diameter characteristic of the shipping spool, and then to the 19 m diameter of the GEM coil. Following the bending experiments, two full scale turns will be roll formed into the 19 m diameter of the GEM coils. The final step is to form 6 full scale turns inside a dummy bobbin.

16.0 SCHEDULE

The summary schedule for the magnet subsystem is shown in Figure 16-1. This schedule is based on the assumption that the magnet subsystem will be authorized to place a major subcontract with an industrial partner or team on 1 January, 1993. Preparations for bidding, awarding, and placing this contract are in progress at this time; an acquisition plan describing the proposed contract and procedures has been prepared and released by the SSC Laboratory. Assuming proper approvals, we intend to release a Request for Proposal (RFP) in late summer 1992 to formally initiate this process. We also intend to undergo a DOE review of the magnet subsystem in the early fall, to allow sufficient scrutiny of our design, plans, and management so that we will be authorized to proceed with this major procurement in advance of the submission of the overall GEM TDR.

Following approval, the three most critical tasks will be: 1) procurement of the conductor (to be performed by SSCL); 2) the design and procurement of the winding tooling (to be done by the industrial team); and 3) to complete the final design of all other hardware. These activities occupy the early critical path for the magnet subsystem as well as the detector as a whole. Reviews are being planned at key points in the schedule, and tentative times are indicated in Fig 16-1 for the following:

SRR - System Requirements Review - to review the vendor's final version of the system requirements, to ensure proper technical understanding of the overall project.

PDR - Preliminary Design Review - to review key long-lead and critical-path items, for which early procurement is required. This will include vacuum vessels, as well as late reviews of coil winding tooling and procedures.

CDR - Critical design Review - to review detailed designs of all remaining hardware prior to procurement actions.

PRR - Production Readiness Review - to review preparations for final assembly on site.

TRR - Test Readiness Review - to review rediness for final acceptance testing above- and below-ground.

These review points will provide SSCL as well as the GEM Collaboration with the desired degree of control over the subcontracting team.

The magnet construction schedule is driven by the need to complete magnet installation and testing in the detector hall by March 1997. The magnet must be completed by this time to allow the installation of the detector components and the activation of the GEM detector by SSC "first-light" in September 1999.

As is typical of large on-site magnet fabrications, the construction schedule critical path is a combination of early facility construction followed by subsequent magnet fabrication and assembly activities. In order to meet the aggressive schedule, the winding of the coils must commence as soon as facilities become available in March 1994. The winding tooling will be developed and ordered early in 1993 for installation at the GEM winding building in February 1994. Early involvement of the magnet prime industrial subcontractor is essential to assure successful winding. Therefore, it is important that the contract for the prime contractor be awarded in January 1993.

The simplified task timelines shown for the major magnet subsystems in Figure 16-1 are derived from a number of sources, traceable to industrial estimates. Estimates of the critical winding and assembly operations were developed by a detailed breakdown of the steps involved. This estimate will be supplemented by a detailed winding plan that is currently being developed by an experienced magnet fabricator. Most elements of the magnet assemblies are near the critical path. The supporting activities of external vacuum pumping systems, power/protection and controls and cryogen supply systems are not deemed critical at this point. The schedule for the major steel erection tasks, the two forward field shapers and supports and the Central Detector support, assumes fabrication in the

United States. Discussions with foreign participants that will occur over the next few months will provide a better basis for determining the schedule impact of these tasks.

While the schedule is ambitious, it is consistent with the construction schedule of other large magnet systems. Timely approval of this detector will assure an orderly and cost-effective fabrication.

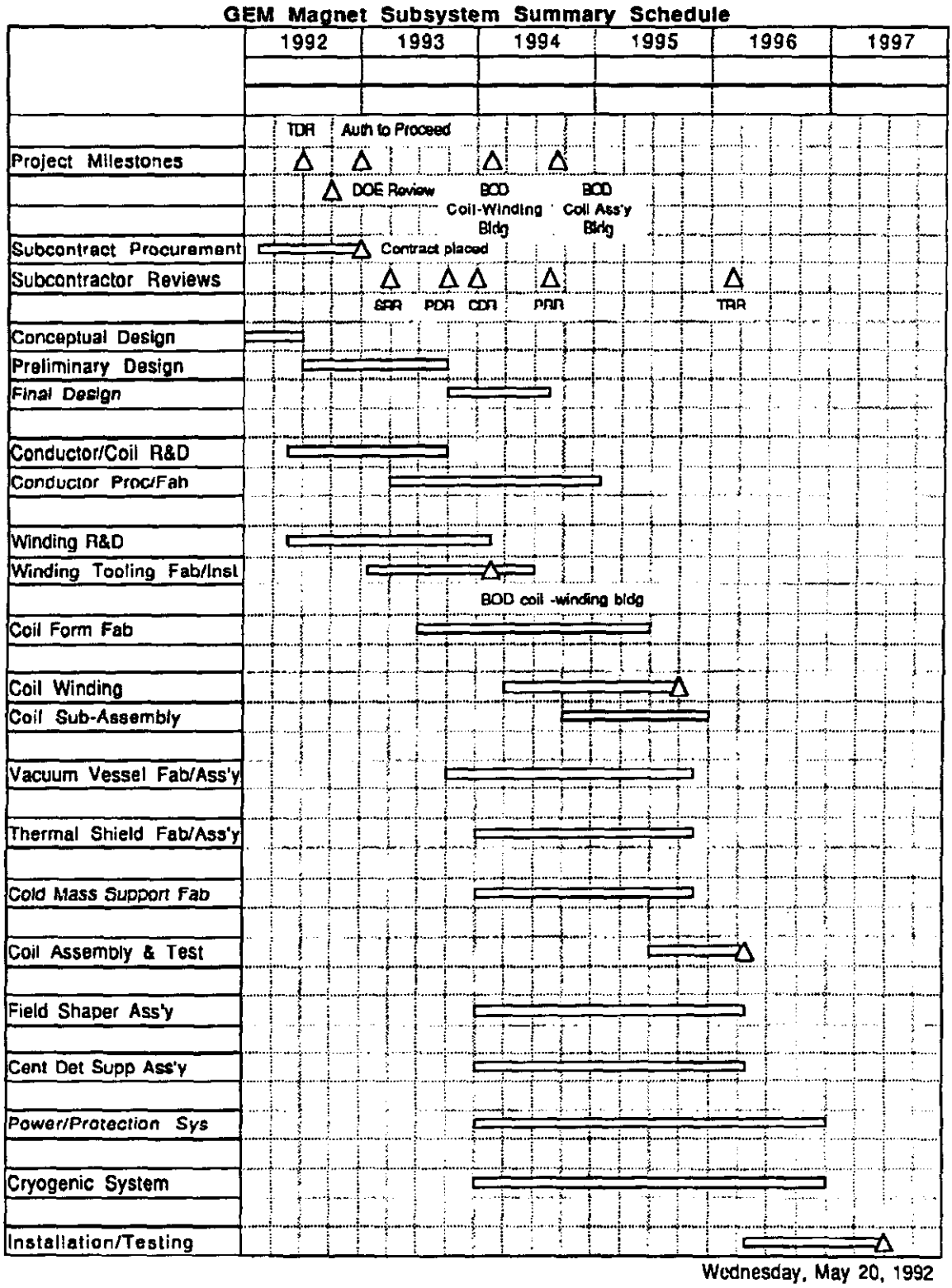

Figure 16-1 - Magnet Subsystem Summary Schedule